2012-12-20

A Case Study on the University of Calgary EEEL Building Large Diameter Earth Tube System

Tan, Li Li

UNIVERSITY OF CALGARY

A Case Study on the University of Calgary EEEL Building Large Diameter Earth Tube System

by

Li Li Tan

A THESIS

SUBMITTED TO THE FACULTY OF ENVIRONMENTAL DESIGN

IN PARTIAL FULFILMENT OF THE REQUIREMENTS FOR THE

DEGREE OF MASTER OF ENVIRONMENTAL DESIGN

FACULTY OF ENVIRONMENTAL DESIGN

CALGARY, ALBERTA

DECEMBER, 2012

Abstract

Building heating, ventilation and air conditioning (HVAC) systems use large amounts of energy. Finding ways to lower that could lead to notable energy savings and reduced emissions.

Earth tube (ET) systems preheat/precool ambient air by directing it through the ground to exploit the relatively stable subsurface temperatures. The technology has been applied in several countries in North America, Europe and Asia.

A 1.2 m inner diameter two-duct ET system at the University of Calgary was studied. The temperature in soil surrounding the ducts was monitored for twenty months. Data were collected and analyzed to evaluate the temperature change of soil surrounding the ducts. It was initially planned to determine if there is a net drawdown of heat in surrounding ground in very cold climates, or if the heat is largely replenished by inflow. However, due to the reverse airflow problem in the south duct, the research was limited to the stabilization of soil remote from the building effect.

Acknowledgements

I would like to express my sincere appreciation to my supervisor Dr. Jim Love for giving me this great study opportunity. He is always generous sharing his vast knowledge in the field of high performance building technologies. His patient instructions on logical thinking, data analysis and professional writing enabled me to reach a higher level of academic research. Without his financial support, this two-year long study would not have been possible.

I would also like to thank my colleague Chris Lashmar for his help in data collection, equipment installation and technical support. Various members of EllisDon, UofC Geoscience department, and UofC facility management also provided valuable information to this research.

Finally, I want to thank my family for their continuous support and encouragement during my study.

Table of Contents

List of Tables

List of Figures

Nomenclature

AHU	Air Handling Unit
ASHRAE	American Society of Heating, Refrigerating and Air-Conditioning Engineers
CAPULA	Canadian Association of Pipeline and Utility Locating Contractors
CDD	Cooling degree-day base 10 ℃ (IP values are converted to SI values for thesis use, the same as below for HDD definition): for any one day, when the mean temperature is more than 10 ℃, there are as many degree-days as degree Celsius temperature difference between the mean temperature for the day and 10 ℃. Annual cooling degree-days (CDDs) are the sum of the degree-days over a calendar year (ASHRAE, 2012, p. 7).
CFD	Computational fluid dynamics
COP	Coefficient of performance. Performance of a refrigeration cycle is usually rated in terms of a coefficient of performance (COP), defined as the benefit of the cycle (amount of heat removed) divided by the required energy input to operate the cycle (ASHRAE, 2009, p. 2.3). For an ET system, its COP means the ratio between its energy gain and the fan electricity use. The COP is calculated with the overall energy gain supplied by the ET system and the mechanical energy used during operation time (Pfafferott, 2003, p. 982).
CSx	Cross section number x
EEEL Building	The Energy Environment Experiential Learning Building
EPA	United States Environmental Protection Agency
ET	Earth Tube
GPR	Ground penetrating radar
GSHP	Ground source heat pump
HDD	Heating degree-day base 18 ℃: for any one day, when the mean temperature is less than 18 ℃, there are as many degree-days as degree Celsius temperature difference between the mean temperature for the day and 18 ℃. Annual heating degree-days (HDDs) are the sum of the degree-days over a calendar year (ASHRAE, 2012, p. 7).
HVAC	Heating, ventilation and air conditioning
Large diameter	Inner diameter of ET usually larger than 1 m
LEED	Leadership in Energy and Environmental Design. It is a third-party certification program and an internationally accepted benchmark for the design, construction and operation of high performance green buildings (Canada Green Building Council, 2012).
NECB	National Energy Code for Buildings
NRCan	Natural Resources Canada
PVC	Polyvinyl chloride
Sx	Sensor number x
Small diameter	Inner diameter of ET usually 10-30 cm
STx	String number x
UofC	University of Calgary

VAV	Variable air volume
VFD	Variable frequency drive

CHAPTER ONE: INTRODUCTION

1.1 Energy Efficiency

The world has limited resources, but human energy needs are growing rapidly. Globally, building energy use has steadily increased to between 20% and 40% of total energy use in developed countries (Pérez-Lombarda et al., 2008, p. 394). Among building services, the growth in heating, ventilation and air conditioning (HVAC) systems energy use has been particularly large. In the U.S., building operations are responsible for 41.1% of all the energy used in 2011 (U.S. Department of Energy, 2012a). Finding ways to lower HVAC system energy use could result in substantial improvements in overall building energy performance which could lead to large financial savings. Moreover, burning of fossil fuels produces greenhouse gases such as carbon dioxide. Increases in greenhouse gas levels in the atmosphere can lead to global warming. The U.S. CO_2 emissions are mainly contributed by building fossil fuel burning, which will account for 40% in 2011 (U.S. Department of Energy, 2012b). This is a notable environmental and social issue and should be addressed quickly.

Alberta Environmental and Sustainable Resource Development (2012) provided strategies to all Albertans in using energy efficiently and reducing greenhouse gas emissions, including to "implement energy efficiency standards in building codes for homes and commercial buildings." Natural Resources Canada (NRCan) updated the National Energy Code for Buildings (NECB) in 2011 and the new code could help improve energy efficiency in new and existed buildings by 25% overall (Natural

Resources Canada, 2011). The International Energy Agency published "25 policy recommendations (2012)" and five of them were to support the 2030 Challenge (Architecture 2030, 2011), which is an international initiative to promote high performance buildings. The 2030 Challenge encourages the research, development and implementation of innovative building energy systems.

Because of the relatively high thermal inertia of the ground, temperatures in the ground lag those at the surface, and their fluctuations decrease with depth below grade (National Research Council Canada, 2005). Moreover, soil temperature gets closer to the mean annual ambient air temperature with increasing depth.

Earth tube (ET) systems (also known as "earth-air heat exchangers") preheat/precool ambient air by directing it through the ground to exploit the relatively stable subsurface temperatures. It was first used in about 3000 B.C. Iranian architects used wind towers and underground tunnels for passive cooling (Bahadori, 1978). It was explored in the late 70s and early 80s but did not gain wide acceptance due to low performance and other problems, such as poor air quality. Over the last two decades, several systems have been installed in China, India, Brazil and some European countries, such as Germany, Sweden and the U.K to condition greenhouse, poultry, office and residential buildings. The potential of using the ground for tempering outdoor air has gained increasing attention during the last few decades, and there has been a surge in research on ET systems (Thevenard, 2007, p. 1). Thevenard's review concluded that "smaller diameters (usually

10-30 cm in diameter (p. 2)) are preferable from a thermal point of view, but they also correspond (at equal flow rate) to higher friction losses." However, large-diameter (> 1 m) ducts could potentially lower friction losses. There could be a way to balance heat transfer and fan power use with large diameter ducts, so that they could be used in large buildings to benefit more people without compromising performance.

1.2 Introduction of Research

In this research, the Energy Environment Experiential Learning (EEEL) ET system at the University of Calgary was studied to investigate its performance in terms of thermal interaction with soil surrounding the ducts. The EEEL Building is a 24,500 m^2 facility housing classrooms, laboratories and offices. The initial ET system design was large enough to condition all outdoor air for the building. Due to budget limitations, the system was downsized to serve only the main floor theatre (floor area of 320 m^2). Temperatures in soil surrounding the ducts were logged continuously at 5-minute intervals for over one year, from February 15th, 2011 to September, 30th, 2012. This thesis presents the key findings.

1.3 Research Objective

Most previous ET studies addressed small, residential systems. More recently, large diameter systems have received more attention due to potentially higher energy savings. Still, there are some areas requiring further research. For instance, for large diameter ET systems in very cold climates, is there a net drawdown of heat in the surrounding ground,

or is the heat largely replenished by inflow? The research objective of this research was initially to characterize the EEEL ET system performance in terms of soil temperature effects.

1.4 Summary of Chapters

Chapter 2 summarizes some of the literature that were most relevant to this author's research, concentrating on heating performance of large diameter systems in cold climates. A few studies on small diameter system heating performance and ground heat depletion were also reviewed.

Chapter 3 introduces the location, weather condition, studied ET system parameters and the method applied in this research.

Chapter 4 describes several research limitations encountered in this research, such as uncertainty of string locations, backward airflow in the south duct of the ET system, and landscape change during data collection.

Chapter 5 provides the analyses of the collected data on soil temperature surrounding the ETs and soil remote from the building. The data collection lasted about twenty months.

Chapter 6 provides the conclusions and suggestions for future work.

CHAPTER TWO: LITERATURE REVIEW

2.1 Introduction

In this chapter, this author reviewed some heating studies conducted on large and small diameter ET systems in cold climates, and several small diameter systems in mild to hot climates. The studies used both experimental and simulation techniques. This chapter also summarises the studies on soil heat depletion surrounding the ETs and both horizontal and vertical ground source heat pump systems.

Table 2.1 summarizes the key literature that were reviewed in this chapter. The literature suggest that ET systems can provide heating for all types of climates and some of the systems provided enough to be viable financially if a very long time frame is considered.

Table 2.1 Literature Summary on ET Heating Performance

Source	Location	Climate (HDD), Weather Station	Reported Temperature Rise (usually maximum)
Cold Climate – Large Diameter – Measured			
Heiselberg (2004)	Grong, Norway	4186 (Oslo-Blindern) (ASHRAE, 2009, p. 14.41)	7 ℃ (Figure 3)
Earth Rangers Centre (2010)	Ontario, Canada	3956 (Toronto Lester B. Person International Airport) (ASHRAE, 2009, p. 14.29)	Claims 15 ℃ based on values from building management system
Parsons (2011)	Ontario, Canada	3956 (Toronto Lester B. Person International Airport)	19 ℃
Schild (2001)	Nesodden municipality, Norway	4344 (Oslo/Fornebu, Norway)	Maximum 6 ℃ (Figure 4a)
Cold Climate – Large Diameter – Estimated			
Jeong (2002)	Grong, Norway	4186 (Oslo-Blindern)	Estimated 12 ℃ (Figure 4.4)
Tjelflaat (2000), Wachenfeldt (2003), Zhang & Haghighat (2005)	Grong, Norway	4186 (Oslo-Blindern)	Estimated 18 ℃ (Figure 7)
Athienitis et al. (2005)	Montreal, Canada	4319 (Montreal-Est) (ASHRAE, 2009, p. 14.30)	Estimated 9 ℃
Cold Climate – Small Diameter – Measured			
Gustafson (1993)	Linkoping, Sweden	4289 (Stockholm) (ASHRAE, 2009, p. 14.44)	15 ℃ for one, 12 ℃ for another
Pfafferott (2003)	Hamm/Freiburg/ Weilheim, Germany	3117 (Guetersloh)/ 3303 (Zurich-Kloten)/ 3337 (Munich)	15 ℃ (Figure 5)/ 16 ℃ (Figure 6)/ 16 ℃ (Figure 7)
Cold Climate – Small Diameter – Estimated			
Stål (2002)	Stockholm, Sweden	4289 (Stockholm)	Estimated 5 ℃ for 1-duct PVC, 11 ℃ for 4-duct PVC, 12 ℃ for 4-duct concrete (Figures 3 and 4)

Source	Location	Climate (HDD), Weather Station	Reported Temperature Rise (usually maximum)
Other Climates – Heating Mode			
Baxter (1992)	Knoxville, Tennessee, USA	2008 (Knoxville Mcghee Tyson AP) (ASHRAE, 2009, p. 14.26)	Maximum 22 ℃ (Figures 2b)
Sharan and Jadhav (2003)	Gujarat, India	11 (Ahmadabad) (ASHRAE, 2009, p. 14.36)	Averaged 11.9 ℃ (Table 2)
Sharan and Jadhav (2004)	Kothara, India	11 (Ahmadabad)	13-14 ℃

2.2 Studies of Earth Tube Systems for Heating in Cold Climates

ASHRAE Standard 90.1-2010 defined climates into eight zones (Table B-4, p. 144). Number 7 represents "very cold", with a heating requirement of $4982 < HDD \leq 6982$. 6A and 6B represent cold-humid and cold-dry climates respectively, both with a heating requirement of $3982 < HDD \leq 4982$.

Energy performance of ET systems in cool to cold climates has been evaluated by several researchers, such as for

- Grong, Norway (Tjelflaat, 2000; Jeong, 2002; Wachenfeldt, 2003; Zhang & Haghighat, 2005; Zhang & Haghighat, 2009; Zhang et al., 2009; Zhang, 2009; Tjelflaat et al., 2011), Nesodden, Norway (Schild, 2001; Schild, 2002);
- Woodbridge, Ontario, Canada (OCCDC, 2010; Parsons, 2011);
- Montreal, Canada (Athienitis et al., 2005);
- Sweden (Gustafson, 1993; Stål, 2002), and

- Germany (Pfafferott, 2003).

Most of these researchers, except Gustafson, Ståhl, and Pfafferott, addressed large diameter ET systems. Calgary has a "very cold" climate (ASHRAE 90.1, 2010, p. 142, 144), experiencing about 5086 HDD and 37 CDD (ASHRAE, 2009, p. 14.28), which makes these studies especially relevant.

2.2.1 Studies of Large Diameter Earth Tubes

An addition to the Mediå School in Grong, Norway, has a 15 m long ET system with a 1.5 m wide by 2 m high cross section (Tjelflaat, 2000, p. 10). The addition's floor area was 1000 m^2, and used displacement ventilation coupled with the ET system. This was a hybrid ET system, intended to use fan-assisted wind forces and stack effect to drive the airflow. The duct inlet was buried about 1.5 m from grade to duct ceiling (Zhang, 2009, p. 27), and the duct was buried with a 5% slope from discharge to inlet. The HDD for Oslo-Blindern is about 20% lower than that of Calgary (Table 2.1), and the floor area of the addition is about three times that of the EEEL building main floor theatre. The findings from the studies of the Mediå School addition were particularly informative for the study of the EEEL ET system.

The initial data collection on the indoor environment and energy use at the Mediå School addition was conducted by Tjelflaat (2000). Other researchers (e.g., Jeong 2002, Zhang & Haghighat 2009) used his data for validation of simulations of whole building energy

performance (Jeong) and detailed ET airflow (Zhang & Haghighat). Tjelflaat reported the cooling effect of the ET caused as much as 8 ℃ temperature drop from air intake to discharge, giving an average heat transfer rate of 60 W/m^2. This was enough to satisfy all the cooling requirements of the school. He concluded that adding the large cross-sectional area ET system was beneficial and that the extra cost was acceptable for a long-life building. It was also easy to inspect and maintain the ventilation system due to the large cross section.

The climate data for Grong (Table 2.1) indicate that the heating performance of the ET system is more critical in terms of annual energy use. However, the literature on the Medi åSchool mostly focused on its cooling performance. Jeong (2002) performed multiple simulations on the thermal and ventilation performance of the building in heating mode with ESP-r, and indicated that "the long underground concrete duct could dampen swings in supply air temperature compared to outdoor temperature (p. 54)." His first reported simulation indicated that the duct raised the supply air temperature by as much as 12 ℃ (from -7 ℃ to 5 ℃) (Figure 4.4, p. 55). However, the simulation seemed to result in a supply air (duct discharge) temperature equal to the duct surface temperatures, which were set to a constant 6.1 ℃ duct wall boundary condition (p. 47). The duct wall temperatures used by Jeong did not reflect actual conditions. This will be discussed below in the review of Heiselberg's (2004) article. Moreover, Jeong provided few details to explain his results. In his second reported simulation of both building thermal performance and airflow volume distribution, the ET raised supply air

temperature by as much as 11 ℃ (from -7 ℃ to 4 ℃) (Figure 4.7, p. 60 and Figure 4.9, p. 64). Although the temperature rise from the two simulations was similar, the second simulation produced a supply air temperature profile that fluctuated with the inlet air temperature. Jeong mainly studied whole building simulation without focusing on the air pre-heating performance of the ET.

Wachenfeldt simulated the performance of the addition to the Medi å School, using data collected by Tjelflaat's group for validation. Wachenfeldt's (2003a) thesis summary first stated the difficulty of predicting energy performance of natural (wind- and buoyancy-driven) ventilation systems, because of variations in airflow paths and rates, sensitive to both internal parameters and the outdoor environment. He stated the importance of fans in enhancing convective heat transfer between air and duct walls. He also indicated that during a hot period in June, more than 60% of the cooling effect of the embedded intake duct was due to conduction to the ground, the remainder being due to diurnal energy storage and lag in the duct walls. Wachendfeldt (2003b) concluded that many empirical correlations from previous research produced convective heat transfer coefficients that were only useful for small diameter ET systems. If the correlations were used on large diameter systems, the convective heat transfer would be substantially underestimated.

While Wachenfeldt's thesis provided no information on temperature rise through the ET during the heating season, Zhang and Haghighat (2005, p. 1421), using data collected by Tjelflaat's group for validation of simulation models, reported a temperature rise of about

18 ℃ with an ambient air temperature of -10 ℃. They compared the corresponding heat transfer coefficients with ones Wachenfeldt determined from measurements and stated that they were in close agreement. Zhang and Haghighat (2009, p. 1896) also conducted lab-based experimental testing of a 1 m by 1.5 m lab system, the equivalent of a section of ET, to validate a simulation model. They noted that using large ducts lowered pressure drop, thus avoiding the need for high power fans and reducing energy use. The authors developed several CFD models that produced results with maximum errors of 8% in prediction of discharge air temperature. However, they expressed the need for further research in order to accurately simulate large cross-sectional area hybrid ET ventilation systems.

Another study addressing the heating potential of the Medi åSchool ET system was conducted by Heiselberg (2004, p. 4). He indicated in his paper that the duct air temperature variation from bottom to top of the ET was as much as 7 ℃. Duct surface temperature variations at the inlet side of the ET were also shown in an infrared photo (Figure 4, p. 5). The maximum temperature difference was 3 ℃. This showed the error in Jeong's assumption of constant duct wall surface temperatures of 6.1 ℃. Heiselberg found that cold air was flowing in the bottom half of the duct and warmer air was pushed to the top. As the discharge vents to the classrooms were positioned near the top of the duct, the supply air temperature was much higher than the average temperature in the duct. This resulted in lower heating energy use. However, the author concluded that heat transfer models then available missed this temperature variation and were therefore

unable to predict the heat transfer properly. He did not provide any detailed explanation of experimental procedures or data. This author thinks the temperature variation across the cross section of a large diameter duct can be used more effectively by controlling top and bottom vents dampers to draw supply air in response to space conditioning requirements. In heating season, the bottom vent damper could be fully closed while the top vent damper could be fully opened, and vice versa in cooling seasons. This could improve system performance even further.

Zhang et al. (2009) performed a study on the Medi å School ET using CFD simulations and compared their results with field measurements. The results showed their CFD model to have reasonable accuracy for airflow and heat transfer. The CFD analysis also showed that flows in large cross-sectional ET systems are complex and different from the turbulent flow in small diameter systems. This causes the convective heat transfer coefficient to be complicated and models for calculating the convective heat transfer coefficient from previous small diameter ET studies to be inaccurate and underestimate the heat transfer when used on large diameter ET systems. The authors' findings confirmed those of Zhang and Haghighat (2005) and indicated that more research is required.

Tjelflaat et al. (2011) studied the cooling performance of the ET system in the Medi å School, focusing on the effects of the inlet supply fan. They found the ET system performance to be satisfactory in meeting the peak cooling requirement (p. 291) during

the testing period when the inlet axial supply fan was running at close to full speed. They also compared their heat transfer results with other studies, including Wachenfeldt (2003a), and found the inlet axial supply fan to be effective at improving the heat transfer coefficient. This contradicted Zhang and Haghighat's result (2009, p. 1897) that changes in inlet air turbulence had little effect on convective heat transfer. However, Tjelflaat et al. also indicated that the results showed large uncertainties and the subject required further research. This article shows there might be potential to improve the EEEL ET system further by installing an inlet supply fan. However, the authors also mentioned the effectiveness of an axial inlet supply fan in improving convective heat transfer coefficient might be less effective in long ducts (the length of EEEL ET is 43 m compared to 15 m for the ET system in Medi å School), without specifying the limiting length.

It is worth repeating that much of the reported Medi å School work focused on cooling rather than heating, even though it is a cold climate building (Table 2.1).

Schild (2001, p. 50) provided cursory comments on eleven buildings with ET systems in Norway, from its west coast (3200 HDD) to subarctic regions (6300 HDD). Most (eight) of them were school buildings, including Medi å School. However, dimensions of the ETs were omitted; the only details he provided were some evaluations of Jaer School in Nesodden, Norway, close to Oslo/Fornebu, Norway with 4344 HDD and 51 CDD (ASHRAE, 2009, p. 14.41). According to Zhang (2009, p. 31), the Jaer School ET system had two parts, a 1.6 m diameter and 20 m length duct, and a 2 m width, 3 m

height and 35 m length duct. Duct depths were not reported. Schild (2002) reported that the Jaer School ET was coupled with a heating battery at the end of the duct to preheat supply air. He explained that it was impossible to measure the temperature rise through the duct in winter because of the heating battery's (coil's) effects on measurements (p. 21). It would have been helpful if there had been a sensor to measure winter pre-heating performance near the discharge of the duct, removed from and upstream of the heating coil.

Performance of an installation of nine 1 m diameter, 20 m long and 2 m deep ETs supplying 7,000 L/s was reported for the Earth Rangers Centre in Woodbridge, Ontario (OCCDC, 2010, p. 1; Parsons, 2011, p. 15) - climate data in Table 2.1. Parsons claimed it was the largest ET system in North America. A temperature rise of up to 15 ℃ through the ETs was reported (Earth Rangers Centre, 2012). The building operator of the Earth Rangers Centre reported a temperature rise of 19 ℃ through the ET system with an ambient air temperature of -17 ℃ (Parsons, 2011, p. 15). It was also estimated a temperature rise of 10 ℃ to 15 ℃ could be achieved with ambient air temperature of -10 ℃. However, neither article provided other ET performance information.

Another large diameter ET system was built in Montreal (Athienitis et al., 2005) - climate data in Table 2.1. The system was built with 4700 L/s design ambient airflow through two 1 m diameter, 60 m long ducts. Athienitis et al. (2005, p. 28) constructed a numerical model and simulated the heating performance of the ET system. They

estimated a temperature rise of 9 ℃ (from -15 ℃ to -6 ℃ for a winter day) (p. 29) and indicated the system was often capable of providing one-third or more of the building's heating needs without stating how they reached this conclusion.

So far, only a small number of large diameter ET systems have been adapted in cold European countries and a few cold Canadian cities. However, the heating potential of large diameter ETs is noteworthy based on the studies discussed above. Further research on large diameter cold climates ET systems is warranted due to the scarcity of reported rigorous measurements on heating performance.

2.2.2 Studies of Small Diameter Earth Tubes

Gustafson (1993, p. 598) conducted two experimental studies of ETs - climate data in Table 2.1. In the first study, the author used the weather data from January to April, 1988. He attached one 25 m long 16 cm diameter PVC duct to a single family house, and measured the inlet and discharge air temperatures. His figure (p. 600) showed the maximum difference in temperature between the inlet and discharge air streams was as much as 15 ℃. However, during certain periods, much heat was transferred from the air stream to the surrounding ground, which resulted in very low overall ET performance. The author indicated that this discouraging result implied that a colder winter period should be studied. In the second study, he used the weather data from January to April, 1987. A 15 m long and 15 cm diameter PVC duct was attached to another single family house. Winter 1987 was colder than winter 1988, the minimum ambient air temperature

of 1987 was 10 °C lower than that of 1988 (Figure 3, p. 600 and Figure 5, p. 602). The ET was downstream of a solar heater. Gustafson concluded that the ET was ineffective, because heat was transferred from the air stream to the ground. However, the author failed to acknowledge that the ET increased air temperature by about 12 °C when the solar panel was shut down at night.

Similarly to Gustafson, Ståhl (2002) focused his research on ET heating for a single family dwelling with simulating two ET systems 2 m deep, and 16 m long in Sweden - climate data in Table 2.1. One system had a single duct with 0.04 m^2 cross-sectional area, while the other system had 4 parallel ducts each with 0.01 m^2 cross-sectional area. His figure (p. 916) indicated the 1-duct system increased the supply air temperature by about 5 °C while the 4-duct system increased the supply air temperature by about 11 °C. He then changed the 4-duct system to PVC and found a temperature rise of about 12 °C. The author stated that the heat extracted from the ET system was low, satisfying only about 7% of total energy use (p. 918). However, Ståhl made many simplifying assumptions during his simulation, such as the length of the ET was infinite, the model boundaries were adiabatic, and ambient air temperature was a regular sine curve. As well, this analysis was for a "normal" single family dwelling - the fraction of heat supplied would be greater for a high performance dwelling.

Pfafferott (2003) conducted one-year experimental measurements on three office building ET systems in slightly warmer Germany. Their properties and the author's important findings are summarized below:

Table 2.2 Properties of the Three ET Systems Researched by Pfafferott (2003)

	DB Netz AG	**Fraunhofer ISE**	**Lamparter**
Climate	3117 HDD and 114 CDD (Guetersloh (ASHRAE, 2009, p. 14.35))	3303 HDD and 132 CDD (Zurich-Kloten (ASHRAE, 2009, p. 14.44))	3337 HDD and 157 CDD (Munich (ASHRAE, 2009, p. 14.35))
Number of ducts	26	7	2
Length	67-107 m	95 m	90 m
Diameter	0.2 m and 0.3 m	0.25 m	0.35 m
Depths	2-4 m	2 m	2.3 m
Max heating temp rise	15 ℃	16 ℃	16 ℃

It is notable that, although the three systems had completely different configurations, they all achieved similar temperature rise under maximum heating load. This article is one of the very few ET publications that touched on the topic of ground temperature. However, it was only included as a design input parameter (p. 973) and neglected the impact of ET operation on soil temperature. Pfafferott mentioned briefly in the conclusion that thermal recovery was good enough to maintain performance (p. 982).

The studies of the Medi å School and the Earth Rangers Centre showed that large diameter ETs could increase air temperature by anywhere from 7 ℃ to 19 ℃. This was similar to what small diameter ET systems achieved. However, small diameters raise

pressure drop in ducts, resulting in higher fan energy requirements. Athienitis and Santamouris indicated in their book (2002, p. 191) that "pressure drop needed to be reduced to a reasonable value so as not to require very large fans and waste much of the thermal energy potentially saved in fan energy requirements." There is potential to explore the benefits of using larger diameter ducts.

2.3 Studies of Earth Tube Systems for Heating in Other Climates

Heating performance of ET systems in mild to hot climates has also been studied. Only studies on small diameter ET systems were found.

Baxter conducted two experimental studies on heating (1992, p. 277) and cooling (1994, p. 258) with an ET system in Knoxville, Tennessee - climate data in Table 2.1. One 15 diameter, 64 m long corrugated metal pipe was buried 1.8 m underground from grade to pipe centre, with a 1% slope from inlet to discharge. In heating mode, an average temperature increase of 6 ℃ was achieved during the one month of measurements. Peak heating temperature rise during a very cold day was as much as 22 ℃. Baxter placed sensors in both lateral and longitudinal directions to collect ground temperatures (Figure 2.1). Nine thermocouples were installed in a horizontal plane (one at the centre, one on each side of the duct, and three in the ground on each side of the duct spaced 5 cm apart) at each of six stations along the duct. Near the midpoint of the ET, seven thermocouples were placed in the ground at 0.3 m intervals from depths of 0.3 to 2.1 m. Data were recorded hourly for four weeks in the heating study and three weeks in the cooling study.

He found cooling performance in summer was more consistent than heating performance in winter. This was due to more consistent ambient air temperature patterns in summer, which resulted in more stable heat flow from soil to air. Baxter stated that ET cooling and heating performance might differ for other locations.

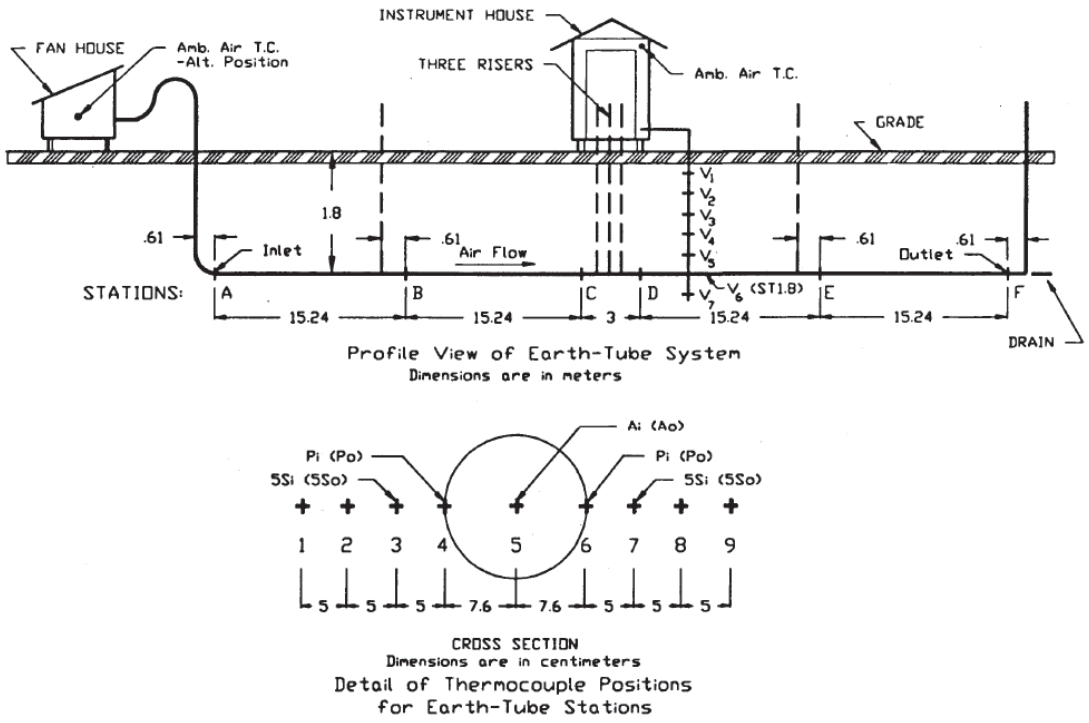

Figure 2.1 Sensor Locations of Baxter's Research (Figure 1, Baxter, 1992, p. 276)

Baxter's choice of lateral soil temperature sensor locations was worth studying for the EEEL ET system research. As seen in Figure 7 (p. 281), the duct wall temperature near the inlet was -5 ℃ and the temperature of soil 5 cm away was 1.7 ℃. This was a large difference of 6.7 ℃ in a short distance. Moreover, the inlet duct wall temperature indicated the soil could be frozen. If so, latent heat exchange would be involved.

Baxter showed a probable freezing soil region that almost reached half the total length of the duct. It would have been good if the duct wall sensors had been installed in the soil instead of in the duct to confirm freezing of the ground and additional sensors in the horizontal plane would have confirmed the soil freeze-thaw pattern. Baxter ignored results from some vertically-arranged sensors during his discussion of soil temperature inversion (Table 1, p. 280). It seemed denser vertical sensor spacing failed to provide any extra information.

Sharan and Jadhav (2003, p. 1) investigated the cooling and heating performance of an ET system in Gujarat, India - climate data in Table 2.1. The system was a single 50 m long, 10 cm diameter duct buried 3 m below ground. Performance data were collected for three consecutive days in each of the twelve months in 2000. As May is the hottest part of summer in the Ahmedabad region and January is the coolest part of winter, only May and January results were presented and discussed in detail. Air temperatures were measured hourly at the inlet of the duct, in the middle (25 m), and at the discharge (50 m). Heating tests were carried out for three nights on January 28th, 29th, 30th, 2000. The authors found a maximum temperature increase of 14.7 ℃ was achieved at 2:00. The average temperature increase was 11.9 ℃.

In later research, Sharan et al. (2004, p. 4) studied the performance of a closed-loop ET system located in a greenhouse in Kothara, India - climate data in Table 2.1. Eight ducts,

spaced 1.5 m apart, were arranged in two tiers; the first tier of four ducts was 3 m deep, and the second tier of four ducts was 1 m above the first tier. Each mild steel duct was 23 m long and 20 cm in diameter. Temperature sensors were placed 1 m above ground at both ends and at the centre of the greenhouse. Two ground temperature sensors were placed at 0.3 m deep and just below the surface. From December 15th to February 15th, the ET system was able to raise the night-time greenhouse temperature from 15 ℃ to 22-23 ℃ after about 30 minutes of operation, while ambient air temperature was 8-9 ℃. The system met the entire heating load easily and at a small cost.

The two studies in India show that ET systems could satisfy peak heating requirements for buildings in mild to hot climates, especially for areas with large differences in between day and night ambient air temperatures.

2.4 Ground Heat Depletion

2.4.1 Studies of Earth Tubes

In predominantly cold climates, average ground temperature around ET systems may decrease after several years of heating operation (heat depletion). As a result, discharge air temperature and the effectiveness of ET systems would decrease.

Accurate ground temperature predictions are essential factors for predicting the sustainability of ET systems. Both the long-term ET-ground heat transfer and the ground temperature should be studied in order to comprehensively evaluate ET systems. However, of the literature reviewed so far, no article covered long-term performance.

Trzaski and Zawada (2011) performed a simulation study of a base case ET system for a single family dwelling in Warsaw, Poland (Warszawa-Okecie, 3771 HDD and 112CDD (ASHRAE, 2009, p. 14.42)). The duct was 0.2 m in diameter, 35 m long and had an inlet depth of 1.5 m and discharge depth of 2 m (p. 1441). They simulated discharge air temperature and temperature of the soil surrounding the discharge relative to ambient air temperature and found the system was able to increase the supply air temperature by as much as 15 ℃ during heating season. The simulation resulted in little change in temperature of the ground surrounding the discharge after one year of operation (p. 1441). Since most heat exchange takes place near the inlet, any notable change in soil conditions would most likely happen around the inlet. It would have been more helpful if the authors researched this topic and for a longer period than one year. The authors' simulation of other environmental parameters such as soil type, ground cover and shading could be very good references for future ET design and application.

2.4.2 Studies of Ground Source Heat Pumps

Another building energy system that takes advantage of the high thermal inertia of the ground is the ground source heat pump (GSHP). This system may also experience ground heat depletion in heating mode. There are two basic types of GSHP systems, horizontal and vertical. The horizontal type is installed much shallower than the vertical one, and is more similar to an ET system. Previous research on soil heat depletion surrounding the horizontal GSHPs could be good references for the effect of ET systems.

2.4.2.1 Studies of Horizontal GSHP Soil Heat Depletion

Several horizontal GSHP systems in Japan, and one in the UK were studied.

Among the studies in Japan, Tarnawski et al.'s (2009) research was for the coldest location. They used data from Sapporo, Japan, with 3673 HDD and 263 CDD (ASHRAE, 2009, p. 14.38). They simulated three horizontal GSHP systems for a typical house for a ten-year period. The two single-layer GSHPs both used 16 cm diameter, 300 m length ducts. One was installed at 0.5 m depth, the other at 1 m depth. The double-layer GSHP had an 8 cm diameter, 300 m length duct, and was buried at 0.5 m and 1 m depths. Ground temperatures at 0.5 m and 1 m depths on June 14th (the end of heating season), and September 30th (the end of cooling season) of ten years after start up were compared with undisturbed ground temperatures (p. 133). Details are shown in Table 2.3.

Table 2.3 Soil Temperatures after Ten Years of Simulation by Tarnawski et al. (2009)

Soil Location	Soil Temperature on June 14th (℃)	Soil Temperature on September 30th (℃)
Undisturbed soil	11.6	14.6
Single-Layer GSHP at 0.5 m depth	9.1	13.5
Single-Layer GSHP at 1 m depth	7.0	11.9
Double-Layer GSHP at 0.5 m and 1 m depths	5.2	11.6

Compared with the undisturbed soil temperature, after the heating season, GSHP vicinity soil temperatures for single-layer GSHP at 0.5 m and 1 m depth, and double-layer GSHP at 0.5 m and 1 m depths decreased by 2.5 ℃, 4.6 ℃ and 6.4 ℃ respectively. After the

cooling season, temperatures of soil surrounding the pipes were close to the undisturbed soil temperature of 14.6 ℃, differences being 1.1 ℃, 2.7 ℃ and 3.0 ℃ respectively. The single-layer GSHP at 0.5 m depth had the best soil heat replenishment. Its soil temperature was barely lower than the undisturbed soil temperature. This supported the use of horizontal GSHP systems as long-term heating system for buildings in these conditions.

Fujii et al. (2012) conducted a study on a developed land area on a hillside in Fukuoka, Japan (1473 HDD and 1021 CDD (ASHRAE, 2009, p. 14.37)). The 500 m long, 2.4 cm inner diameter pipe had an 80 cm diameter for each loop. It was buried in a U-shape trench 72 m long and 1.5 m deep, in a 35 m long by 4 m wide area (p. 56-57). Two thermistors were installed at 1 m depth at the midpoint of each of the supply and return loops, to measure soil temperature. Heat distribution of ground temperature at 1 m and 1.5 m depths (p. 61) was simulated, based on their calculation of 38 days of operation of the system. They indicated that, because of heat extraction, at the depth of 1.5 m, ground temperatures at the pipe inlet were lower than that of undisturbed soil by over 5 ℃, and at the depth of 1 m the temperature difference was about 4 ℃. Horizontally, a 2 ℃ temperature difference comparing with undisturbed soil was observed at about 1 m away from the coil. They concluded that heat from the soil was mainly extracted from above and below the coils. The authors were comparing soil temperature directly above the coil at 1 m depth with undisturbed soil temperature at 1.5 m depth instead of undisturbed soil temperature at the same depth of 1 m. Also, at 1 m depth, soil temperature is more

affected by ambient conditions than at the depth of 1.5 m. Fujii et al., in their numerical simulation, treated the horizontal slinky as a thin plate element, almost two-dimensional (p. 58). This caused the faces of the plate to have much larger heat exchange areas compared to the small vertical area. This may have caused the large heat loss above and below the coils. This simulation technique is also different from that used in ET studies. ET diameters are large enough that three-dimensional analysis is required. This author believes Fujii et al.'s conclusion requires further investigation. No research on potential heat replenishment was conducted.

Wu et al. (2011, p. 2) studied the effects of a horizontal GSHP system on ground temperature in a paddock area in Oxfordshire, UK (close to London Heathrow Airport, 2661 HDD and 94 CDD (ASHRAE, 2009, p. 14.46)). They used both experimental and simulation methods. The system included four parallel slinky heat exchanger loops buried 1.2 m underground in an 80 m long by 20 m wide paddock area. To monitor the soil temperature, they dug one hole above a portion of the system and a reference hole, 2 m from the first hole. Eighteen thermistors were installed in the holes at various depths. Monitoring began on November 6th, 2009, one month after the system started operating. Sensors were read every 10 s and values were averaged over 30 min intervals. Using November 7th, 2009 as an example, they measured and analyzed the ambient air temperature and the soil temperature. Wu et al. compared the temperatures at a range of corresponding depths and at various times during the day and found noticeable differences between heat exchanger and the reference string conditions after only one

month of system operation. The heat exchanger lowered the surrounding soil temperature by over 3 ℃ and the impact could be observed as far as 0.9 m vertically away from the heat exchanger. In the simulation, the system was set as 4 cm diameter, 80 m long and 1.8 m deep. Wu at al. predicted the soil temperature change at various depths after 1, 10, 100 and 600 h from both horizontal and vertical directions. Results showed that long-term performance of the system would be difficult to maintain, although the system had a large short-term heating potential (p. 6). Gonzalez et al. (2012) (same group of researchers) reported results for the same GSHP system for almost a year which further supported their conclusions in Wu et al. The soil temperature difference between the heat exchanger and reference location was 3 ℃ lower than when measurement began (p. 148). However, the authors neglected to investigate the potential for heat replenishment. They mentioned Tarnawski's system was working in both heating and cooling mode, which helped to compensate for some heat loss. Their system operated in heating mode only (p. 148), being in a region with only 94 CDD (ASHRAE, 2009, p. 14.46). Also, shutting down the system during the summer instead of heating domestic hot water and swimming pool would also reduce heat extraction, especially when the difference between soil temperature at heat exchanger and reference location was almost zero by July (p.148). Further research is required to confirm potential for heat replenishment.

The four articles reviewed for horizontal GSHP soil heat depletion had different findings. Tarnawski et al.'s experiment was for the coldest location, was conducted over a long

period and the simulated systems were sustainable. Only Wu et al. found it was hard to maintain long-term operation of the system. This topic still requires further investigation.

2.4.2.2 Studies of Vertical GSHP Soil Heat Depletion

Eugster and Rybach (2000, p. 826) combined experimental and theoretical approaches to measure and predict the long term effects of a single-pipe, 105 m long borehole GSHP on surrounding ground temperatures. The system served a single family house near Zurich, Switzerland and largely operated in heating mode. Zurich-Kloten experiences 3303 HDD and 132 CDD (ASHRAE, 2009, p. 14.44). Eugster and Rybach buried temperature sensors at depths of 1 m, 2 m, 5 m, 10 m, 20 m, 35 m, 50 m, 65 m, 85 m, and 105 m to measure the ground temperatures. The atmospheric temperature variations and all parameters relevant to the operation of the entire system (hydraulic system flow rates, circuit temperatures, power consumption of the GSHP, etc.) were also recorded at 30-minute intervals for five years. It was obvious that the ground around the GSHP cooled in the first few years of operation. However, the rate of temperature drop decreased from year to year until a new ground thermal equilibrium was established at 1-2 ℃ lower than the original temperature. After ten years of operation, the measurement system was restarted. The new temperature profiles showed little further shift towards lower temperatures, thus demonstrating that a quasi-steady equilibrium had been reached after the first few years. Their simulation results of September, 1996 were compared with the measured data. The agreement was excellent, within ±0.1 ℃. Then they modeled the ground temperature changes for over 30 years of GSHP operation and 30 years of

recovery. They found that, after shut-down of GSHP operation, thermal recovery began, initially rapid and later decreasing gradually. They also found that the time to reach a complete recovery depended on how long the GSHP had operated. Principally, the recovery period equalled the operation period. However, the authors only performed one experiment on one system, precluding general conclusions. In summary, the measurements and simulations supported that sustainable heat extraction could be achieved with such systems.

Trillat-Berdal et al. (2005, p. 1246) conducted a numerical study on a borehole GSHP for a single family dwelling in the Savoie region of France, close to Lyon-Satolas (2588 HDD and 309 CDD) (ASHRAE, 2009, p. 14.35). They noted that Eugster and Rybach's (2000) finding that ground temperature stabilized after an initial decline was based on a single system with an effectively infinite amount of surrounding earth. Apparently based on this (and disregarding the limitation of Eugster and Rybach that they had identified), Trillat-Berdal et al. stated in the introduction to their paper that "the natural thermal recovery of the ground is not sufficient to maintain stable performances (p. 1246)". They reported that decrease of performance after 20 years was 4%, and concluded "the ground heat depletion is not too important". The main purpose of their paper was to evaluate approaches, such as solar heating, to reducing ground temperature decline.

Using TRNSYS, Niu et al. (2011, p. 1806) simulated the ground temperature changes and system COP for a borehole GSHP system serving a 25,000 m^2 office building at three

locations in China, the coldest of which was Qiqihar(5426 HDD and 370 CDD) (ASHRAE, 2009, p. 14.33). Results showed that, after 5 years of operation, the average temperature of the ground in the vicinity of the GSHP decreased by 2.4 ℃ in Qiqihar. The annual average change in ground temperature diminished in Beijing and Qiqihar year by year. As was found by Eugster and Rybach (2000), the rate of ground cooling declined annually.

Of the GSHP borehole papers reviewed above, Trillat-Berdal et al., and Niu et al. both investigated ground heat depletion and found an acceptable (small) performance decrease after long term operation. Eugster and Rybach investigated heat depletion as well as recovery, and seemed to indicate that natural heat replenishment was sufficient to maintain ground heat even though it involved periods of non-operation of the GSHP systems. Ground heat depletion and replenishment for ET systems still requires further research.

2.5 Conclusions

The articles reviewed helped this author obtain a clear understanding of the history and current state of research on large diameter ET systems for heating, and the issue of potential duct vicinity soil temperature depletion.

- Large diameter ET systems have great potential in reducing both annual heating energy use and peak cooling loads for cold climates and night heating loads for mild to hot climates. They could make large contributions in reducing building energy use;

- Simulation can be a great help in analyzing ET systems performance and predicting duct surrounding ground temperature change. However, future research to find a more accurate model for determining the convective heat transfer coefficient for large-diameter systems is required;
- A lot of experimental studies have been done to validate numerical models and analyze ET systems performance;
- There is a lack of research on the heating performance of ET systems, especially for large diameter tubes in cold climates.

The lack of research on large-diameter, large-scale ET systems and effects on surrounding ground especially in a very cold climate is evident. This literature review confirms the need for research on this topic and this author will be applying some of the best research techniques learned from these articles to her own research. Some of the techniques include:

- Frequent data collection for long durations for a large sample data size;
- Strategically placed sensors to map out entire temperature field in the duct vicinity ground.

CHAPTER THREE: METHODS

3.1 Case Study Building

The University of Calgary Energy, Environment and Experiential Learning (EEEL) Building (Figure 3.1) is located at the northern edge of the campus. It is a five-story building of about 24,500 m^2, including laboratories, classrooms and spaces for interdisciplinary collaboration (UofC, 2010). The building is expected to receive LEED Platinum certification (Hetu, 2011). The experimental setup included the building's ET system and an array of sensors to monitor ground temperatures.

Figure 3.1 North Façade of the EEEL Building (the Earth Tube Intakes are Highlighted)

Calgary is located in southern Alberta, Canada, at latitude 51 °north and longitude 114 ° west. Its climate is classified as "very cold" by ASHRAE Standard 90.1-2010 (p. 142, 144). The mean annual temperature is 4 ℃. January is the coldest month in Calgary; the mean daily maximum temperature is -2.8 ℃, and the mean daily minimum temperature is -15.1 ℃ (World Meteorological Organization, 2012). July is the hottest month; the mean daily maximum temperature is 22.9 ℃, and the mean daily minimum temperature is 9.4 ℃.

3.2 The Earth Tube System

3.2.1 System Design

The ET system is on the north side of the EEEL building with the ducts running east to west (Figure 3.2). The system consists of two 1219 mm inner diameter (1473 mm outer diameter), 43 m long concrete ducts (Figure 3.2) placed 1554 mm apart. The inlet side of the horizontal portion of the ducts is buried 4.9 m deep from nominal grade to duct centre (Figure 3.3), and that depth on the discharge side is 4.5 m. The ducts slope 0.5 °west to east under a peak height of 1.6 m to 2.3 m layer of dirt above nominal grade, with a ground cover of grass (Figure 3.4).

Three 6 m high and 2 m inner diameter (2.5 m outer diameter) air intakes (Figures 3.1, 3.2, and 3.5) connect the atmosphere to an air shaft (Room 043v, Figures 3.2, 3.3 and 3.6) in the building basement, which connects to the ET duct inlets. The discharges of the ET ducts connect directly to an air plenum (Room 057v, Figures 3.2, 3.3 and 3.7), which has

an airtight door. The air was intended to flow through a 1.2 m by 1.1 m air intake louver (Figure 3.7) to air handling unit 4 (AHU-4) inside Mechanical Room 4, also in the basement of the building. The ET system in relation to the AHUs is shown in Figure 3.8. The original drawings provided by EllisDon are shown in Appendix A.

To install the ducts, the immediate area around the ETs was excavated along with the foundation volume and the ET was backfilled with native soil, which is clay based, alkaline and low in nutrients.

As noted in the introduction, the initial ET system design was large enough to condition all outdoor air for the building. Due to budget limitations, this was downsized to serve only the main floor theatre (floor area of 320 m^2).

AHU-4 (Engineered Air model LM6/C/HRP) serves the main floor theatre (Room 181z) with 180 seats. Two 3.73 kW TECO TEFC motor driven fans draw the ambient air through the ducts. The air flow rate varies from a normal flow of 4720 L/s to a minimum of 1652 L/s when operating (Appendix B).

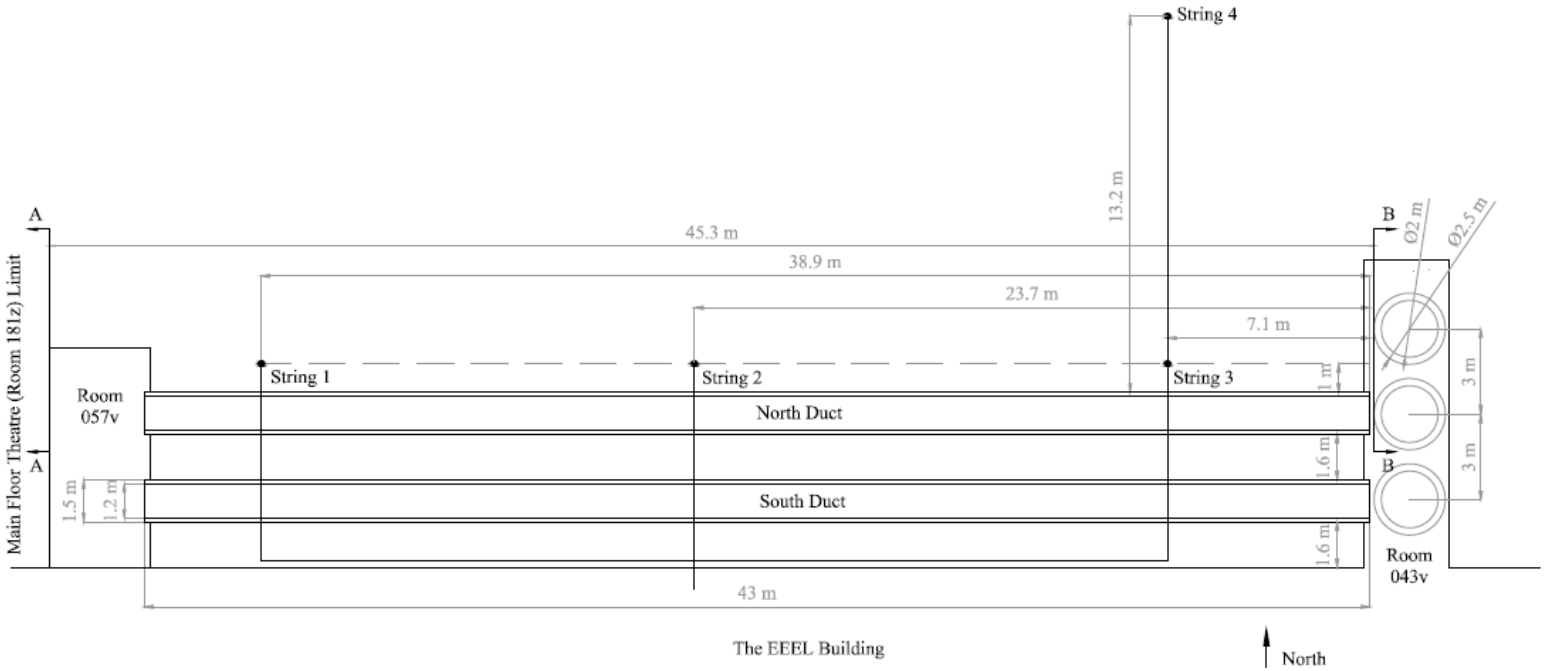

Figure 3.2 Plan of the ET System

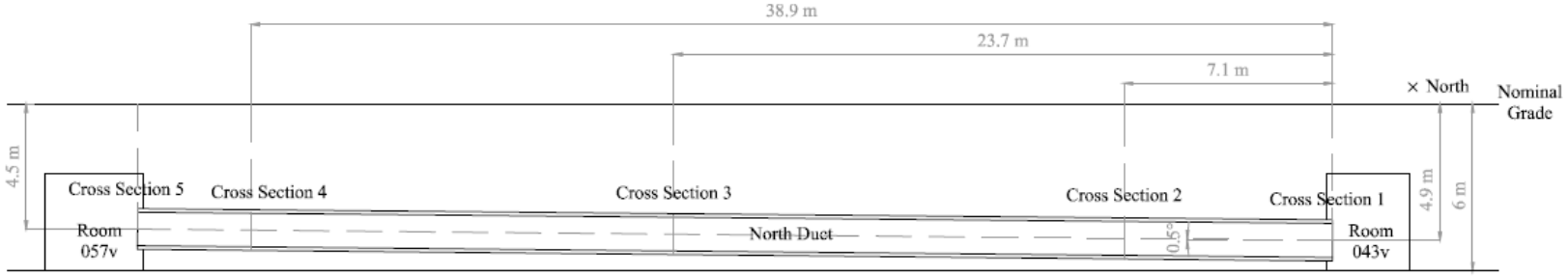

Figure 3.3 West-East Section of the ET System

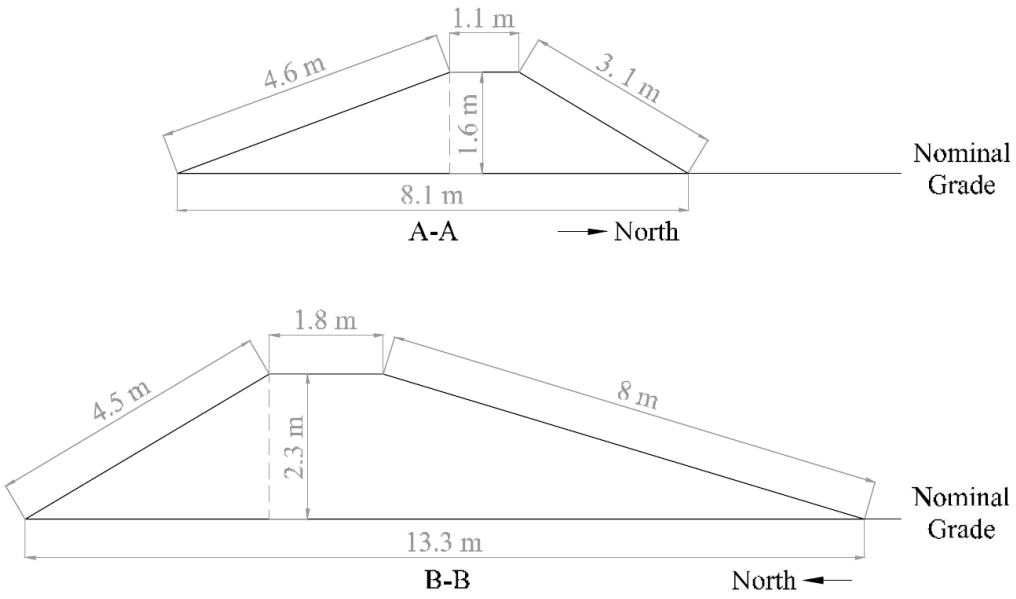

Figure 3.4 Cross-sections A and B of the Layer of Dirt above Nominal Grade

Figure 3.5 Air Intakes

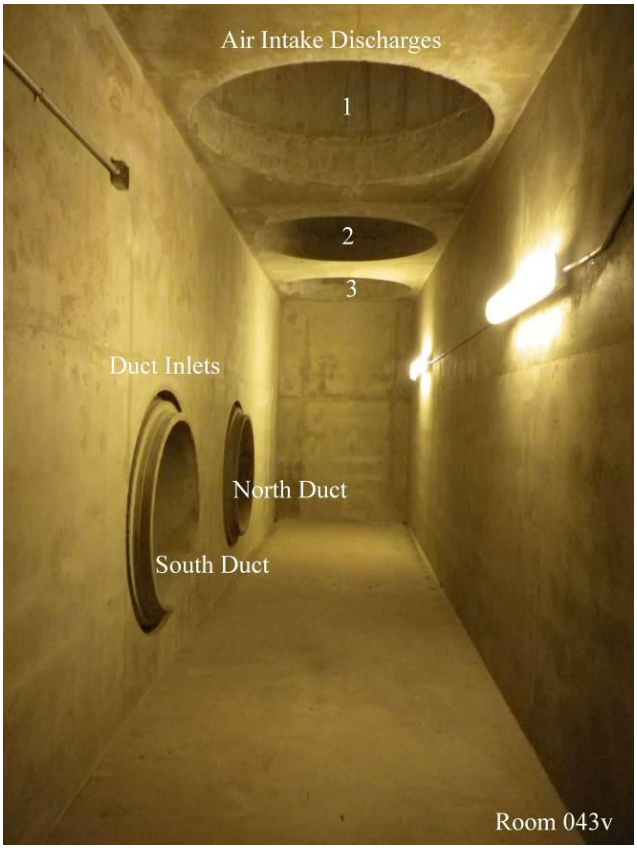

Figure 3.6 Air Intake Discharges and Duct Inlets in Room 043v

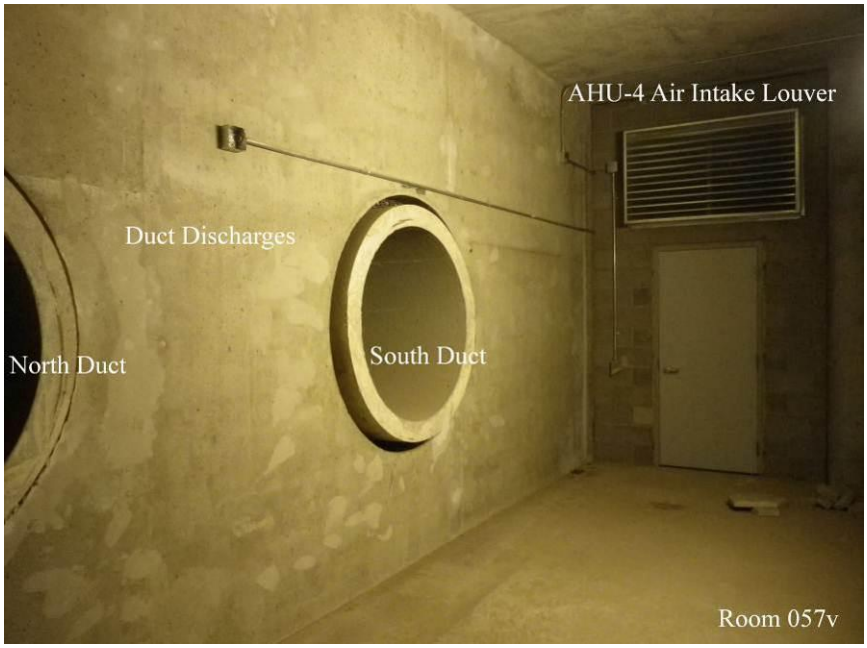

Figure 3.7 Duct Discharges and AHU-4 Air Intake Louver in Room 057v

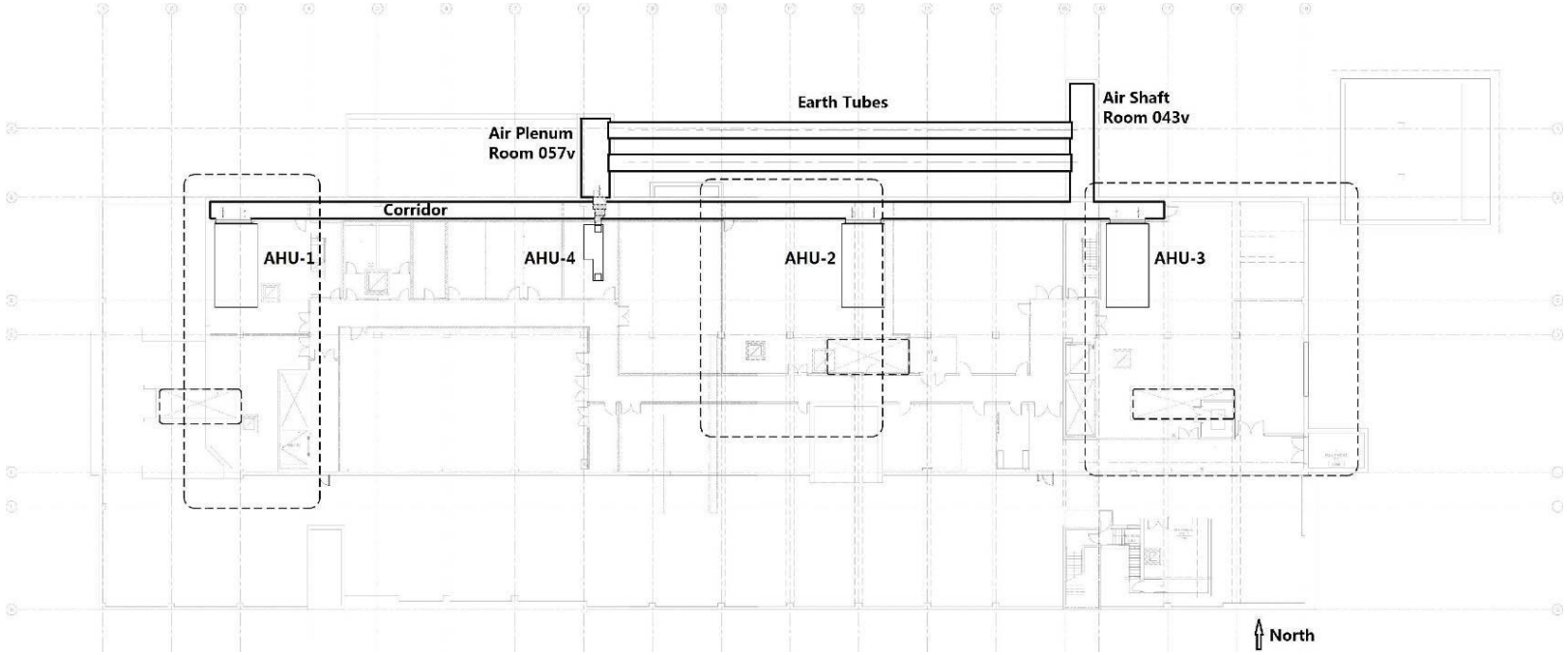

Figure 3.8 The Relationship between the ET system and the AHUs (combination of EllisDon Drawings M2.40 and M2.41, simplified)

3.2.2 System Operation

The building air distribution system started operation with two LEED flushes. LEED flush (also known as "flush out" for obtaining LEED certification) aims to remove indoor air pollutants from a newly constructed or renovated building before occupancy, by forcing a large amount of tempered outdoor air through the building ventilation system (EPA, 2012). The EEEL LEED flushes lasted from September 8th to September 28th, 2011. After the LEED flushes, air handler operation was controlled by space temperature and return air CO_2 concentrations. Supply and return fans of AHU-4 and the other four air handling unit were equipped with variable frequency drives (VFD) so airflow could vary with temperature and CO_2 concentrations.

AHU-4 is scheduled on from 6:00 to 22:00, Monday to Friday and 7:00 to 17:00 on Saturday. The fan speeds are controlled by several variables, such as ambient air temperature, and occupancy loads via sensing of CO_2 concentration. During the first year of occupancy (approximately September 2011 to August 2012), the AHUs were operated by the contractor and controls subcontractor, who did not collect fan speed and fan energy use data.

The other AHUs are scheduled to run 24/7. AHU-1 serves the west side of the building (all floors), AHU-2 and 2A serve the core (all floors), and AHU-3 serves the east side (all floors). The AHUs all provide variable airflow (VAV).

3.3 Installation of Ground Temperature Sensors

In order to determine whether there was a net drawdown of heat in soil surrounding the ducts, sensors were designed to be placed up to 10 m deep in the soil surrounding the ducts. However, underground water was encountered at about 7 m during drilling of the boreholes. This caused the walls of the bore holes to collapse before the strings could be placed below about 8 m depth, based on observation of the sensor positions in the strings relative to grade.

Twenty 109BAM temperature probes (Campbell Scientific, 2010) with 61 m cables were grouped into four strings (Figures 3.2, 3.9 and Table 3.1). All sensors were calibrated before installation. Information regarding sensor calibration and accuracy is provided in Appendices C and D. The sensor leads were bundled together to achieve the offsets shown in Figure 3.9. Boreholes were 1 m north of the north duct to avoid damage during the drilling. Boreholes were created by a truck-mounted auger and manually backfilled with the soil removed during the drilling. A 0.1 m diameter protective PVC sleeve was used to route the strings to the foundation wall of the building. The strings were connected to an AM16/32B multiplexer (Campbell Scientific, 2009), operated by a CR1000 datalogger (Campbell Scientific, 2011). The logger, multiplexer and sensor lead connections were installed inside a wall-mounted cabinet in Mechanical Room 2 in the basement of the building. The extra lengths of sensor leads were coiled in a second cabinet above the logger cabinet.

All depths in Table 3.1 have a consistent datum as nominal grade as shown in Figures 3.3, 3.4 and 3.8. These values will remain constant regardless of the change in surface landscape.

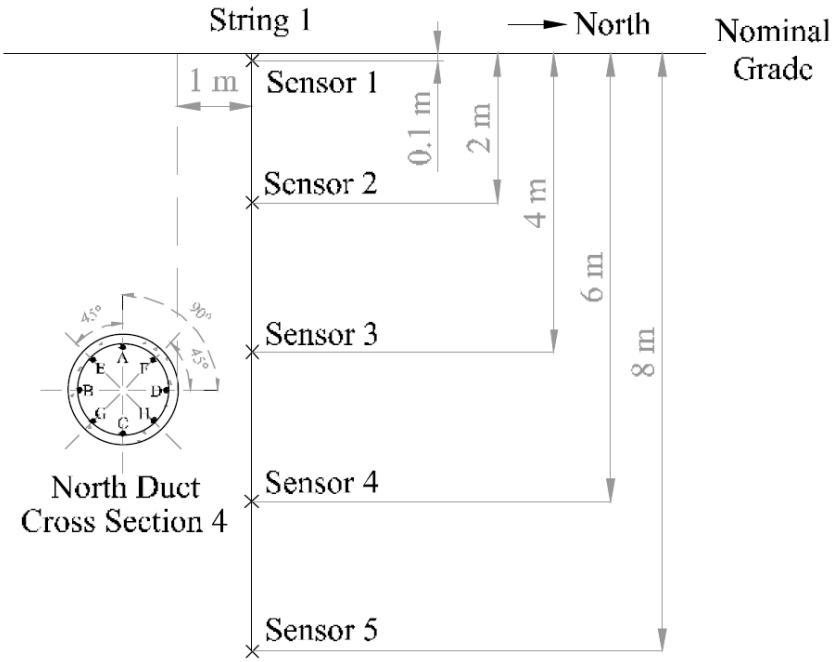

Figure 3.9 South-North Section

Table 3.1 Ground Temperature Sensor Locations

Depth	Sensor			
	String 1 (ST1)	**ST 2**	**ST 3**	**ST 4**
0.1 m	Sensor 1 (S1)	S6	S11	S16
2 m	S2	S7	S12	S17
4 m	S3	S8	S13	S18
6 m	S4	S9	S14	S19
8 m	S5	S10	S15	S20

CHAPTER FOUR: PRELIMINARY FINDINGS

Several problems occurred during the research. These included uncertainty regarding the string locations, reverse airflow discovered inside the south duct, and the landscape changes above nominal grade. Although the problems still exist, the processes and approaches to addressing the problems enlightened this author regarding avoiding them in future research.

4.1 Uncertainty Regarding String Locations

During data collection and analysis, this author found that temperature of ST3 sensors (near intake) were almost always lower in summer and higher in winter than those of corresponding ST1 (near discharge) and ST2 (midpoint) sensors.

4.1.1 Reverse of Expectations

This was the opposite of the expected temperature pattern. The amount of heat exchange should decrease as outdoor air flows through the duct. In winter, ambient air temperature is usually lower than that of the ground. When ambient air flows into the north duct, the heat exchange between the duct wall and ground surrounding the duct happens first at the point corresponding to ST3. Travelling between ST3 and ST2, the air should be heated by the ground when colder than the ground. When the air reaches ST2, the temperature difference between the air and the surrounding ground should be smaller than at ST3, and the amount of heat exchange at this cross section should be smaller. Therefore, in winter, the ground at ST3 should experience more heat depletion and temperature should

be lower than at ST2 and ST1. Heat transfer should also diminish with distance along the ET in summer; however, the air temperature will generally be above the ground temperature and heat should be transferred to the ground.

4.1.2 Measurements of Duct Wall Temperature and Duct Air Velocity

The expected pattern of lower temperature with distance along the ET was also inconsistent with the duct wall temperatures measured by this author as explained below in this section. As this author was not involved in the initial design of the ground temperature sensor system, she was only able to observe the drilling and installation of the last string (ST1). It was possible that ST1 and ST3 were installed in the wrong locations, ST1 at inlet and ST3 at discharge. If this were true, the data would be more consistent with expectations as explained above.

This author went to the ET ducts on the mornings of November 8th, November 9th, December 6th, 2011, January 17th, and July 9th, 2012. An Omega OS950 series infrared thermometer (model OS953 based on its "target temperature range") (OMEGA, 2012, p. 14) was used to measure the duct wall temperatures. Details can be seen in Tables 4.2-4.7 below.

Five positions were chosen along each duct (Figure 3.3). Cross section 2 (CS2), CS3 and CS4 coincided with the string positions. CS1 was at the duct inlets, and CS5 was at the

duct discharges. The duct surface temperature was measured at eight points at each position (Figure 3.9).

Table 4.1 shows the results for Nov. 8th at 11:00. The hourly average ambient air temperature was 3.4 ℃. It is obvious that wall temperatures increased from inlet to discharge along the north duct, as expected. These data were reversed from the ground temperature pattern. It is possible that the contractors installed ST1 and ST3 in reverse order from the provided design. However, the wall temperature of the south duct decreased from the inlet to the discharge, opposite to the north duct trend. At the intended ET discharges (Room 057v), this author faced the openings of each of the ducts. The non-movement of this author's hair showed there was no air exiting the south duct, while air was obviously exiting the north duct as shown by this author's hair being blown away from the duct opening.

Table 4.1 Duct Wall Temperatures on November 8th, 2011

Distance to Inlet (m)	Corresponding String	Corresponding Cross Section	Measured Spots	Temperature of the North Duct Wall (℃)	Temperature of the South Duct Wall (℃)
7.1	ST3	CS2	A	2.8	5.5
			B	2.4	5.8
			C	2.8	5.0
			D	2.4	5.4
			E	2.5	5.8
			F	2.5	5.5
23.7	ST2	CS3	A	3.5	4.9
			B	3.0	4.7
			C	3.2	4.7
			D	3.3	4.5
			E	3.4	5.0
			F	3.2	4.7
38.9	ST1	CS4	A	3.9	4.2
			B	3.6	4.0
			C	3.6	4.2
			D	3.8	4.3
			E	3.7	4.1
			F	3.5	4.0

Table 4.2 shows the duct wall temperatures measured on Nov. 9th at 9:00. The hourly average ambient air temperature was -7 ℃. This author wanted to see how much the duct wall temperatures were affected by cold air after a cold night (ambient air temperature was below zero during the entire night). The fan was operating at 50% speed during the measurements.

Table 4.2 Duct Wall Temperatures on November 9th, 2011

Distance to Inlet (m)	Corresponding String	Corresponding Cross Section	Measured Spots	Temperature of the North Duct Wall (℃)	Temperature of the South Duct Wall (℃)
7.1	ST3	CS2	A	0.6	4.9
			B	0.5	4.9
			C	0.1	4.1
			D	0.1	4.3
			E	0.3	5.2
			F	0.2	4.8
			G	0.0	4.9
			H	0.1	4.5
23.7	ST2	CS3	A	3.0	4.5
			B	2.4	4.8
			C	1.6	4.0
			D	2.4	4.2
			E	2.4	4.8
			F	2.7	4.6
			G	1.9	4.6
			H	1.9	3.8
38.9	ST1	CS4	A	3.6	3.2
			B	2.8	3.1
			C	1.9	2.7
			D	2.4	3.3
			E	2.9	3.2
			F	2.7	3.1
			G	1.9	3.3
			H	1.9	2.9

The duct wall temperature trends were the same as those of Nov. 8th. It was also found by the direction of this author's hair was blown that air exited the north duct from nominal inlet to nominal discharge, but from nominal discharge to nominal inlet for the south duct. Air speed was measured by this author hand-holding an air speed sensor (model TSI 8475-12, serial number 60070034) near the centre of both ducts at the five

measurement positions described above, while an assistant carried the battery and read the air speed values. Details can be seen in Table 4.3. It should be noted that this air velocity was a rough measurement. It did not follow the "Round Duct Traverse Method" described in ASHRAE Standard 111-2008 (p. 70). Moreover, during the measurements, there were two people inside the ducts. Although both people stayed downstream of the instrument, it could still have affected the airflow values. However, as the aim for this measurement was to show the general airflow condition inside ducts, those effects could be ignored.

Table 4.3 Duct Air Velocity Measured on November 9th, 2011 (from Nominal Duct Inlet to Nominal Discharge) - Negative Values Indicate Reverse Flow.

Measurement Positions	**Air Velocity in the North Duct (m/s)**	**Air Velocity in the South Duct (m/s)**
CS1 Centre	>2.5 (exceeded the equipment's measurement range)	-0.9
CS2 Centre	2.0	-1.1
CS3 Centre	2.2	-1.3
CS4 Centre	2.3	-1.0
CS5 Centre	1.6	-1.3

Another measurement was conducted on December 6th, 2011 at 10:00, when the hourly average ambient air temperature was 7.2 ℃. Details are shown in Table 4.4.

Table 4.4 Duct Wall Temperatures on December 6th, 2011

Distance to Inlet (m)	Corresponding String	Corresponding Cross Section	Measured Spots	Temperature of the North Duct Wall (℃)	Temperature of the South Duct Wall (℃)
0	Duct Inlet	CS1	A	0.6	4.9
			B	0.5	4.9
			C	0.1	4.1
			D	0.1	4.3
43	Duct Discharge	CS5	A	3.0	4.5
			B	2.4	4.8
			C	1.6	4.0
			D	2.4	4.2

A final measurement for winter was planned for January 17th, 2012 at 9:00; however, the hourly average ambient air temperature was -30.2 ℃, beyond the working temperature range of the infrared thermometer, no data were collected.

Duct wall temperatures and duct air velocities during summer were measured on July 9th, 2012 at 10:00. The average hourly ambient air temperature was 27.4 ℃ at that time. In the north duct, duct wall temperatures at CS2 (corresponding to ST3) were higher than those at CS3 (ST2) and CS4 (ST1). This was still contrary to the collected soil temperature data.

Airflow direction was checked by suspending a piece of thread in the duct. The duct air still flew backwards in the south duct, from nominal duct discharge to nominal inlet. In the north duct, the flow was from nominal inlet to nominal discharge. Details are shown in Tables 4.5 and 4.6.

Table 4.5 Duct Wall Temperatures on July 9th, 2012

Distance to Inlet (m)	Corresponding String	Corresponding Cross Section	Measured Spots	Temperature in the North Duct Wall (℃)	Temperature in the South Duct Wall (℃)
0	-	CS1	A	19.4	17.9
			B	19.7	17.3
			C	19.7	18.0
			D	19.2	17.9
			E	19.7	17.4
			F	19.2	17.8
			G	19.7	17.3
			H	19.4	17.9
7.1	ST3	CS2	A	16.3	13.4
			B	16.6	13.3
			C	16.9	13.5
			D	16.6	13.8
			E	16.5	13.3
			F	16.5	13.9
			G	16.9	13.2
			H	16.8	13.7
23.7	ST2	CS3	A	15.2	13.8
			B	15.7	13.9
			C	15.5	13.8
			D	15.3	13.9
			E	15.3	13.7
			F	15.2	13.9
			G	15.7	13.7
			H	15.5	13.9
38.9	ST1	CS4	A	15.3	15.1
			B	15.3	15.4
			C	15.1	15.2
			D	14.7	15.2
			E	15.2	15.2
			F	14.8	15.2
			G	15.1	15.2
			H	14.9	15.4
43	-	CS5	A	17.0	17.0
			B	16.7	17.2
			C	16.5	17.1
			D	16.6	17.1

Distance to Inlet (m)	Corresponding String	Corresponding Cross Section	Measured Spots	Temperature in the North Duct Wall (℃)	Temperature in the South Duct Wall (℃)
43	-	CS5	E	16.8	17.2
			F	16.7	17.0
			G	16.6	17.1
			H	16.8	17.0

Table 4.6 Duct Air Velocity Measured on July 9th, 2012 (from Nominal Duct Inlet to Nominal Discharge) - Negative Values Indicate Reverse Flow

Measured Spots	Air Velocity inside the North Duct (m/s)	Air Velocity inside the South Duct (m/s)
CS1 Centre	>2.5	-0.7
CS2 Centre	2.1	-0.7
CS3 Centre	1.8	-0.7
CS4 Centre	1.8	-0.7
CS5 Centre	1.4	-1.2

4.1.3 Measurements of String Lengths

As a second check of string placement, this author scaled and measured the design drawings (Appendix E). As all four string cables were 61 m long, the rest of ST3 cables should be almost the same length as those of ST1. However, the measurements showed that the lengths of the ST3 cables in the cable cabinet were about 4.5 m longer than those of ST1, suggesting that ST3 was closer to the EEEL building. There is no simple way to determine the whether the strings are in the specified locations. One reason for the unexpected differences in length might be that some portions of the ST1 cables were routed more circuitously to the cable cabinet.

4.1.4 Signal Tests

One more technique was applied to check for string placement. A plasma ball can generate a signal, which could be picked up by sensor wires, and monitored from an oscilloscope or datalogger. This author went to perform tests on site on June 25th and 28th, 2012 with the help of an assistant. One person was to use a plasma ball to try to trace the sensor wires from ground surface, and the other person was to stay at Mechanical Room 2 to monitor the devices. Two way radios were used for communication during the tests, as there was no cell phone signal in Mechanical Room 2 in the basement. It was hoped that the sensors would pick up the plasma ball signal.

The tests on June 25th, 2012 were conducted from 9:10 to 10:35. S1 (on string ST1) and S11 (on string ST3) were both disconnected from the datalogger mounted on the wall, with one re-connected to the oscilloscope, the other to another CR1000 datalogger. Ground temperature data of this period were necessarily missing from the raw data. The person at the ground surface tried to scan the areas where ST1 and ST3 were buried. The plasma ball was placed 2 cm, 1 m and 2 m north of the junction box, 1 m and 2 m east and 1 m north of the box, 1 m and 2 m west and 1 m north of the box. Signals appeared and disappeared at all the locations. The results were not reliable. Later that day, it was discovered that a person touching the ball with one hand and the wire with the other hand, greatly increased the signal strength.

The second test was conducted on June 28th, 2012 from 8:05 to 9:00 following the same procedure as the first test, but with the improvement of sticking several metal rods about 23 cm into the ground, first 1.8 m and then 0.5 m north of the junction box mounted on the exterior wall of EEEL. S1 and S2 (on string ST1) and S11 (on string ST3) were all disconnected from the datalogger mounted on the wall during the test. S1 and S2 were connected to another datalogger and S11 was connected to the oscilloscope. Videos were taken from both tests on the ground and the signal graph shown on the oscilloscope from Mechanical Room 2 for comparison. The plasma ball was placed 2 cm, 1 m and 2 m north of the junction box, 1 m east and 1 m north of the box, 1 m west and 1 m north of the box. Unfortunately, all signals received by the sensor wires were weaker than during the first test. This method of using a plasma ball to locate sensor strings failed.

4.2 Design and Operation Problems of the EEEL ET System

The two parallel ET ducts were intended to serve AHU-4. However, site inspections by this author revealed a circular path for outdoor air on every occasion the ET system was visited: west through the north duct and east through the south tube. Detailed calculations on the duct airflow Reynolds (Re) number under the various operating conditions are provided in Appendix F.

As noted in Tables 4.3 and 4.6, the airflow direction in the south duct was from duct nominal discharge to nominal inlet, and this was first noticed in late October, 2011, when this author was attaching sensors to the duct walls. It was later confirmed with

measurement by observation of a suspended thread and by measurements with air speed sensors. This is because all four AHUs draw air from the three air intake towers, and make the pressure in the Room 043v (connected to the air intakes) much higher than that of the air plenum Room 057v and the plenum connected to AHU-1, AHU-2 and AHU-3 (Figure 3.2, Appendix A). The pressure difference made the north duct, Room 057v and the south duct a U-shaped duct, with the north duct inlet pressure higher than the south duct inlet. As a result, fresh air moves through the U-shaped duct. With air flowing two ways in the ETs, there would be a cancellation effect, with warmed air in the south duct losing heat to the ground and offsetting the heating of westward flowing air in the north duct in heating season. This is not the way a system should be designed and operated.

4.3 Change of Landscape and Unanticipated Situations

The research method was designed before the building and its surrounding area were completed. The change of the site landscape on the north side of the building, where the ET system and sensors were located, affected the research plan by making the sensor depths inconsistent during the data collection. Subsequent to the installation of ST1 to ST4 after backfilling, the soil distributions above nominal grade were changed a few times prior to completion of the building. Unanticipated situations also occurred during the installation of the ground temperature sensors. These required this author to search for solutions and further adjust the research plan.

4.3.1 Uncertainty of Sensor Depths

Besides the locations of the strings, an effort was made to determine the depths of the ground temperature sensors more precisely.

Ground-penetrating radar (GPR) was used as a means to confirm string depth more precisely. A PulseEkko Pro with dual100MHz antennas and handles, and a 250MHz Noggin cart based ground penetrating radar (GPR) system were borrowed from a University of Calgary Geoscience Department research group, and a test was performed on December 15th, 2011. Neither system provided useful results. A second test inside the duct area was performed on January 25th, 2012, using the Noggin 500MHz unit. Based on the graphs the equipment generated, no sensors were observed. All the GPR equipment was manufactured by Sensors and Software Inc.

All members of Canadian Association of Pipeline and Utility Locating Contractors (CAPULC) in Calgary were contacted about approaches to locating the sensors. Half of them replied, but the conclusion was that the sensors were too tiny to be found using their equipment. However, through the email conversation with a technical specialist from 3M, this author learned about a kind of electronic marker (3M, 2010, p. 2), which could locate underground facilities easily and faster. The marker's working range is only up to 1.5 m (p. 4) underground. This depth is insufficient to mark the depths of the sensors in this research, but it at least could show the locations of the strings. This kind of marker could be used in similar future studies.

Finally, this author decided to make some assumptions based on the available information. There are five sensors in each string, and the distance between two sensors is 2 m as designed. The distance between the shallowest and the deepest sensors in each string should theoretically be 8 m. However, during the installation, the strings could be bended on the way down. Also, there was underground water encountered at about 7 m. As there was no way to check the exact depths of the sensors, and soil temperature below 2 m depth underground will not have obvious difference within small distances, such as 10 cm, this author decided to assume that the strings were straight with 2 m between each two sensors. This author assumed the shallowest sensor was located at 0.1 m depth, because the temperatures of sensors at this depth changed quickly following ambient air temperature.

4.3.2 Changes in Soil Distribution above the Ducts

Both ducts were buried at the same depth below nominal grade. However, a 1.6 to 2.3 m high layer of dirt (Figure 3.4) was placed on top of the duct area and moved back and forth, the condition and even the data were affected and the research plan had to be revised.

The dirt was sloped on both north and south and was located with its peak on top of the ST1, ST2 and ST3 area. This meant the north duct was buried deeper than the south duct, by about 0.3 m. The depths of both ducts and the three strings were not consistent from

the beginning of data collection on February 15th, 2011 until September 30th, 2011. This affected below grade temperature conditions. ST4 sensors were no longer at the same depth as those of ST1, ST2 and ST3. However, ST4 sensors could still be used as comparison to the other string sensors, but at slightly less comparable conditions. The effect of extra dirt on ground temperatures was positive because the north duct was deeper. At 2 m depth, the effect was very easily observed in the temperature trends.

CHAPTER FIVE: RESULTS AND DISCUSSION

5.1 Ambient Air Temperature

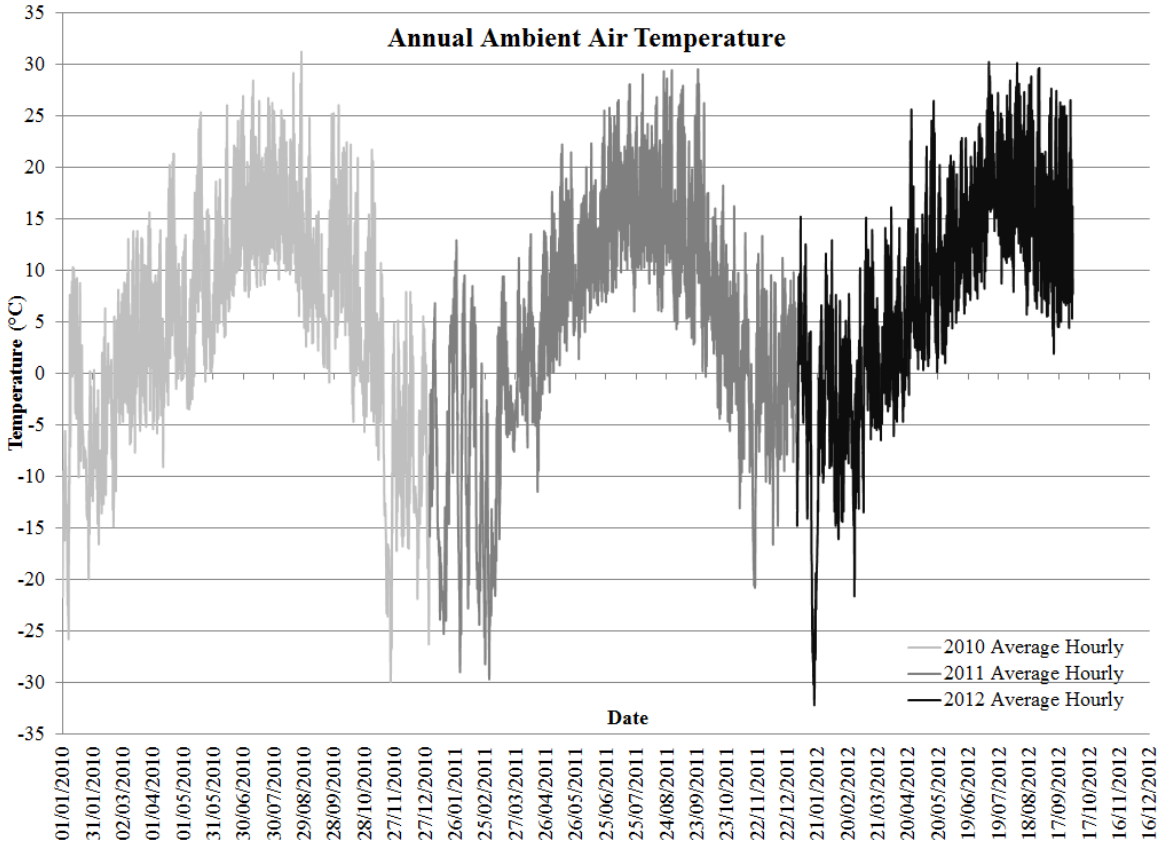

Figure 5.1 Average Hourly Ambient Air Temperatures for 2010 to 2012

Figure 5.1 shows the hourly average ambient air temperatures from 2010 to 2012 (September 30th). The mean annual air temperature was 4.5 ℃ in 2010 and 4.4 ℃ in 2011 (Tables 5.1 and 5.2). January and February of 2010 were generally warmer and November and December of 2010 colder than the corresponding months in 2011. The other corresponding months of both years had similar ambient air temperatures. The

winter average ambient air temperature (calculated from November 1st of previous year to March 31st) was -3.7 ℃ in 2010, -7.3 ℃ in 2011, and -2.3 ℃ in 2012 (Table 5.4).

Table 5.1 Average Yearly and Monthly Ambient Air Temperatures (℃) for 2010

	Average	Max	Min	Range
2010	**4.5**	**31.2**	**-29.9**	**61.1**
January	-6.3	10.3	-25.8	36.1
February	-4.5	8.1	-16.6	24.7
March	3.0	15.6	-7.7	23.3
April	4.9	21.3	-9.1	30.4
May	7.6	25.3	-3.5	28.8
June	13.5	26.9	2.0	24.9
July	16.2	28.4	7.4	21.0
August	15.0	31.2	2.6	28.6
September	9.1	25.2	-0.9	26.1
October	7.5	26.0	-5.7	31.7
November	-4.4	21.7	-29.9	51.6
December	-8.6	7.9	-26.3	34.2

Table 5.2 Average Yearly and Monthly Ambient Air Temperatures (℃) for 2011

	Average	Max	Min	Range
2011	**4.4**	**29.5**	**-29.7**	**59.2**
January	-8.6	12.9	-29.0	41.9
February	-9.1	9.5	-28.2	37.7
March	-6.1	11.2	-29.7	40.9
April	2.0	13.8	-11.5	25.3
May	9.6	22.2	0.1	22.1
June	13.2	25.7	4.0	21.7
July	16.8	29.0	6.0	23.0
August	16.4	29.4	6.0	23.4
September	14.2	29.5	0.2	29.3
October	6.0	18.2	-5.6	23.8
November	-2.0	13.6	-20.8	34.4
December	-0.9	11.1	-16.6	27.7

Table 5.3 Average Monthly Ambient Air Temperatures (℃) for 2012

	Average	Max	Min	Range
January	-5.1	15.2	-32.2	47.4
February	-4.4	12.8	-21.6	34.4
March	0.6	15.1	-13.5	28.6
April	4.9	25.6	-6.1	31.7
May	9.7	26.4	0.1	26.3
June	13.9	24.2	4.4	19.8
July	18.6	30.2	8.2	22.0
August	17.3	30.1	5.7	24.4
September	14.0	27.6	1.9	25.7

Table 5.4 Winter Average Ambient Air Temperature (℃) of 2010, 2011 and 2012 (Winter Average Ambient Air Temperature: from November 1st of Previous Year to March 31st)

Winter	Average	Max	Min	Range
2010	-3.7	19.6	-32.4	52.0
2011	-7.3	21.7	-29.9	51.6
2012	-2.3	15.2	-29.9	45.1

Some parameters in the experiment may vary a lot from year to year: ambient air temperature, climate conditions (more/less snow or rain each year), etc. The geographic location of Calgary means its winter weather is influenced greatly by Chinooks. In January (usually the coldest month of the year), 2012, Calgary experienced both a few very cold days (such as median temperature of -30 ℃ on January 17th, 2012) and a few warm days (such as median temperature of 8 ℃ on January 8th, 2012).

5.2 Related Information to Soil Temperature Change

5.2.1 Related Heat Exchanges

Some important heat exchanges related to this ET research are described below:

- Between ambient air and ground: "Ambient air temperature influence surface and subsurface temperature by affecting the rate at which heat is transferred to or from the atmosphere and the ground (Williams & Gold, 1976)." Ground surface temperature follows consistently with ambient air temperature. In summer, ground surface gains heat from solar radiation, and ground surface temperature rises first. In winter, heat is extracted from ground to ambient air, which makes ground surface temperature decrease first. Below the ground surface, however, because of the relatively high thermal inertia of the ground, temperature fluctuations decrease with depth below grade;
- Between outdoor air and ET: when outdoor air goes through ETs, in winter, temperature in soil (deeper than 2 m from ground surface) surrounding the ducts are higher than average outdoor air temperature, heat in soil surrounding the duct is conducted into the duct wall, and then convected into passing supply air. In this case, supply air passing through ETs is heated, while duct wall and soil surrounding the duct is cooled. In summer, the opposite happens, supply air passing through ETs is cooled, and duct wall and soil surrounding the duct is heated. However, as this ET system was not properly designed, this heat transfer was negated by counter flowing air in the north and south earth tubes;
- Between ground and building foundation: as building indoor air temperature is usually maintained above 20 ℃ throughout the year, the temperature of a building foundation will always be higher than that of the surrounding soil. Therefore, heat

will be conducted from the building interior through the foundation into the surrounding soil.

5.2.2 Data Collection Description

Ground temperature data collection was initiated on February 15th, 2011 at 16:00. Data were recorded at 1-minute intervals until the interval was revised to 5 minutes after 13:35 on February 23rd, 2011, because inspection of the data showed that soil temperature changes would be adequately recorded with a 5 minute interval. The data include pre- and operation conditions. They were downloaded from the datalogger to a laptop computer, and then imported into an Excel spreadsheet to analyze median daily ground temperature. An SC32B interface (Campbell Scientific, 2003) with an SC12 cable was used for attachment to the datalogger and a 10873 cable from the interface to the laptop. The data recorded between February 15th, 2011 at 16:00 and September 30th, 2012 at 23:00 were analyzed to explore the temperature changes of shallower ST1, ST2 and ST3 sensors due to soil distribution change above nominal grade, and the stabilization of ST4 sensor temperatures. The ambient air temperature data were obtained from Environment Canada (2012).

Two important external conditions changed during data collection and should be considered during analysis:

- One was the theatre LEED flush that began on September 8th, 2011, followed by the normal operation of AHU-4. From November, 2010 to September, 2011, the ET system was buried, but there was no mechanical airflow;
- The other one was changes in the depths of ST1, ST2 and ST3 sensors. One layer of dirt was placed on top of the three strings between July 5th and August 15th, 2011, moved away and then another higher pile of dirt was moved back permanently on September 28th, 2011. These major events were noted in Figures 5.2-5.6. Details will be provided in later sections.

5.3 Soil Temperature Change

5.3.1 Ground Temperature Changes due to Soil Distribution Change above Nominal Grade

Because the EEEL ET system was not designed correctly (see discussion of reverse flow in the south duct in Chapter 4), there was no point in evaluating the ground heat transfer for ST1, ST2 and ST3. However, as the soil distribution changed above nominal grade, the actual depths of sensors in ST1, ST2 and ST3 increased unevenly from 1.6 m to 2.3 m deeper from nominal grade than the original design. Changes of temperature trends at 0.1 m and 2 m depths were still of interest and should be analyzed.

Figures 5.2 and 5.3 show the temperature trends of the soil at 0.1 m and 2 m depths. The soil temperatures of ST1-ST3 sensors at 0.1 m and 2 m depths were lower in the first few months of data collection than one year later. Other than the soil distribution changes

noted above, the difference between average hourly ambient air temperatures for winters 2011 and 2012 (Table 5.4) should also be considered.

At 0.1 m depth, in winter 2011, S11 reached its minimum on March 2nd, 2011 at -11.2 ℃, while ambient air temperature was the lowest at -24.7 ℃. The ground temperature then rose following ambient air temperature. Beginning April 2nd, 2011, S16's temperature stayed quite stable just below 0 ℃ till May 13th, 2011. S1, S6, and S11 reached just below 0 ℃ on May 15th, May 10th, and May 12th respectively. As stated in Schoeneich's paper (2011, p. 1), "During snow melting, the snow cover will first lose its isolation capacities by both the compaction of the snow and the increase of its water content, leading to a progressive warming of the ground surface temperature. When melt water percolates to the ground surface, the ground surface temperature will enter a phase at 0 ℃, lasting until complete snow melt, and called zero curtain." The period during early April to mid-May was when all the heat from the ambient air was consumed by the ground as latent heat. After the ground completely melted, the temperatures of all sensors began to rise rapidly, and followed ambient air temperature more closely.

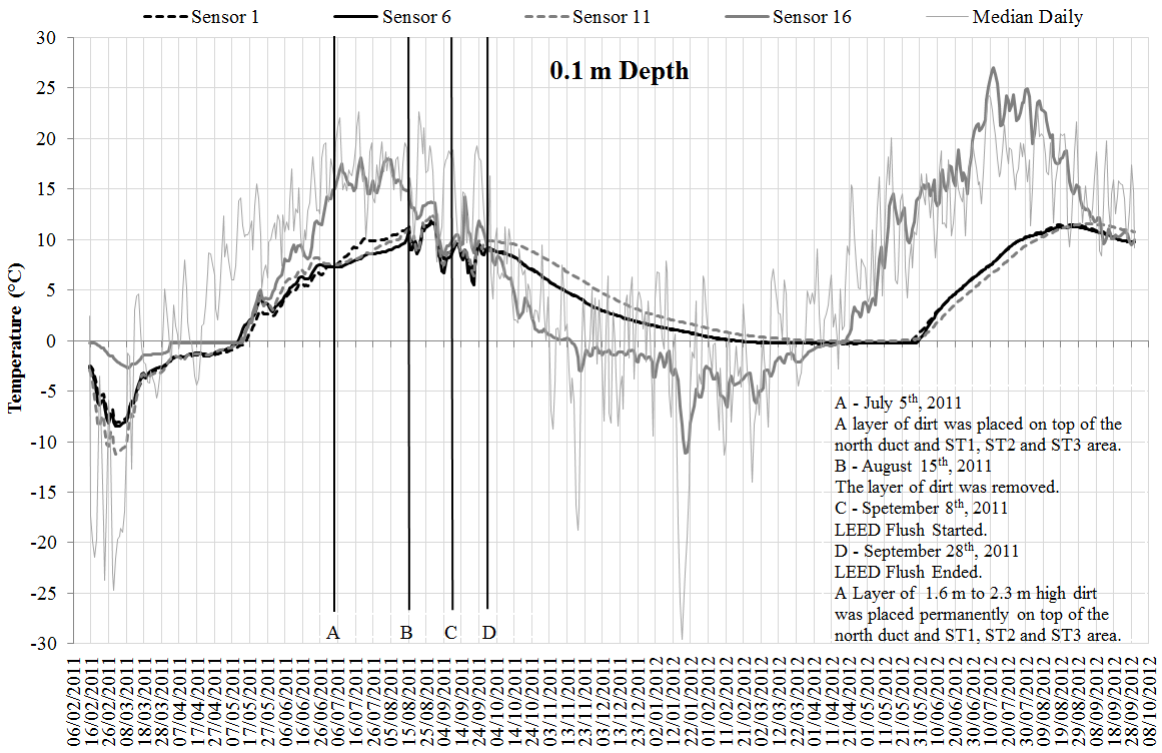

Figure 5.2 Median Daily Ground Temperatures at 0.1 m Depth

The extra dirt placed above ST1, ST2 and ST3 (period between A and B in Figure 5.2) both

- delayed S1, S6 and S11's peaking by just over a month, and lowered their peak temperatures by about 6 ℃ compared with S16 (all the related dates, peak and minimum temperatures of the twenty sensors can be found in Table 5.5) and
- resulted in the temperatures of S1, S6 and S11 remaining stable, while the temperature at S16 (in ST4) experienced big fluctuations following the ambient temperature.

After point D in Figure 5.2, the extra soil was permanently placed above nominal grade. Temperatures of S1, S6 and S11 became stable and decreased slowly, while the temperature of S16 fluctuated with ambient air temperature and decreased rapidly. The effect of the large layer of dirt was obvious.

In winter 2012, the temperature at S16 first fell below 0 ℃ on November 15th, 2011. It reached as low as -11.1 ℃ on January 19th, 2012, two days after the ambient air temperature reached a winter low of -29.6 ℃. Temperatures at S1, S6, and S11 decreased below 0 ℃ beginning on February 15th, 2012, and stayed stable just below 0 ℃. Their "zero curtains" of winter 2012 were quite different from those of winter 2011. Their durations were all longer than S16: February 15th to May 26th for S1, February 18th to May 30th for S6, and April 4th to May 16th for S11.

Following the rise of ambient air temperature, the temperature of S16 experienced a much shorter period of zero curtain than winter/spring, 2011, from April 5th (-0.5 ℃) to April 19th (-0.1 ℃). This was because it was closer to ground surface and received latent heat from ambient air quicker than the other three sensors (covered by extra soil). Moreover, the winter average ambient air temperature in 2012 was -2.3 ℃, while that of 2011 was -7.3 ℃. The latent heat required for melting was much less in spring, 2012.

Table 5.5 Peaks and Troughs of Median Daily Soil Temperature (℃) of Winter and Summer, 2011 and 2012

Depth	Sensor	Winter, 2011	Summer, 2011	Winter, 2012	Summer, 2012
0.1 m	S1	March 2nd -8.1	August 28th 11.9	April 6th -0.3	August 26th 11.5
	S6	March 2nd -8.5	August 28th 11.9	April 11th -0.3	August 27th 11.3
	S11	March 2nd -11.2	August 28th 12.6	April 24th -0.1	September 1st 11.6
	S16	March 9th -2.7	July 19th 18.1	January 19th -11.1	July 12th 27.1
2 m	S2	March 15th -1.7	September 1st 10.3	April 11th 0.2	September 4th 11.0
	S7	April 24th -0.4	September 5th 9.2	April 11th 0.4	September 14th 10.5
	S12	March 21st -0.8	October 13th 9.5	April 29th 0.6	-
	S17	May 19th 0.9	September 5th 10.3	May 5th 0.6	August 22nd 13.8
4 m	S3	April 25th 1.1	October 2nd 9.7	March 31st 1.4	-
	S8	April 8th 0.9	September 30th 9.4	March 29th 1.2	-
	S13	April 30th 0.9	October 6th 9.3	April 14th 1.7	-
	S18	June 10th 3.3	October 21st 8.3	May 23rd 3.1	-
6 m	S4	April 26th 3.1	October 3rd 8.8	March 29th 3.0	-
	S9	April 8th 2.8	October 2nd 8.7	March 28th 2.8	-
	S14	May 3rd 2.5	October 7th 8.6	April 12th 3.1	-
	S19	July 1st 5.0	November 13th 7.3	June 5th 4.8	-
8 m	S5	May 10th 5.0	October 20th 7.9	April 25th 4.8	-
	S10	May 2nd 5.0	October 18th 7.4	April 25th 4.9	-
	S15	May 17th 4.6	October 25th 7.4	April 29th 4.9	-

Depth	Sensor	Winter, 2011	Summer, 2011	Winter, 2012	Summer, 2012
8 m	**S20**	August 5th 6.0	December 17th 7.0	July 8th 5.8	-

After the "zero curtain", S1, S6 and S11 all increased rapidly and smoothly following ambient air temperature. The processes of S1, S6 and S11 peaking were much smoother than that they experienced in year 2011 (period between B and D in Figure 5.2). This was because during that time the extra soil above these sensors was removed. The pile of dirt substantially changed the temperature profiles of ST1, ST2 and ST3 sensors at this depth.

At 2 m depth, the soil could be either affected by the ETs or by the ambient air. It is hard to tell which effect is greater.

The maximum depth of frost penetration in Calgary is 1.8 m (The Canadian Geotechnical Society, 2006, p. 192). In this research, the ground temperature at 2 m depth fell below 0 ℃ during February and March, 2011, and this did not occur in 2012. This could be because:

- the area around the ducts was excavated during the installation of the ETs in November, 2010. It is reasonable temperature in this area was lower than normal;
- the extra soil located above nominal grade since late September, 2011.

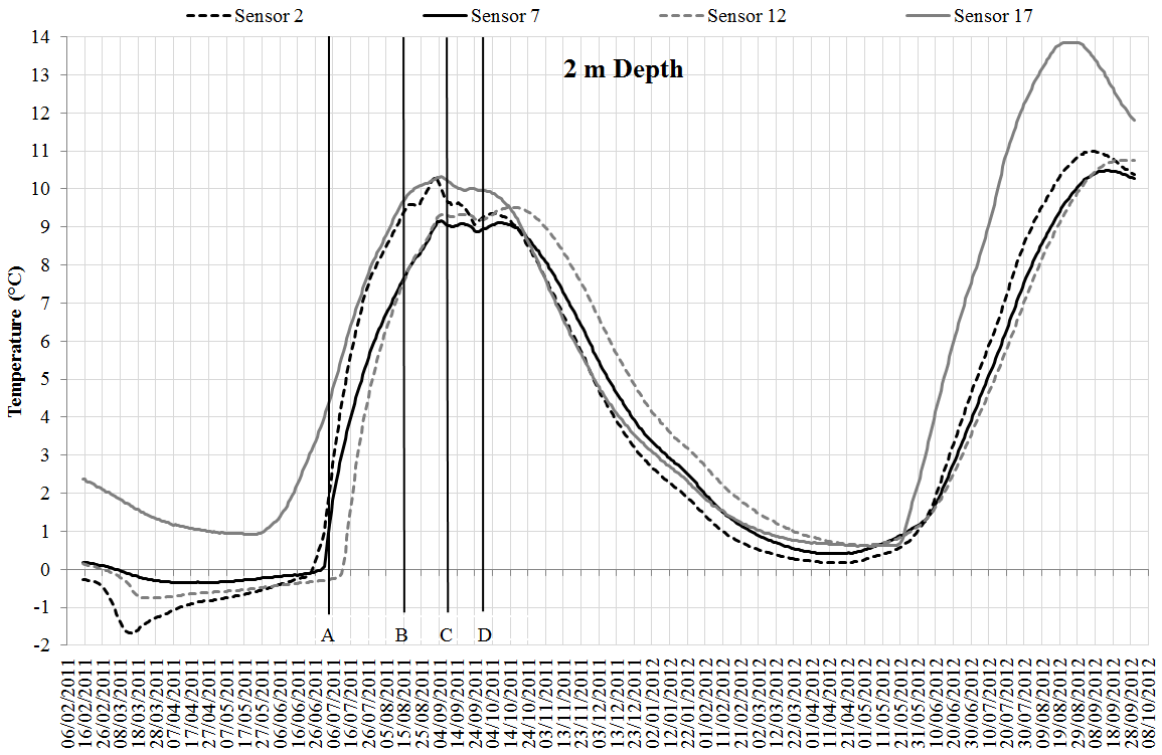

Figure 5.3 Median Daily Ground Temperatures at 2 m Depth

As stated above, ST4 is the farthest from the building and ducts, and the least affected by their related heat transfer. The ground around S17 (in ST4, 2 m deep) never froze, and the temperature began to rise on May 26th, 2011. This was much earlier than at corresponding points on S2 (ST1), S7 (ST2) and S12 (ST3). The ground near the duct at S2, S7 and S12 froze in winter 2011. Their readings rose to 0 ℃ one by one from late June to mid-July 2011. The zero curtain phenomenon occurred. The temperatures at the three sensors all rose rapidly after the ground melted, and peaked around September, 2011.

The effect of the removal of extra soil between period B and D also showed at 2 m depth. The fluctuations of S2, S7 and S12 caused by ambient air temperature during that period experienced a two-week time lag relative to sensors at 0.1 m depth, because of the 1.9 m extra depth.

The temperatures of the sensors at 2 m depth reached their minimums in mid-April all above 0 ℃ (see details in Table 5.5). Again this could be because both the extra soil and the 5 ℃ warmer winter temperature of 2012.

By September 28th, 2012, AHU-4 had been operated normally for one year after LEED flush. Based on the data given in Table 5.6, comparing to September 28th, 2011,

- the median daily soil temperature at 0.1 m depth had risen 8.7% (average of all three sensors), while the median daily ambient air temperature was higher by 75%;
- the median daily soil temperature at 2 m depth had risen 15.2%.

It could be noticed that the temperature rise at 2 m was higher. This could be because the extra layer of dirt above normal grade. The effective sensor depths increased and the winter average ambient air temperature of 2012 was 5 ℃ higher than that of 2011 (Table 5.4).

Table 5.6 Temperature Changes (℃) of Sensors at 0.1 m and 2 m after One-Year of Normal Operation

String	Sensor	September 28th, 2011	September 28th, 2012	Temperature Changes
0.1 m	S1	9.1	9.8	0.7
	S6	9.1	9.8	0.7
	S11	9.8	10.8	1.0
	S16	9.9	9.5	-0.4
2 m	S2	9.2	10.4	1.2
	S7	8.9	10.3	1.4
	S12	9.2	10.8	1.6
	S17	10.0	11.9	1.9
Ambient Air Temperature		10.0	17.5	7.5

5.3.2 Stabilization of the Ground Temperature Remote from the Building

As ST4 was remote from the ducts and the building, it was the least influenced and would be expected to correspond more closely to the undisturbed ground temperature. It provides some reference data on the stabilization of the ground temperatures for the disturbed soil especially at 4 m, 6 m and 8 m depths.

It can be seen from Figures 5.4-5.7 and Table 5.7 that the deeper the ground, the more stable ST4 ground temperature remained.

The ducts were buried at 4.9 to 4.5 m from nominal grade to the centres of inlet and discharge. The temperature in soil surrounding ducts will be affected more at the depths of 4 m and 6 m than at 0.1 m, 2 m and 8 m. Temperatures at these two depths were analyzed and compared.

Figures 5.5 and 5.6 show that ground temperatures at 4 m and 6 m in ST4 were always above 0 ℃; the deeper the sensors, the higher the temperatures, the smaller temperature range, and the larger the temperature time lags with respect to the ambient air temperature. The temperature ranges for ST4 sensors at 4 m and 6 m were 6.4 ℃ and 2.5 ℃, while those of ST1-3 sensors were about 9 ℃ and 6 ℃ respectively.

Table 5.7 Median Monthly Temperature Ranges (℃) for Sensors at 4 m, 6 m and 8 m Depths (from February 15th, 2011 to September 30th, 2012)

String	Sensor	Maximum Temperature	Minimum Temperature	Temperature Range
4 m	**S3**	September, 2012 10.3	April, 2011 1.1	9.2
	S8	September, 2012 10.0	April, 2011 0.9	9.1
	S13	September, 2012 9.9	April, 2011 1.0	8.9
	S18	September, 2012 9.5	May, 2012 3.1	**6.4**
6 m	**S4**	September, 2012 8.9	April, 2011 3.1	5.8
	S9	September, 2012 8.9	April, 2011 2.9	6.0
	S14	September, 2012 8.9	April, 2011 2.6	6.3
	S19	November, 2011 7.3	June, 2012 4.8	**2.5**
8 m	**S5**	October, 2011 7.8	April, 2012 4.9	2.9
	S10	October, 2011 7.4	April, 2012 4.9	2.5
	S15	October, 2011 7.4	May, 2011 4.6	2.8
	S20	February, 2011 7.2	July, 2012 5.8	**1.4**
Ambient Air		July, 2012 18.2	February, 2011 -16.8	35.0

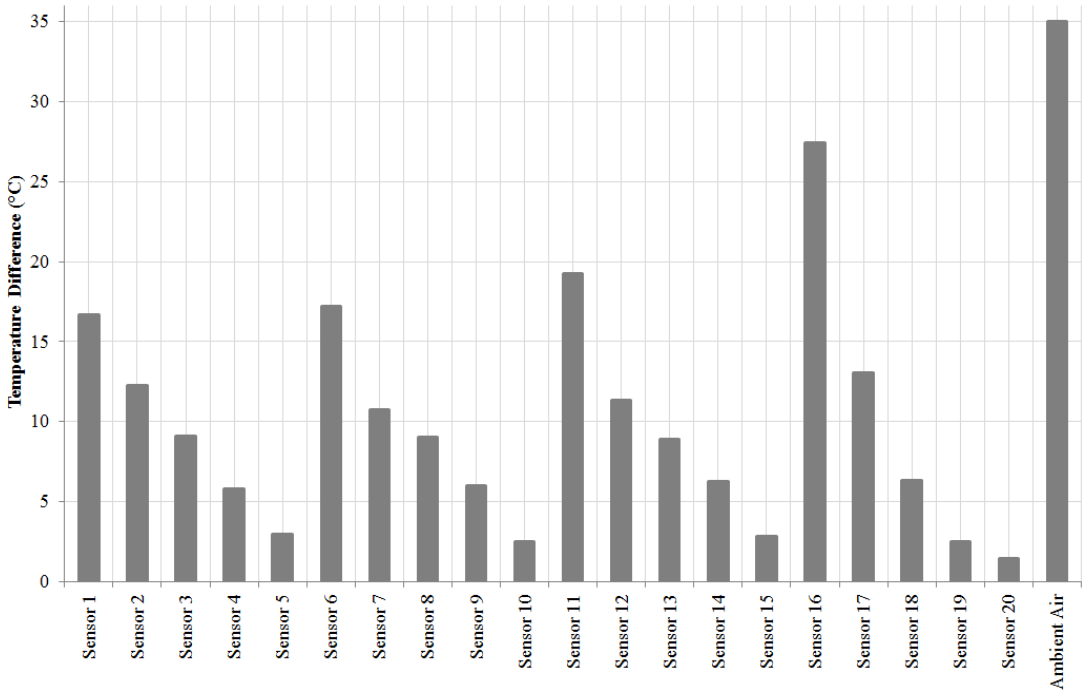

Figure 5.4 Median Monthly Temperature Ranges for Ground Temperature Sensors

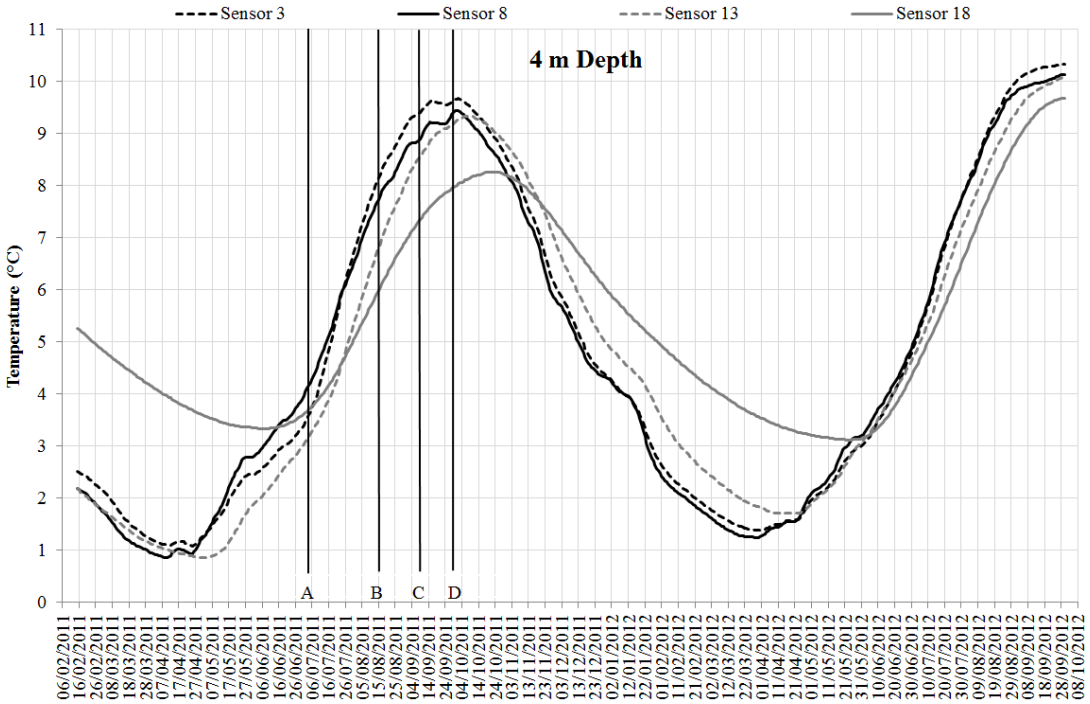

Figure 5.5 Median Daily Ground Temperatures at 4 m Depth

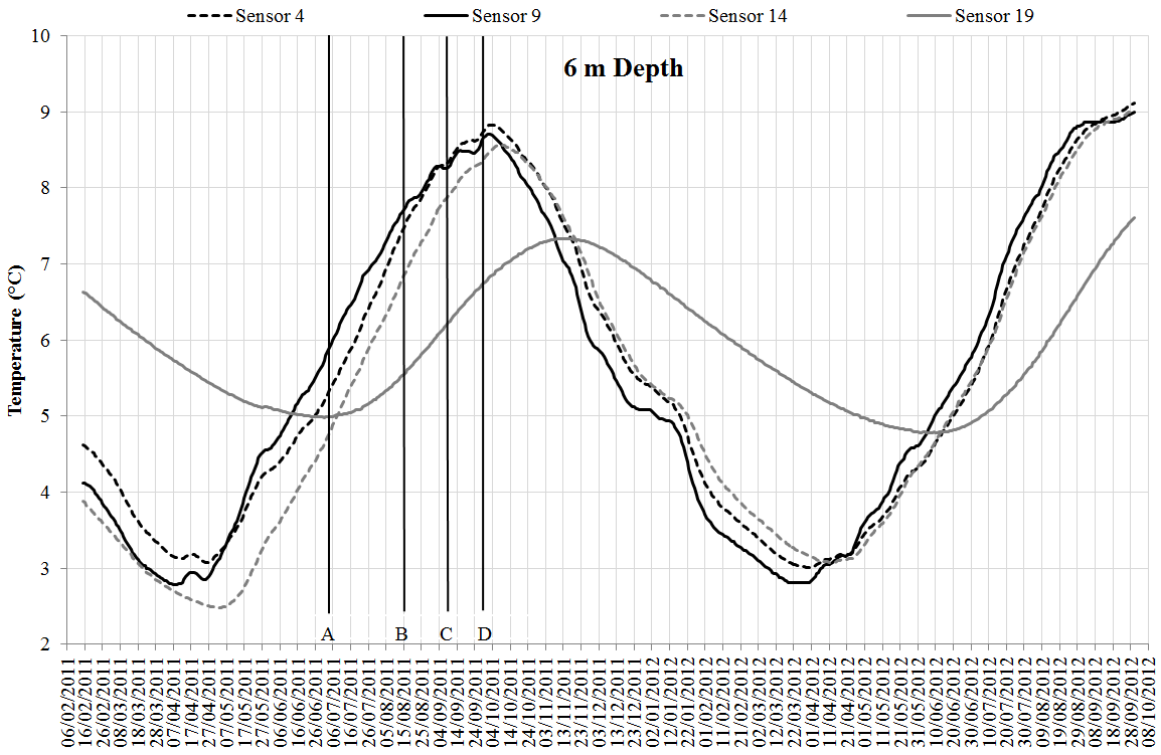

Figure 5.6 Median Daily Ground Temperatures at 6 m Depth

Temperatures of all the ST1, ST2 and ST3 sensors began to rise around April, 2011 and peaked around October, 2011, both much earlier than the corresponding sensors in ST4. The peak of S18 (ST4) at 4 m depth was about 1.2 ℃ lower and two weeks later than those of the ST1-ST3 sensors at the same depth. That of S19 (ST4) at 6 m depth was about 1.4 ℃ lower and six weeks later than those of the ST1-ST3 sensors at the same depth.

After peaking in October, 2011, temperatures of the ST1-3 sensors decreased rapidly with delay of about 3 to 4 days compared to ambient air temperature. During the weeks of November 27th-December 3rd, December 18th-December 24th and December 25th-

December 31st, 2011, the rates of temperature decrease of S3, S8 and S13 (at the depth of 4 m), and S4, S9 and S14 (at the depth of 6 m) slowed. This was because ambient air temperatures were relatively high during that period (higher than ground temperatures during daytime) and heat was transferred from the incoming air to the ground surrounding the ducts. This was expected as these two sets of sensors were closest to the ducts and they were affected. The rates of temperature drop clearly increased for the same set of sensors during the cold week of January 15th-January 21st, 2012. During both temperature rate changes of ST1-3, the temperatures of ST4 sensors were more stable and their curves were much smoother. The stabilization effects of soil remote from the building and the ducts were obvious.

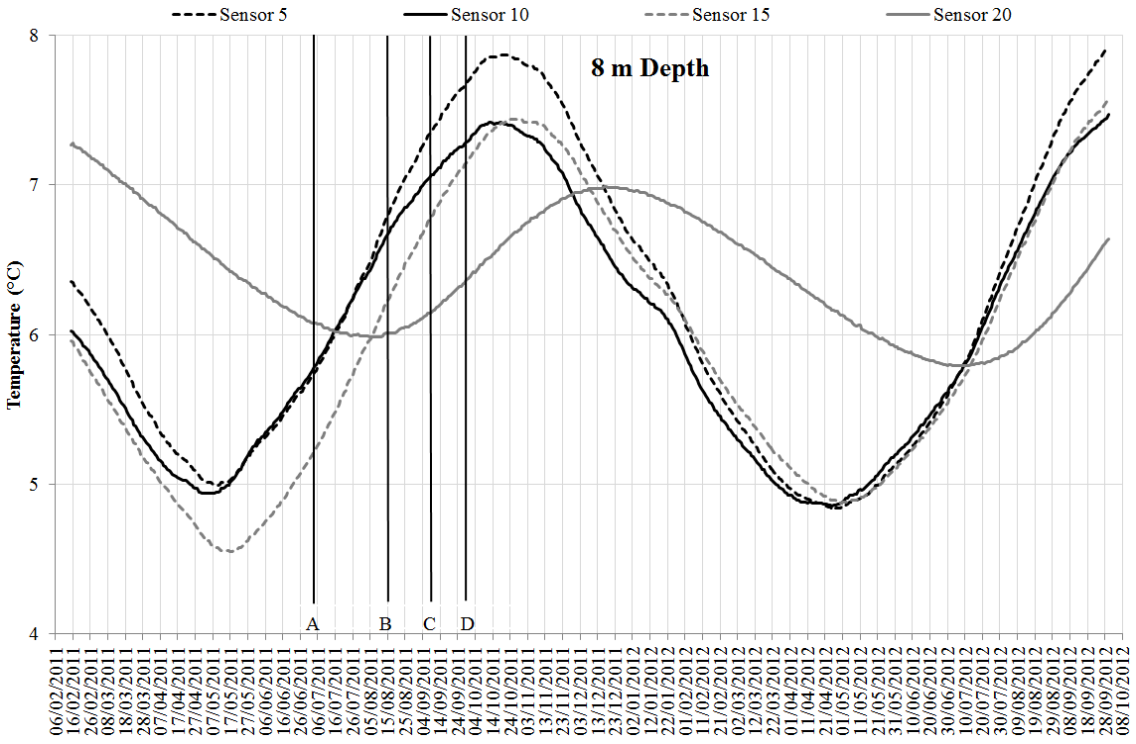

Figure 5.7 Median Daily Ground Temperatures at 8 m Depth

At 8 m depth, the temperature at S20 was the most stable. The highest temperatures at S20 occurred in mid-February, 2011, almost a half-year of time shift relative to the ambient air temperature. The temperature range of S20 was 1.4 ℃, about half of the other sensors' at this depth. This further shows that undisturbed ground temperature stays very stable during a complete year when depth is sufficient (such as at 8 m).

Figure 5.7 shows that S5, S10 and S15 reached their minimums around mid-May, 2011 while S20 reached its around mid-August, a three-month delay. However, the temperatures of sensors at 8 m depth fluctuated less than those at other depths. After the system started operating, temperatures at S5, S10 and S15 peaked around October 20th, 2011. Temperature of S20 peaked in mid-December, 2011. However, the peak was lower than it was in early 2011 (or late 2010). As S20 is in ST4 and far from the ducts, the temperature change should be mostly related to the undisturbed ground temperature which is affected by ambient air temperature, but no influence by the ETs.

Figures 5.8-5.11 show the vertical temperature gradient for each string from the beginning of October, 2011 to the end of September, 2012. It could be seen that ST4 profile has a much more typical and narrower funnel shape, while ST1, ST2 and ST3 sensors had similar temperature profiles. At all strings the temperature ranges for each sensor diminished with depth. Temperature ranges for ST4 sensors at 0.1 m and 2 m were larger than those of ST1, ST2 and ST3 sensors. The effect of the extra dirt on top of ST1, ST2 and ST3 was obvious. At 4 m, 6 m and 8 m, the ranges of ST4 sensors were

only about half of those for ST1, ST2 and ST3. The stabilization of soil remote from the building and the ducts is obvious.

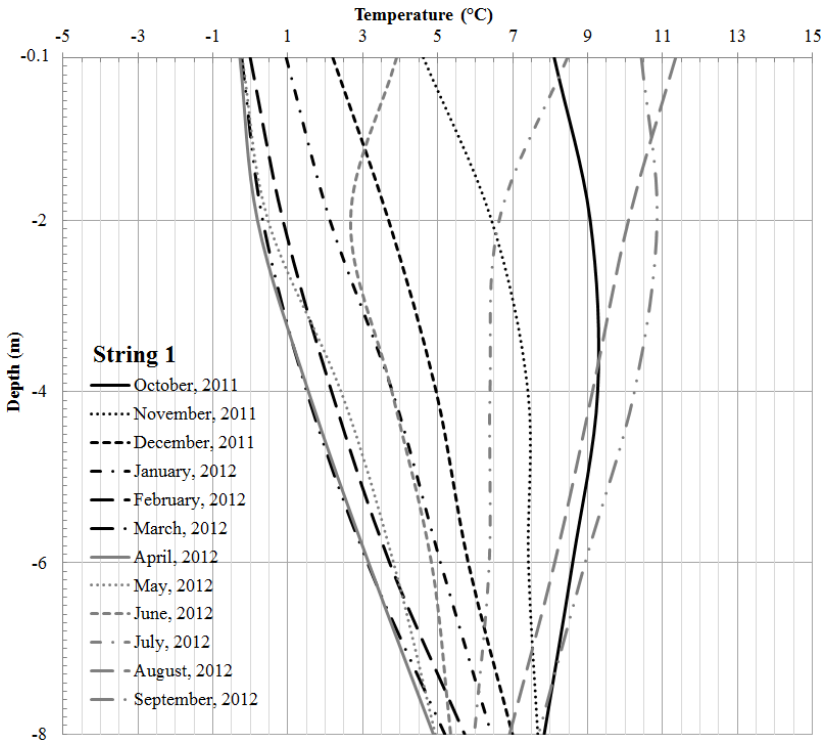

Figure 5.8 Median Monthly Ground Temperatures at ST1 for 12 Months

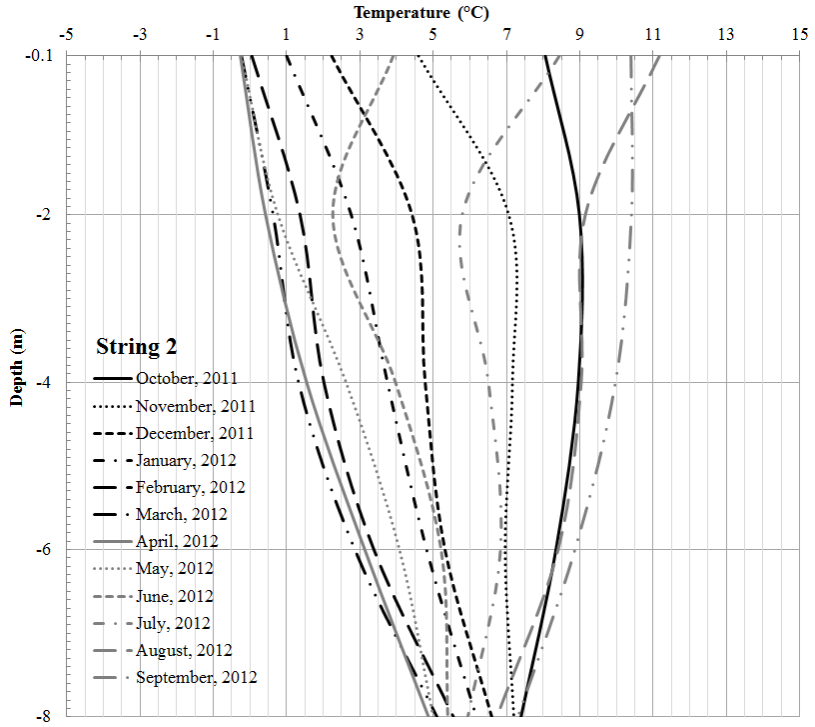

Figure 5.9 Median Monthly Ground Temperatures at ST2 for 12 Months

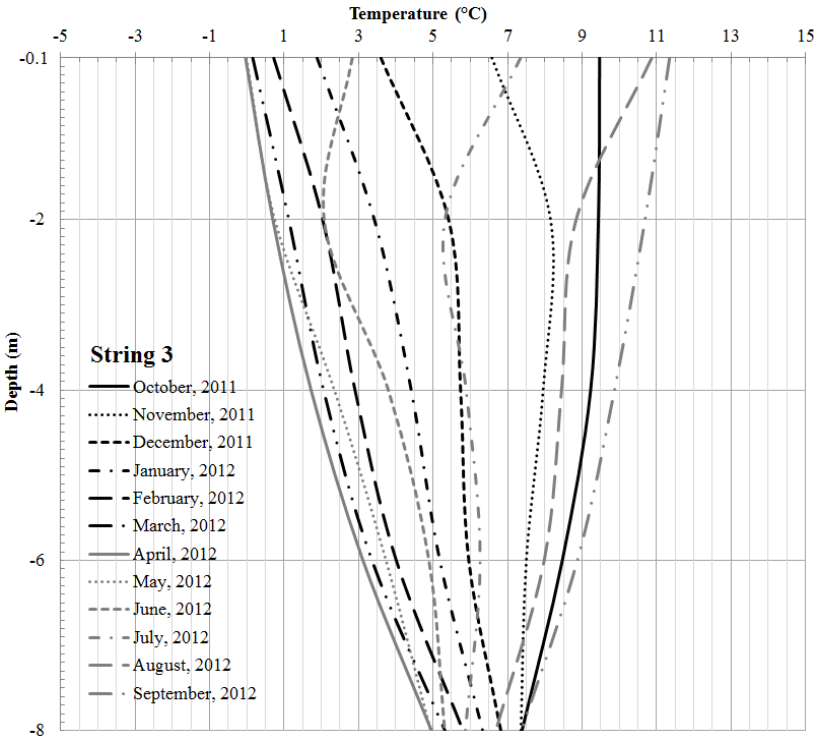

Figure 5.10 Median Monthly Ground Temperatures at ST3 for 12 Months

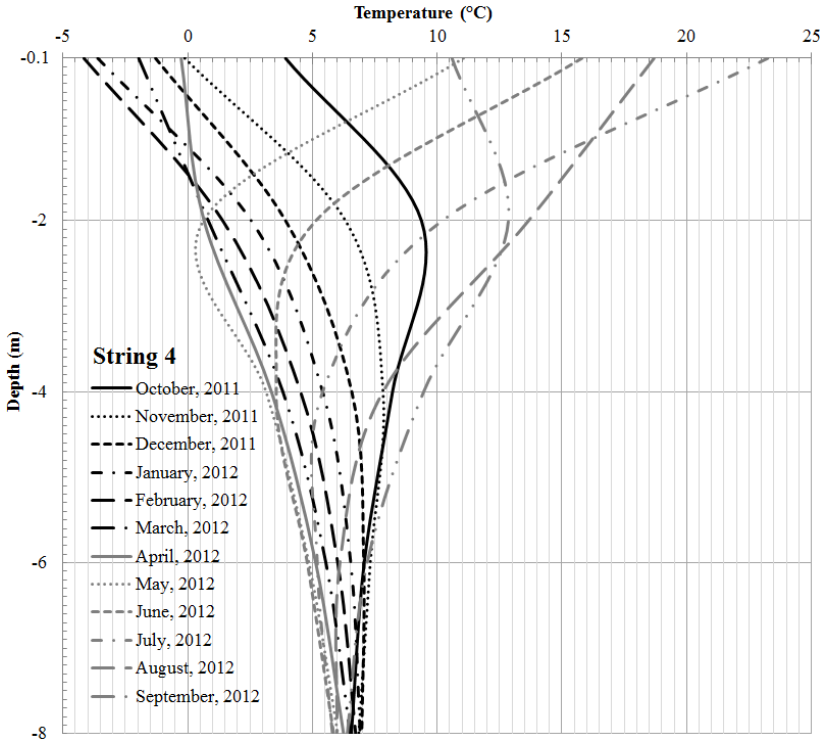

Figure 5.11 Median Monthly Ground Temperatures at ST4 for 12 Months

CHAPTER SIX: CONCLUSIONS

6.1 Findings on Soil Temperature Change

The purpose of this research was to analyze ET effects on soil temperatures. Among the topics considered were the soil temperature changes due to soil distribution change above nominal grade, and the stabilization of soil temperature remote from the building and the ducts.

First of all, the combination of the following outside factors affected soil temperature:

- Soil excavation during ET installation;
- The change of landscape above nominal grade had resulted in the change of depths of soil temperature sensors;
- AHU-4 started operating more than six months after measurement started;
- Winter average ambient air temperature of 2011 was 5 ℃ lower than that of 2012.

The findings on soil temperature change are below:

- At 0.1 m and 2 m depths, soil temperatures were affected by the soil distribution change above nominal grade. This change made the soil at these two depths more stable. The "zero curtain" phenomenon occurred in both winters 2011 and 2012 for soil temperature at 0.1 m, but only in winter 2011 for that at 2 m. This could be because the soil was excavated and disturbed in November, 2010 or the relatively warm winter 2012;

- Comparing to sensors in ST1-3, soil temperatures at 4 m, 6 m and 8 m depths of ST4 were very stable. As soil at these three depths was remote from the building and the ducts, the deeper the ground, the smaller temperature ranges were, and the larger time delays were.

6.2 Inspirations from this Research

6.2.1 Documentation

The site construction was still ongoing during the early period of data collection and lasted until late September, 2011. The soil distribution above nominal grade of the duct and string area changed a few times during that time. This influenced the soil temperature data trend. Frequent photo-taking during the research was helpful in recording project progress, initial conduit cable and asphalt path locations. The photos were especially useful for later comparison between data analysis results and landscape conditions.

6.2.2 Measurement

This author planned to collect ET duct wall temperatures on January 17th, the coldest day of 2012, when ambient air temperature was -30 ℃ at 10:00. An OMEGA OS950 series infrared thermometer was used for temperature collection. However, as it was quite windy and cold down at the ETs, the infrared thermometer only worked for the first two minutes and then was frozen. The user's guide said the instrument operating range is 0 ℃ to 50 ℃ (OMEGA, p. 10), and its storage range is -30 ℃ to 60 ℃. Becoming

familiar with equipment before using would save time and make one's research more confident. It was unfortunate that the data were unavailable for detailed analysis. Moreover, pen worked poorly at the cold environment. It is better to use pencil.

6.2.3 Communication

Visit the site frequently was helpful during the research to observe events that occurred during the research that required the researchers' attention, such as landscape and system changes.

Communication was also important during this research. The more questions you ask, the more you learn. This author discussed the mechanical system and architectural questions with people from EllisDon, the EEEL construction company. She also tried to obtain the initial design from the designer of the ET system, Tim McGinn of Design Dialog. She asked questions and received valuable data and control system information from Siemens staff and University facility management personnel.

At the beginning of the research, when this author went to the duct air plenum (Room 057v) in the basement, she could smell sewer gas from the drainage. The room is the only path for outdoor air to go into AHU-4, transporting polluted air into the occupied space. Moreover, as air in that room will also flows back to Room 043v through the south duct, the malodourous air would also have been drawn into AHU-1, AHU-2 and AHU-3. This means sewer gas, even at low concentration, would permeate the building.

According to ASHRAE Standard 62.1 Table 6-1 (2007, p. 13), the air class for theatre and lecture classroom should both be 1. The definition of air class 1 (p. 9) is "Air with low contaminant concentration, low sensory-irritation intensity, and inoffensive odour." Circulation of polluted supply air inside the EEEL building was a possibility. This author reported the situation to the facility manager Doug Morton. He informed the EllisDon site Superintendent. It was found that a device that should be installed was missing. In the meantime, this author went to the main floor theatre and found she could easily smell the gas there.

To confirm every step of sensor installation, temperature measurement, and data collection is very important. Because some of the steps are not reversible, one missing item could result in important mistakes in data prediction and analysis. If people in charge of installation are not familiar with the details and standards, it is possible for them to ignore things and make mistakes. This will lead to useless data and research uncertainties. The possibility of ST1 and ST3 installed backwards could be a bad example. Communication is important. The installers and designers should keep good communications open and discuss, agree on and record any changes to the original design.

6.3 Recommendations for Future Work

The results of this experiment could provide general results on soil temperature change due to soil distribution change above nominal grade, and the stabilization of soil remote from the building and the ducts. It is only the basic step of the system evaluation.

However, because of the incorrect design of the EEEL ET system, the system's effects on temperature in soil surrounding the ducts failed to show. Ground temperature change requires long-term monitoring. Corrections of the design problem and long-term monitoring are required to explore the ground heat depletion surrounding the ducts, in order to evaluate if the system can maintain long-term stable operation in a very cold climate. Questions such as how long will it take for the ground heat to self-recover, if the ground heat is not sufficient to maintain a satisfy operation, will there be any technology that can help the heat recovery economically, all need to be answered.

Moreover, the air distribution inside the ducts, such as the air velocity, temperature, and boundary layer contacting the duct walls should be analyzed to further improve the experiment. Simulation tools, such as using a CFD model to analyze the heat distribution inside the ducts and even ground surrounding the ducts might be helpful.

The ET system's effect on the scope of the whole EEEL building should also be explored. This will require building simulation with proper software, which can model not only the inside building HVAC system but also the ET system buried underground next to the building. Once the model analysis data are compared with real experimental data, and the accuracy of the model is confirmed, it can be used to analyze how much energy is saved per year with the ET system and calculates its payback period.

Several recommendations for future work are as below:

- Figure out how air moves in the south duct under various conditions of the AHUs operations;
- Finding possible solutions to the reverse airflow problem. The backward airflow in the south duct must be corrected so as to make full use of the ET system;
- Install duct air temperature sensors, collect data and find temperature difference after air moves through the ETs so as to calculate system's coefficient of performance (COP);
- Confirm ST1 and ST3 locations, see if they are installed backward;
- The soil sensors of EEEL ET were 1 m laterally from the north duct wall. The soil immediately surrounding the ducts could be frozen during winter time. This information could be useful for future EEEL ET studies as simulation input;
- Work with building operator to alternate between operation and non-operation of the ET system to examine the ground heat self-replenishment;
- Simulate the building with the ET system and evaluate energy savings;
- Questionnaires for students, teachers and staff regarding indoor environment comfort to further evaluate the ET system.

REFERENCES

3M. (2010). *Recommendations for Marking Power Facilities Using 3M™ EMS Electronic Markers*. 3M Track and Trace Solutions.

Alberta Environmental and Sustainable Resource Development. (2012). *Energy Efficiency-Conserving and Using Energy Efficiency.* Retrieved July 24, 2012, from http://environment.alberta.ca/02799.html

Architecture 2030. (2011). *The 2030 Challenge.* Retrieved July 24, 2012, from http://architecture2030.org/2030_challenge/the_2030_challenge

ASHRAE. (2007). *ANSI/ASHRAE Standard 62.1-2007, Ventilation for Acceptable Indoor Air Quality*. Atlanta, GA: American Society of Heating, Refrigerating and Air-Conditioning Engineers, Inc.

ASHRAE. (2008). *ANSI/ASHRAE Standard 111-2008, Measurement, Testing, Adjusting, and Balancing of Building HVAC Systems*. Atlanta, GA: American Society of Heating, Refrigerating and Air-Conditioning Engineers, Inc.

ASHRAE. (2009). *ASHRAE Handbook, Fundamentals, S-I Edition*. Atlanta, GA: American Society of Heating, Refrigerating and Air-Conditioning Engineers, Inc.

ASHRAE. (2010). *ANSI/ASHRAE/IESNA Standard 90.1-2010, Energy Standard for Buildings Except Low-Rise Residential Buildings, I-P Edition*. Atlanta, GA: American Society of Heating, Refrigerating and Air-Conditioning Engineers, Inc.

Athienitis, A. K., & Santamouris, M. (2002). *Thermal Analysis and Design of Passive Solar Buildings.* London, UK: James and James Pub.

Athienitis, A. K., Roy, M., & Zhao, M. (2005). Design and Simulation of a Hybrid Ventilation System with Earth-Air Heat Exchanger. *9th International Building Performance Simulation Association Conference*, 27-32.

Bahadori, M. N. (1978). Passive Cooling Systems in Iranian Architecture. *Scientific American, 238*(2), 144-154.

Baxter, D. O. (1992). Energy Exchanges and Related Temperatures of an Earth-Tube Heat Exchanger in the Heating Mode. *Transaction of the ASAE, 35*(1), 275-285.

Baxter, D. O. (1994). Energy Exchanges and Related Temperatures of an Earth-Tube Heat Exchanger in the Cooling Mode. *Transactions of the ASAE, 37*(1), 257-267.

Bernier, M. A. & Shirazi, A. S. (2007). Solar Heat Injection into Boreholes: a Preliminary Analysis. *Proceedings of the 32e Annual Conference of the Solar Energy Society of Canada and the Second Canadian Solar Research Network Conference*, 1-8.

Canada Green Building Council. (2012). LEED: The International Mark of Excellence. Retrieved October 23, 2012, from http://www.cagbc.org/AM/Template.cfm?Section=LEED

Campbell Scientific. (2003). *SC32B Optically Isolated RS-232 Interface Instruction Manual.* Campbell Scientific, Inc.

Campbell Scientific. (2009). *AM16/32B Relay Multiplexer Instruction Manual.* Campbell Scientific, Inc.

Campbell Scientific. (2010). *109B & 109BAM Temperature Probe Instruction Manual.* Campbell Scientific (Canada) Corp.

Campbell Scientific. (2011). *CR1000 Measurement and Control System Operator's Manual.* Campbell Scientific, Inc.

Canadian Geotechnical Society. (2006). *Canadian Foundation Engineering Manual 4th Edition.* BC, Canada: The Canadian Geotechnical Society.

Earth Rangers Centre. (2012). *About the Earth Tubes at the Earth Rangers Centre for Sustainable Technology*. Retrieved June 29, 2012, from http://www.ercshowcase.com/earth_tubes/index.html

Environment Canada. (2012). *Climate Data Online*. Retrieved August 25, 2011, from http://www.climate.weatheroffice.gc.ca/climateData/canada_e.html

EPA. (2012). Controlling Pollutants and Sources. Retrieved October 23, 2012, from http://www.epa.gov/iaq/schooldesign/controlling.html#Air%20Out%20and%20Flush%20Out

Eugster, W. J., & Rybach, L. (2000). Sustainable Production from Borehole Heat Exchanger System. *Proceedings World Geothermal Congress 2000*, 825-830.

Fujii, H., Nishi, K., Komaniwa, Y., & Chou, N. (2012). Numerical Modeling of Slinky-Coil Horizontal Ground Heat Exchangers. *Geothermics, 41*(1), 55-62.

Gonzalez, R. G., Verhoef, A., Vidale, P. L., Main, B., Gan, G., & Wu, Y. (2012). Interactions between the Physical Soil Environment and a Horizontal Ground Coupled Heat Pump, for a Domestic Site in the UK. *Renewable Energy, 44*(1), 141-153.

Gustafsson, S. (1993). Are Earth Tube Heat Exchangers of Interest When Heating Buildings? *International Journal of Energy Research, 17*(7), 597-604.

Heiselberg, P. (2004). Building Integrated Ventilation Systems-Modeling and Design Challenges. *CIB 2004 World Building Congress*, 1-8.

Hetu, E. (2011). New Building on Track to Receive LEED Platinum Certification. Retrieved July 30, 2012, from http://www.ucalgary.ca/news/utoday/december20-2011/leed

International Energy Agency. (2012). *25 Energy Efficiency Policy Recommendations – 2011 Updated.* Retrieved October 19, 2012, from http://www.iea.org/publications/freepublications/publication/name,3782,en.html

Jeong, Y. (2002). *Modeling of a Hybrid-Ventilated Building : "Grong School"* . Unpublished Master's Thesis, Concordia University, Montreal, Quebec, Canada.

National Research Council Canada. (2005). Archived – CBD-180. Ground Temperatures. Retrieved October 13, 2012 from http://archive.nrc-cnrc.gc.ca/eng/ibp/irc/cbd/building-digest-180.html

Natural Resources Canada. (2011). *ecoENERGY Efficiency for Buildings.* Retrieved July 24, 2012 from http://oee.nrcan.gc.ca/corporate/8803

Niu, F. X., Ni, L., Yao, Y., Jiang Y. Q., & Ma, Z. L. (2011). Thermal Accumulation Effect of Ground-Coupled Heat Pump System. *Electric Technology and Civil Engineering (ICETCE), 2011 International Conference*, 1805-1807.

OCCDC. (2010). Earth Ranger Wildlife Centre. *Case Study, 3*(4), 1-2.

Parsons, B. (2011). Earth Rangers Revisited. *Canadian Consulting Engineer, 52*(3), 14-18.

OMEGA. (2012). *OS950 SERIES Handheld Infrared Thermometers User's Guide.* OMEGA Engineering Inc.

Pérez-Lombarda, L., Ortiz, J., & Pout, C. (2008). A Review on Buildings Energy Consumption Information. *Energy and Buildings, 40*(3), 394-398.

Pfafferott, J. (2003). Evaluation of Earth-to-Air Heat Exchangers with a Standardised Method to Calculate Energy Efficiency. *Energy and Buildings, 35*(10), 971–983.

Schild, P. G. (2001). An Overview of Norwegian Buildings with Hybrid Ventilation. *Hybrid Ventilation: An Integral Solution for Ventilation, Health and Energy, Second International One-Day Forum,* 49-68.

Schild, P. G. (2002). Pilot Study Report: Jaer School, Nesodden Municipality, Norway. *International Energy Agency Energy Conservation in Building and Community Systems Annex 35: HybVent.*

Schoeneich, P. (2011). Guide Lines for Monitoring: GST Ground Surface Temperature. *PermaNET, 3,* 1-8.

Sharan, G., & Jadhav, R. (2003). Performance of Single Pass Earth-Tube Heat Exchanger: An Experimental Study. *Journal of Agricultural Engineering, 40*(1), 1-18.

Sharan, G., Prakash, H., & Jadhav, R. (2004). Performance of Greenhouse Coupled to Earth-Tube-Heat-Exchanger in Closed-Loop Mode. *Indian Institute of Management Ahmedabad Working Papers, WP2004-03-02.*

Tarnawski, V. R., Leong, W. H., Momose, T., & Hamada, Y. (2009). Analysis of Ground Source Heat Pumps with Horizontal Ground Heat Exchangers for Northern Japan. *Renewable Energy, 34*(1), 127-134.

Thevenard, D. (2007). *Bibliographic Search on the Potential of Earth Tubes*. Numerical Logics Inc.

Tjelflaat, P. O. (2000). Pilot Study Report: Medi å School, Grong, Norway. *International Energy Agency Energy Conservation in Building and Community Systems Annex 35: HybVent.*

Tjelflaat, P. O., Zhang, J., & Haghighat, F. (2011). Measurements of Cooling Performance for an Earth-to-Air Heat Exchanger with an Axial Entrance Fan. *The 12th International Conference on Air Distribution in Rooms*, 291-298.

Trillat-Berdal, V., Souyri, B., & AchAaurgdu, G. (2005). Numerical Study of the Evolution of Ground-Coupled Heat Pump System Performance. *9th International Building Performance Simulation Association*, 1245-1252.

Trzaski, A., & Zawada, B. (2011). The Influence of Environmental and Geometrical Factors on Air-Ground Tube Heat Exchanger Energy Efficiency. *Building and Environment, 46*(7), 1436-1444.

UofC. (2010). *Energy Environment Experiential Learning.* Retrieved August 22, 2011 from http://www.ucalgary.ca/fmd/buildings/eeel

U.S. Department of Energy. (2012a). *Buildings Energy Data Book.* Retrieved October 20, 2012, from http://buildingsdatabook.eren.doe.gov/TableView.aspx?table=1.1.3

U.S. Department of Energy. (2012b). *Buildings Energy Data Book.* Retrieved October 20, 2012, from http://buildingsdatabook.eren.doe.gov/TableView.aspx?table=1.4.1

Wachenfeldt, B. J. (2003a). *Natural Ventilation in Buildings Detailed Prediction of Energy Performance*. Doctoral Dissertation summary, Norwegian University of

Science and Technology, Trondheim, Norway. Retrieved August 19, 2011, from http://ntnu.diva-portal.org/smash/record.jsf?pid=diva2:126227

Wachenfeldt, B. J. (2003b). *Natural Ventilation in Buildings Detailed Prediction of Energy Performance*. Unpublished Doctoral Dissertation, Norwegian University of Science and Technology, Trondheim, Norway**.** in Zhang, J., & Haghighat, F. (2005). Simulation of Earth-to-Air Heat Exchangers in Hybrid Ventilation Systems. *9th International Building Performance Simulation Association Conference*, 1417-1424.

Williams, G. P., & Gold, L. W. (1976). Ground Temperatures. *Canadian Building Digests, Division of Building Research, National Research Council Canada, UDC 551.525*, CBD180-180-4.

World Meteorological Organization. (2012). *World Weather Information Service*. Retrieved August 22, 2011 from http://www.worldweather.org/056/c00622.htm

Wu, Y., Gan, G., Gonzalez, R. G., & Verhoef, A. (2011). Prediction of the Thermal Performance of Horizontal-Coupled Ground-Source Heat Exchangers. *International Journal of Low-Carbon Technologies, 6*(4), 261-269.

Zhang, J., & Haghighat, F. (2005). Simulation of Earth-to-Air Heat Exchangers in Hybrid Ventilation Systems. *9th International Building Performance Simulation Association Conference*, 1417-1424.

Zhang, J., & Haghighat, F. (2009). Convective Heat Transfer Prediction in Large Rectangular Cross-Sectional Area Earth-to-Air Heat Exchangers. *Building and Environment, 44*(9), 1892–1898.

Zhang, J., Haghighat, F., Wachenfeldt, B. J., Tjelflaat, P. O., & Inger, A. (2009). Field Measurements and CFD Simulations of a Large Cross-Sectional Area ETAHE. *The 11th International Conference on Air Distribution in Rooms*, 1-7.

Zhang, J. (2009). *Investigation of Airflow and Heat Transfer in Earth-to-Air Heat Exchanger*s. Unpublished Master's Thesis, Concordia University, Montreal, Quebec, Canada.

APPENDIX A: EEEL AHUS VENTILATION PLAN

Provided by EllisDon.

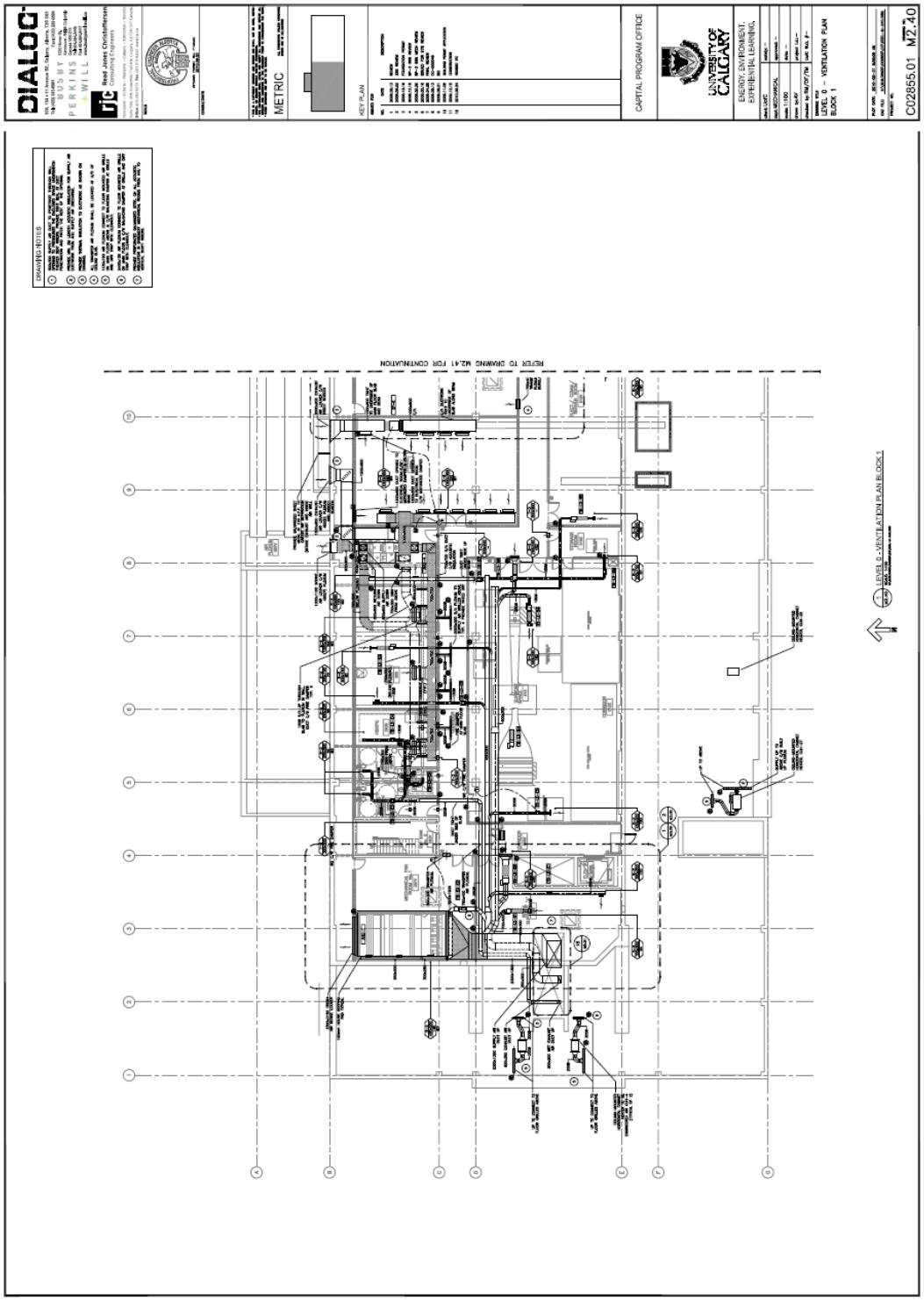

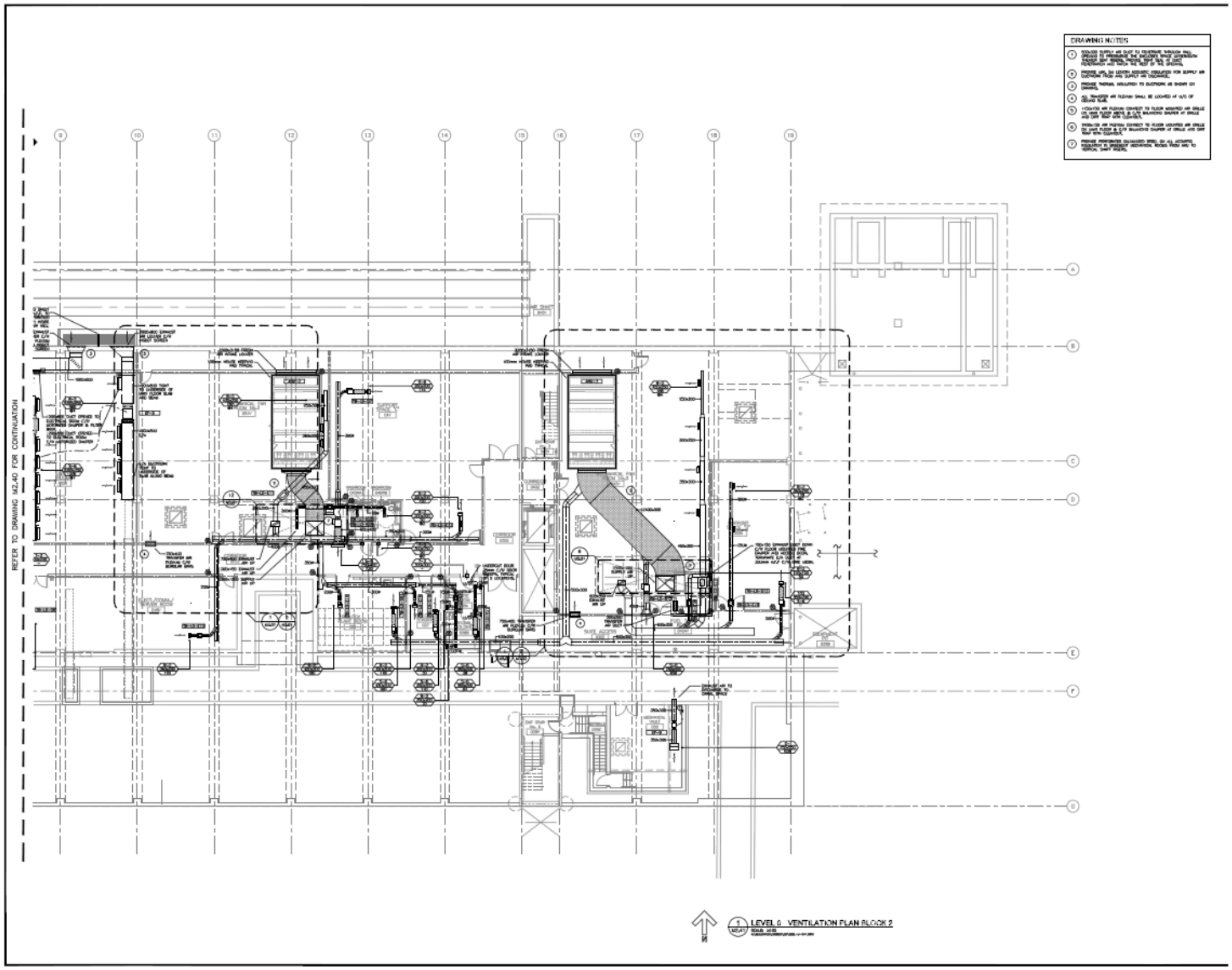

DIALOG

BUSBY PERKINS + WILL

rjc Read Jones Christoffersen Consulting Engineers

METRIC

KEY PLAN

ISSUED FOR

NO.	DATE	DESCRIPTION
1	2020/05/12	REVIEW
2	2020/06/03	SDE REVIEW
3	2020/06/18	FOR DESIGN REPORT
4	2020/07/15	DP-1 DDE REVIEW
5	2020/08/26	DP-2 SDE MECH. REVIEW
6	2020/09/18	ISSUED FOR SITE REVIEW
7	2020/09/28	FINAL REVIEW
8	2020/10/12	IC-ISSUED
9	2020/10/21	IBC
10	2020/11/25	BUILDING PERMIT APPLICATION
11	2020/12/15	CONSTRUCTION
12	2021/01/04	REVISED #1

CAPITAL PROGRAM OFFICE

UNIVERSITY OF CALGARY

ENERGY ENVIRONMENT EXPERIENTIAL LEARNING

drawn: DaVC	editing: --
dept: MECHANICAL	approved: --
scale: 1:100	date: --
drawn by: RV/JF	project: tube --
checked by: RM/DF/TM	sub: mod. # --

DRAWING TITLE
LEVEL 0 - VENTILATION PLAN
BLOCK 2

PLOT DATE: 2021-01-12 3:08:01 PM

CAD FILE: M:\2020\C02855.01\ARCH\CAD\REVIT\C02855_M_BLOCK2.RVT

PROJECT NO.
C02855.01

DRAWING NO.
M2.41

APPENDIX B: AHU-4 SPECIFICATION

Provided by EllisDon.

EngA ENGINEERED AIR

SUBMITTAL RECORD

JOB NAME: EEEL-BP3 BUILDING RENOVATION **JOB NO:** 45819(C35996)

CUSTOMER: TROTTER & MORTON BUILDING **ENGINEER:** COHOS EVAMY

EngA MODEL: LM6/C/HRP **QTY:** 1 **TAG:** AHU-4

SHIPPING AND APPROVAL INFORMATION

MOUNTING Indoor Base Mounted **ACCESS** As Per Drawing

NO. OF PIECES 1 Unit **SHIPPING WEIGHT** 10750 lb (4886 kg)

- CETL approval.
- Unit operates at the altitude of 0-4500 ft(0-1372 m).

SUPPLY AIR DATA

AIR FLOW 5,000 CFM (2,360 l/s) **FAN SIZE** (2) 182 MPQN **TSP** 5.0 in w.c. (1245 Pa) **RPM** 2269

MOTOR SIZE 5 HP (3.73 kW) **TYPE (RPM)** TECO TEFC (1750) **ESP** 2.0 in w.c. (498 Pa) **BHP** 2.98 BHP (2.22 kW)

- Supply air fan c/w direct drive motor and 2"(51 mm) deflection spring vibration isolation.
- Unit mounted Danfoss adjustable speed drive. Normal operating airflow of 5,000CFM (2,360 l/s) at 71Hz operating frequency. Minimum operating airflow of 1,750 CFM (826 l/s) at 25Hz operating frequency c/w input line reactors, load reactors and manual bypass.

EXHAUST AIR DATA

AIR FLOW 5,000 CFM (2,360 l/s) **FAN SIZE** (2) 182 MPQN **TSP** 3.3 in w.c. (822 Pa) **RPM** 1913

MOTOR SIZE 3 HP (2.24 kW) **TYPE (RPM)** TECO TEFC (1750) **ESP** 2.0 in w.c. (498 Pa) **BHP** 1.93 BHP (1.44 kW)

- Exhaust air fan c/w direct drive motor and 2"(51 mm) deflection spring vibration isolation.
- Unit mounted Danfoss adjustable speed drive. Normal operating airflow of 5,000CFM (2,360 l/s) at 60Hz operating frequency. Minimum operating airflow of 1,750 CFM (826 l/s) at 21Hz operating frequency c/w input line reactors, load reactors and manual bypass.

AIR OPENING DATA

AIR OPENING	LOCATION	DAMPER TYPE	OPERATION
SUPPLY AIR	Top		
RETURN AIR	Top		
OUTSIDE AIR	Back	See Below [1]	By Others
EXHAUST AIR	Top		

- [1] - TAMCO Series 1000 Low Leakage Aluminum Air-foil Opposed Blade
- Damper operators supplied and installed by others where damper shaft terminated inside unit.

CONSTRUCTION DATA

UNIT CABINET	16 gauge satin coat galvanized sheet metal c/w 2" (51 mm) 3 lb/ft³ (48 kg/m³) insulation on entire unit casing.
UNIT LINER	24 gauge perforated liner throughout except any filter sections, coil sections and unit underside.
	22 gauge solid liner on any filter sections, coil sections, humidifier section and unit underside.
	22 gauge stainless steel liner on cooling coil and humidifier sections.
UNIT FLOOR	14 gauge welded black iron checker plate c/w rust inhibitor coating and 1.5" (38mm) upstands on entire unit floor.
EXTERIOR PAINT	Electrostatically applied enamel(gray colour) on all exterior surface but not including unit underside.
AIRSIDE DOOR	Filter, blower and plenum access - AJ doors c/w lockable lever type door handles and double pane tempered glass window.
	Humidifier access - AJ doors c/w lockable lever type door handles
SERVICE DOOR	Electrical access - hinged c/w lockable lever type door handle

DATE 14-Oct-2009 - 1 - Continued on page 2

EngA ENGINEERED AIR

SUBMITTAL RECORD

JOB NAME: EEEL-BP3 BUILDING RENOVATION JOB NO: 45819(C35996)

CUSTOMER: TROTTER & MORTON BUILDING ENGINEER: COHOS EVAMY

EngA MODEL: LM6/C/HRP QTY: 1 TAG: AHU-4

CONSTRUCTION DATA (CONTINUED)

DRAIN PAN Stainless steel drain pan c/w drain connection through casing on cooling coil section.
Stainless steel drain pan c/w floor drain connection through base frame on humidifier section and heat pipe supply and exhaust section.

- Heat Pipe : (1) QDT Heat pipe energy reclaim coil installed (See attached performance data) c/w aluminum tubes/fins, galvanized steel casing and R134A refrigerant.
- Humidifier plenum is for future use with grids supplied by others.
- Humidifier plenum is 36" (914mm) in length, but the absorption distcance is 16" (406mm) before the top discharge opening due to length restrictions.
- Paint is lead and cadmium free.

ELECTRICAL DATA

POWER SUPPLY	MAIN FEEDER AMPACITY	MAXIMUM FUSE(D.E.)	MAXIMUM BREAKER
575 / 3 / 60	18.1 AMPS	25 AMPS	25 AMPS

- See Electrical Data Sheet for details.
- (7) marine lights c/w an on/off switch with indicating light and (1) service receptacle unit mounted on unit exterior - 120V/1PH/ 60HZ power supply by others.

SUMMER AND WINTER FILTER SECTION DATA - Side Loaded

FILTER TYPE Farr 30/30 Pleated Filter c/w Metal Frame with MERV 8 (25-30% Eff)

QTY/SIZE 2 - 24 x 12 x 2" (610 x 305 x 51 mm) QTY/SIZE 2 - 24 x 20 x 2" (610 x 508 x 51 mm)

TOTAL GROSS AREA 10.67 SQ.FT. (0.99 SQ. MTRS) FACE VELOCITY 469 FPM (2.38 m/s)

- Filters may be shipped loose or mounted in the tracks.
- 1 spare set of filters - shipped loose
- Dwyer series 2000 magnehelic gauge 0-1" wc across summer filter section

FINAL FILTER SECTION DATA - Side Loaded

FILTER TYPE EngPac Syn Rigid Filter c/w header with MERV 13 (90-95% Eff)

QTY/SIZE 2 - 24 x 12 x 12" (610 x 305 x 305 mm) QTY/SIZE 2 - 24 x 20 x 12" (610 x 508 x 305 mm)

TOTAL GROSS AREA 10.67 SQ.FT. (0.99 SQ. MTRS) FACE VELOCITY 469 FPM (2.38 m/s)

- Filters may be shipped loose or mounted in the tracks.
- Dwyer series 2000 magnehelic gauge 0-2" wc across final filter section c/w valve for winter pre-filter section

EXHAUST FILTER SECTION DATA - Side Loaded

FILTER TYPE Farr 30/30 Pleated Filter c/w Metal Frame with MERV 8 (25-30% Eff)

QTY/SIZE 2 - 24 x 12 x 2" (610 x 305 x 51 mm) QTY/SIZE 2 - 24 x 20 x 2" (610 x 508 x 51 mm)

TOTAL GROSS AREA 10.67 SQ.FT. (0.99 SQ. MTRS) FACE VELOCITY 469 FPM (2.38 m/s)

- Filters may be shipped loose or mounted in the tracks.

HYDRONIC HEATING COIL DATA

COIL SIZE 48 (1219) x 30 (762) x 2R x 12 FPI VELOCITY 500 FPM (2.54 m/s)

CAPACITY 433,010 Btuh (126.9 kW) AIR P.D. 0.19 in.wc. (47 Pa)

ENTERING AIR DB -20°F (-28.9°C) LEAVING AIR DB 71.6°F (22.0°C)

FLUID MEDIUM 50% Propyl-Glycol CONN. SIZE (In & Out) 1 1/2 in (38 mm) FLUID P.D. 4.4 FT (13 kPa)

FLUID FLOW RATE 23.6 US.GPM (1.5 l/s) ENTERING FLUID TEMP 170°F (76.7°C) LVG. FLUID TEMP 129.1°F (53.9°C)

- Heating coil c/w MPT connections.

EngA ENGINEERED AIR

SUBMITTAL RECORD

JOB NAME: EEEL-BP3 BUILDING RENOVATION JOB NO: 45819(C35996)

EngA MODEL: LM6/C/HRP QTY: 1 TAG: AHU-4

HYDRONIC HEATING COIL DATA (CONTINUED)

- Freeze protection by others.

HYDRONIC COOLING COIL DATA

COIL SIZE 48 (1219) x 30 (762) x 3R x 12 FPI		VELOCITY 500 FPM (2.54 m/s)	
CAPACITY 138,570 Btuh (40.6 kW)		AIR P.D. 0.34 in.wc. (85 Pa)	
ENTERING AIR DB / WB 90°F (32.2°C) / 62.0°F (16.7°C)		LEAVING AIR DB / WB 61.0°F (16.1°C) / 51.7°F (10.9°C)	
FLUID MEDIUM Water	CONN. SIZE (In & Out) 2 in (51 mm)	FLUID P.D. 6.6 FT (20 kPa)	
FLUID FLOW RATE 28.8 US.GPM (1.8 l/s)	ENTERING FLUID TEMP 50°F (10.0°C)	LVG. FLUID TEMP 59.6°F (15.3°C)	

- Cooling coil c/w stainless steel casing, stainless steel drain pan and MPT connections.

SHIPPED LOOSE ITEMS (See filter sections for filters and spare filters)

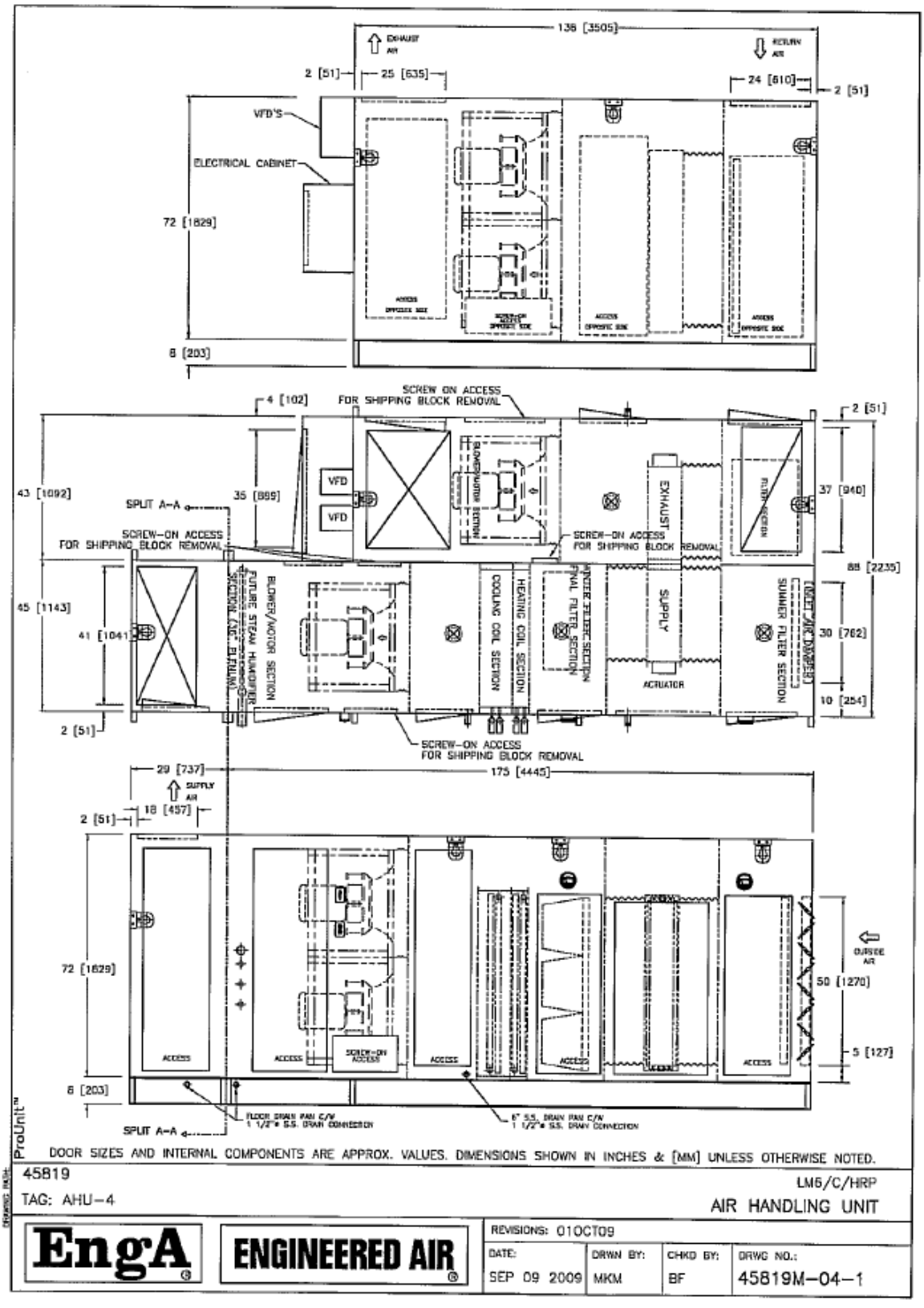
138 [3505]
EXHAUST AIR
RETURN AIR
2 [51]
25 [635]
24 [610]
2 [51]
VFD'S
ELECTRICAL CABINET
72 [1829]
8 [203]
ACCESS OPPOSITE SIDE
4 [102]
SCREW ON ACCESS FOR SHIPPING BLOCK REMOVAL
2 [51]
43 [1092]
SPLIT A-A
35 [889]
VFD
VFD
BLOWER/MOTOR SECTION
EXHAUST
FILTER SECTION
37 [940]
SCREW-ON ACCESS FOR SHIPPING BLOCK REMOVAL
SCREW-ON ACCESS FOR SHIPPING BLOCK REMOVAL
88 [2235]
45 [1143]
41 [1041]
FUTURE STEAM HUMIDIFIER SECTION (24" DEPTH)
BLOWER/MOTOR SECTION
COOLING COIL SECTION
HEATING COIL SECTION
FINER FILTER SECTION
FINAL FILTER SECTION
SUPPLY
ACTUATOR
SUMMER FILTER SECTION
MIXING AIR DAMPER
30 [762]
10 [254]
2 [51]
SCREW-ON ACCESS FOR SHIPPING BLOCK REMOVAL
29 [737]
175 [4445]
SUPPLY AIR
18 [457]
2 [51]
72 [1829]
ACCESS
SCREW-ON ACCESS
OUTSIDE AIR
50 [1270]
5 [127]
8 [203]
FLOOR DRAIN PAN C/W 1 1/2" S.S. DRAIN CONNECTION
6" S.S. DRAIN PAN C/W 1 1/2" S.S. DRAIN CONNECTION
SPLIT A-A
ProUnit™
DOOR SIZES AND INTERNAL COMPONENTS ARE APPROX. VALUES. DIMENSIONS SHOWN IN INCHES & [MM] UNLESS OTHERWISE NOTED.
45819
TAG: AHU-4
LM6/C/HRP
AIR HANDLING UNIT
EngA
ENGINEERED AIR
REVISIONS: 01OCT09
DATE: SEP 09 2009
DRWN BY: MKM
CHKD BY: BF
DRWG NO.: 45819M-04-1

EngA | ENGINEERED AIR

HEAT PIPE PERFORMANCE DATA
Version 1.2.4

JOB NAME: EEEL-BP3 BUILDING RENOVATION
JOB NO: 45819(C35996)
CUSTOMER: TROTTER & MORTON BUILDING
ENGINEER: COHOS EVAMY
LOCATION: Calgary, AB
ALTITUDE: 3540 ft (1078.9 m)
EngA MODEL: LM6/C/HRP QTY: 1 TAG: AHU-4

Heat Pipe Selection Data - HVAC			
		Supply	Exhaust
Winter Design (Note 1)	Fan Location	Heat Pipe Outlet	Heat Pipe Outlet
	Air Flow Through Pipe	5000 ACFM	5000 ACFM
	Standard Velocity Thr Pipe	507 fpm	449 fpm
	Entering Temp. DB/WB	-22.0/-22.0°F	70.0/58.0°F
	Leaving Temp. DB/WB(RH)	18.1/12.0°F(12%)	40.9/40.9°F(100%)
	Air Pressure Drop	0.57"wc	0.60"wc
	Energy Recovery	211.5	
	Supply Recovery Factor	43.6% (Note 2)	
	Tilt Conirol Factor		9425
	Moisture Condense Out		0.98 Lbs/Min
	Frost Point		-14.6°F

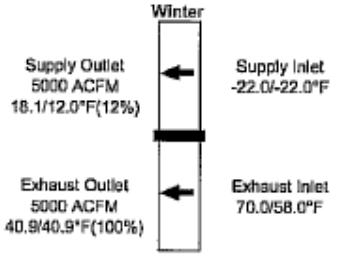

System: (1) Tru in an integrated tilt package Type: Corrugate Aluminum fin, 5/8" O.D. aluminum tube										
Unit ID	TRU Model	Face Height	Face Length	Row	Exh FPI	Sup FPI	Type	Exh Length	Sup Length	Weight (LBS)
1	TRU-120	- 49.5	- 58	- 6	- 10E	- 10S	- AC5	- 30	28	414

Unit(Dimensions are in inches)	Length	Width	Height
Integrated tilt package model: TP-120-3E-20	62	36	64
Integrated tilt package crated dimensions:	68	40	67

Unit	Weight in lbs
TRU unit weight	414
Integrated tilt package w/o Tru(s)	589
Total system weight	1003
Crated system weight	1298

Notes: 1. Pipe performance in the winter design section includes the effects of frost control.
2. Without taking frost control into account, the Supply Recovery Factor is 52.6%.

DATE: 21-Sep-2009 SUBMITTED BY: MKM

EngA ENGINEERED AIR

ELECTRICAL DATA

JOB NAME: EEEL-BP3 BUILDING RENOVATION **JOB NO:** 45819(C35996)

EngA MODEL: LM6/C/HRP **QTY:** 1 **TAG:** AHU-4

Power Supply	Main Feeder Ampacity	Terminal Block to Accept	Maximum Fuse (Dual Element)	Maximum Breaker	Minimum Unfused Conductor
575 / 3 / 60	12.1 AMPS	14 Awg	15 AMPS	15 AMPS	14 Awg

Components	Model	Minimum Conductor Size	Ampacity FLA / LRA
Supply Fan Motors #1 and #2	TECO TEFC (1750) 3 HP	14 Awg	3.3
Exhaust Fan Motors #1 and #2	TECO TEFC (1750) 2 HP	14 Awg	2.1
Main Control Xfmr		14 Awg	.4

WIRING DRAWING LEGEND

AFS	Auto Fan Switch	DM	Damper Motor	LAR	Low Ambient Relay
C	Contactor	FR	Fan Relay	NFD	Non Fused Disconnect
CCH	Compressor Crankcase Heater	GV1	Low Stage Gas Valve	OL	Thermal Overload
CFC	Condenser Fan Control	GV2	High Stage Gas Valve	OP	Oil Failure Switch
CLC	Compressor Loading Control	HR	Heating Relay	PV	Pilot Gas Valve
CPM	Compressor Protection Module	HLPC	High/Low Pressure Control	R	Relay or Contactor
CP	Internal Compressor Protection	HL	High Limit Control	SS	Sail Switch
CR	Cooling Relay	IGN	Ignition Control	TB	Terminal Block
CUC	Cylinder Unloading Control	LAC	Low Ambient Control	TDR	Time Delay Relay
CUS	Cylinder Unloading Solenoid	LPC	Low Pressure Control	TC	Time Clock

UNIT FUNCTION

Disconnect switch (by others) 'on', duct high pressure limit contact (by others) 'closed' service switch 'on', fan unit on/off contact (by others) 'closed', outside air damper opens, blowers delay on and run continuously to a minimum airflow of 1,750CFM (25Hz).

The QTRAC with an adjustable integral set point set at 70°F (21.1°C) will tilt the heatpipe as required to provide leaving air temperature regulation, summer/winter changeover, and frost control when required.

Fan on/off contact (by others) 'off', blowers shut down, unit is off.

Note 1 - Refer to manuals shipped with unit for a more detailed explanation of maintenance, component(s) and/or controller(s).

DATE: 22-SEP-2009 **SUBMITTED BY:** STEVE KUZMA / MKM

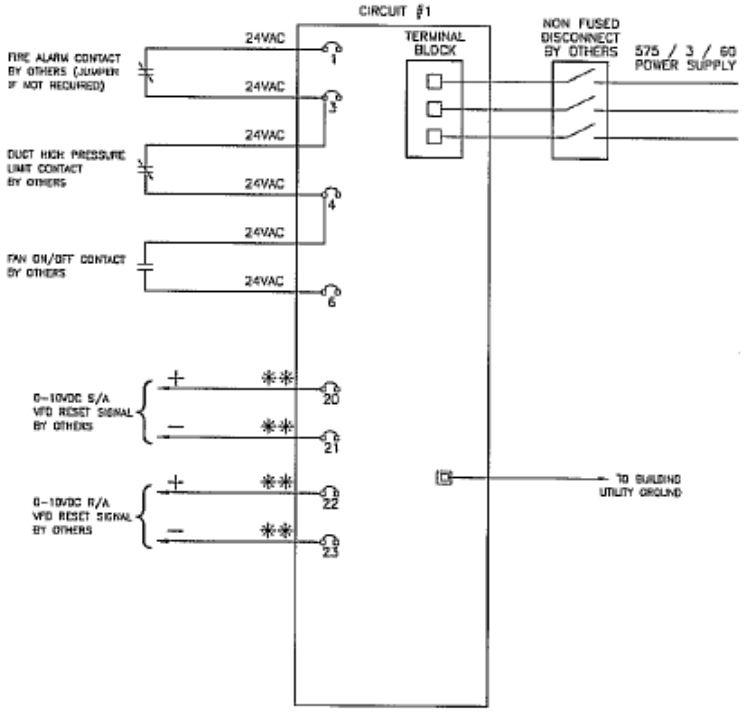

MAXIMUM CONTROL CIRCUIT AMPACITY 10.42 AMPS AT 24 VAC

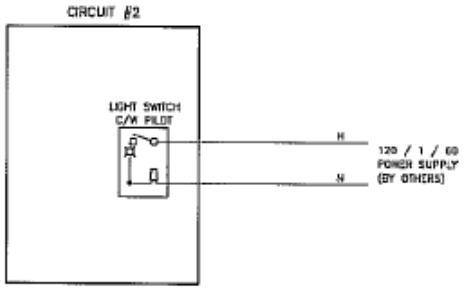

** SHIELDED WIRE IS REQUIRED WITH BMS ANALOG SIGNALS. TAPE OTHER END OF GROUND WIRE & SHIELD ENDS OF ANY UNUSED WIRES.

1. FIELD WIRING VOLTAGE DROP NOT TO EXCEED 10%.
2. ALL WIRING SHOWN SHALL BE COMPLETED BY INSTALLER.
3. ALL WIRING TO COMPLY WITH THE CANADIAN ELECTRICAL CODE.

TAG: AHU-4

FIELD WIRING DIAGRAM
LM SERIES

EngA ENGINEERED AIR

REVISIONS:			
DATE:	DRN.BY:	CHKD.BY:	DRWG.NO.:
15SEP09	MKM	BF	45819F-04-1

45819

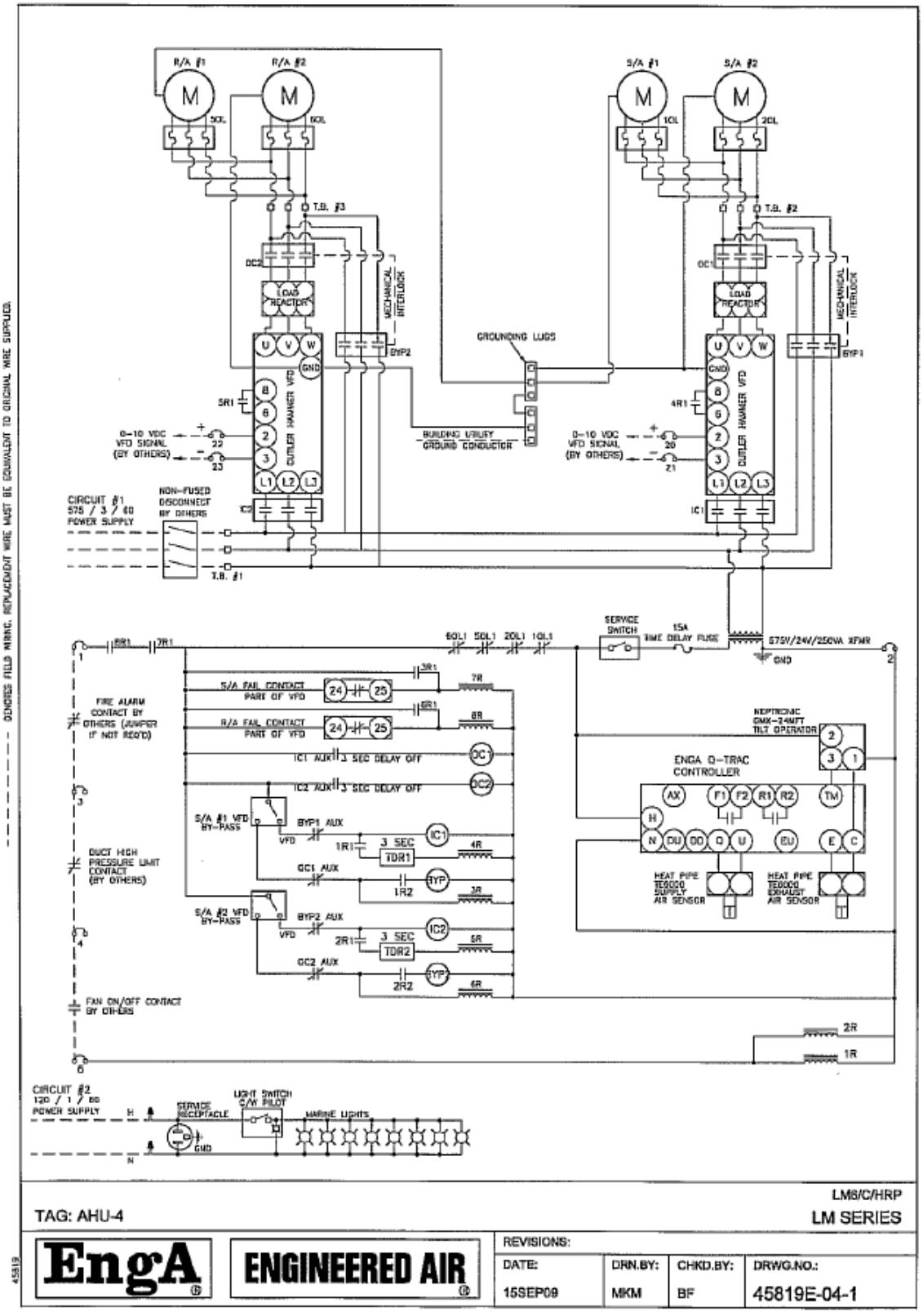

LM6/C/HRP

TAG: AHU-4

LM SERIES

EngA ENGINEERED AIR

REVISIONS:			
DATE:	DRN.BY:	CHKD.BY:	DRWG.NO.:
15SEP09	MKM	BF	45819E-04-1

82

Customer:	Fan Tag: S/A FAN AHU-4
Job ID:	Model: 182 MPGN

CFM:	2,500
SP:	5 in.wg
RPM:	2375
BHP:	2.98
Outlet Velocity:	480
Density:	0.066

Corrected for:
% width: 60%
Altitude 3,540

TWIN CITY FAN AND BLOWER PERFORMANCE CURVE

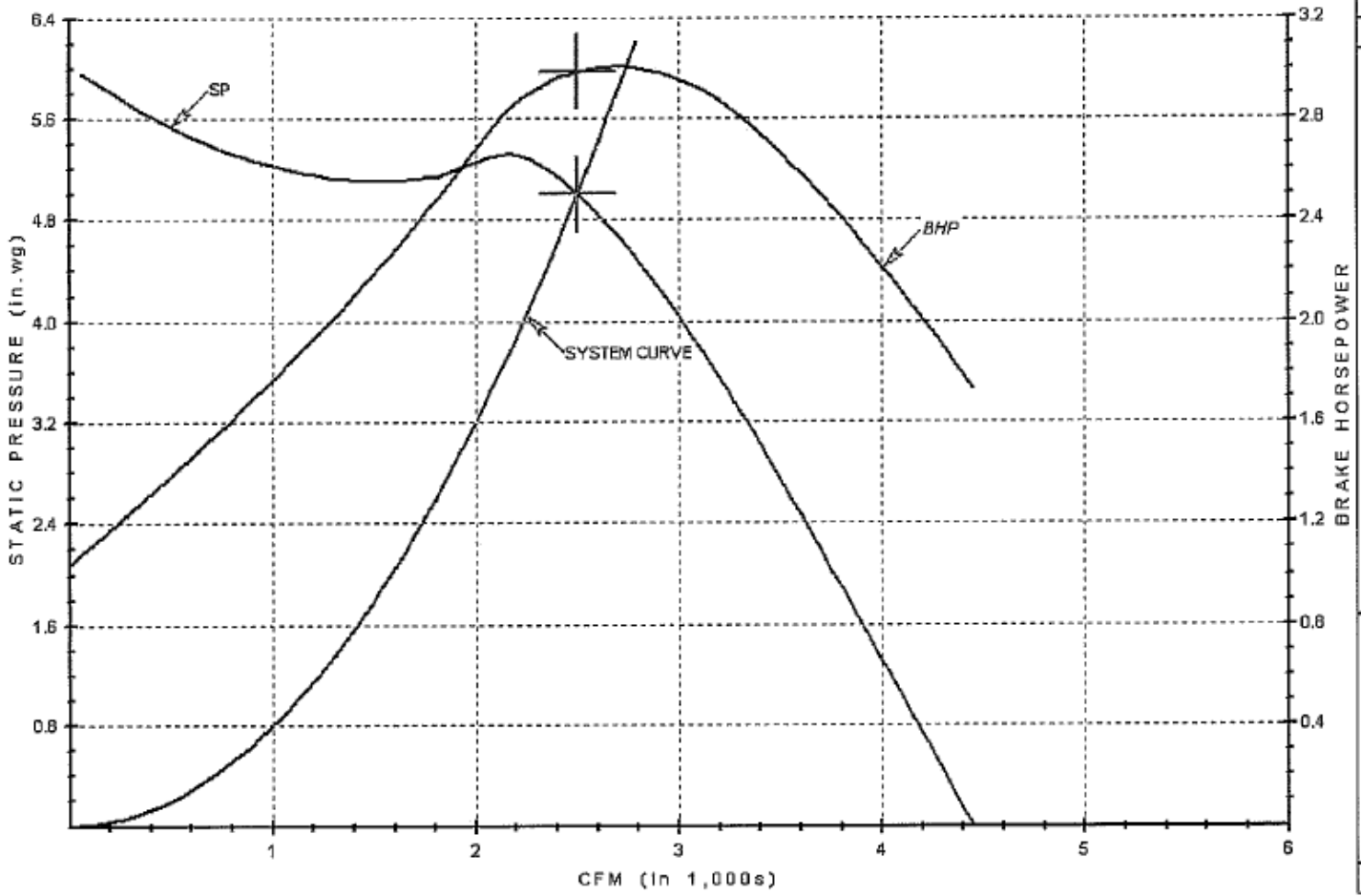

Sound Power Level

Octave	In/Out
1	79 / 83
2	79 / 82
3	77 / 75
4	82 / 77
5	72 / 72
6	74 / 71
7	69 / 67
8	65 / 67

In db re 10^{-12} watts

10/16/2009 09:06

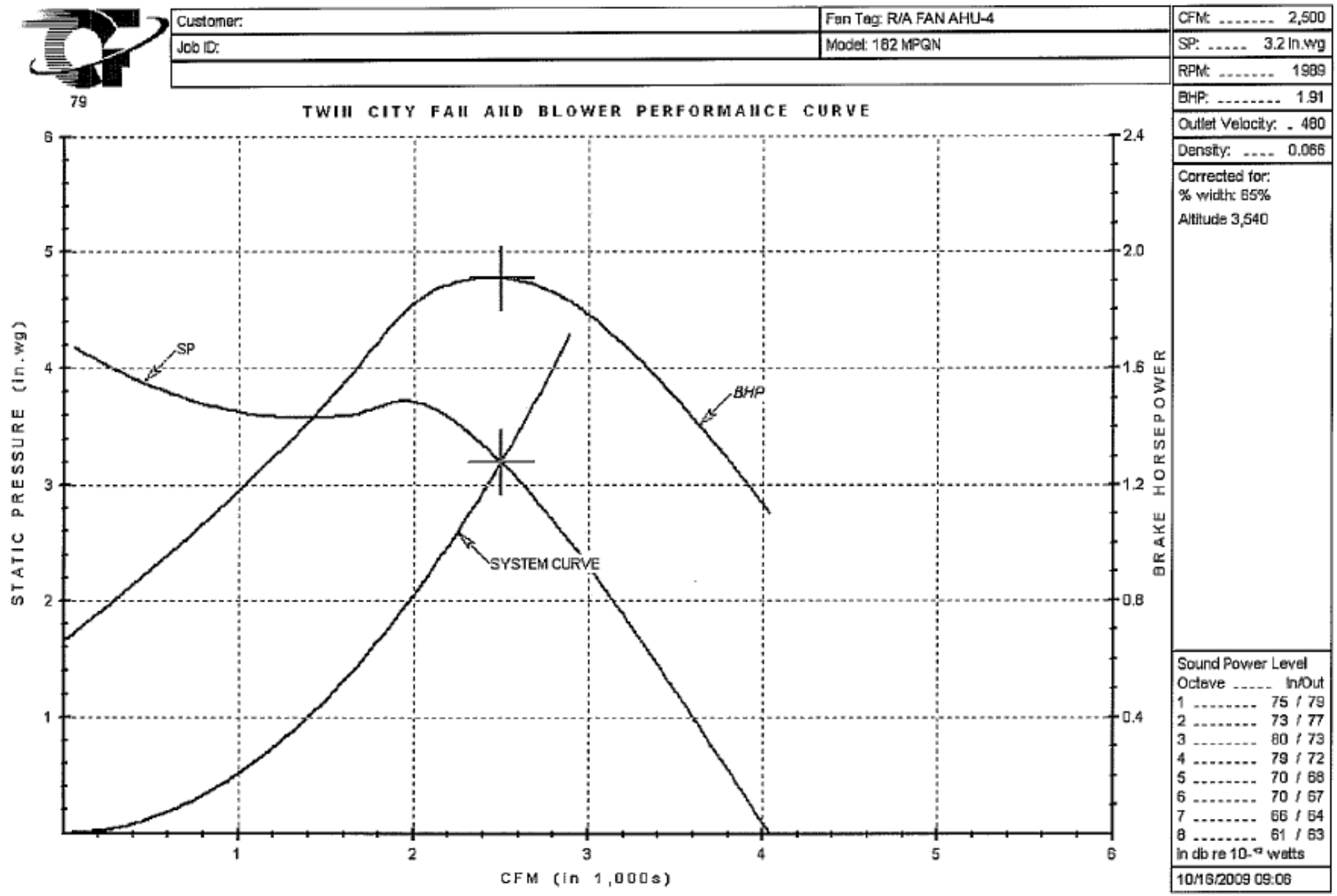
79
Customer:
Job ID:
Fan Tag: R/A FAN AHU-4
Model: 182 MPQN
CFM: 2,500
SP: 3.2 in.wg
RPM: 1989
BHP: 1.91
Outlet Velocity: 480
Density: 0.066
Corrected for:
% width: 65%
Altitude 3,540
TWIN CITY FAN AND BLOWER PERFORMANCE CURVE
STATIC PRESSURE (in.wg)
BRAKE HORSEPOWER
CFM (in 1,000s)
SP
BHP
SYSTEM CURVE
Sound Power Level
Octave In/Out
1 75 / 79
2 73 / 77
3 80 / 73
4 79 / 72
5 70 / 68
6 70 / 67
7 66 / 64
8 61 / 63
10/16/2009 09:06

APPENDIX C: EEEL SENSOR CALIBRATION NOTES

Prepared by Chris Lashmar, July, 2012

C.1 Disclaimer

These notes were constructed in 2012, two years after the June 2010 calibration test, using email, files and personal memory. Additional notes may have existed in a logbook but it was stolen.

C.2 Method

Twenty labelled 109BAM temperature sensors were submerged in a bath of water with ice. A pump circulated the water to ensure even temperature distribution of the water. The sensors were connected to a multiplexor that was connected to a CR1000. The CR1000 program that was probably used is shown in Appendix C.1.

Results were recorded over the period of June 24th and June 25th, 2010. The wiring that was probably used until 9:09 June 25th is described in Appendix C.2. For referral purposes here, this period will be referred to as Test 1. After 9:09, sensors S5-S8 were disconnected and sensors S17-S20 were connected to the terminals previously occupied by S5-S8. This period will be referred to as Test 2.

C.3 Results

The data collected for Test 1 showed a discrepancy of about 0.5 ℃ between two sets of sensors: S1-S4 and S17-S20 comprised one set and S5-S16 comprised the other set. On

June 25th, 2010, an email sent by Chris Lashmar to Jim Love on behalf of Danielle Coolman and Chris refers to a 'doubling up' on the ports with S1-S4 and S17-S20. It is for this reason that sensors S5-S8 were disconnected and S17-S20 were connected to the terminals previously occupied by S5-S8. Because sensors S9-S16 should be the least affected by the wiring changes, the average values of sensors S9-S16 at each measurement interval are used as the baseline for comparison. To compare sensors, temperature values from each sensor are subtracted from the baseline and graphed over time. Ideally, this difference would always be zero for all sensors.

Figure C.1 shows the difference between sensor values from S5-S16 and the baseline for Test 1.

Figure C.2 shows the difference between sensor values from S1-S4, S17-S20 and the baseline for Test 1. Because these results appear incorrect and Test 2 appears to correct the problem, the mean and standard deviation from these sensors for Test 1 are not calculated.

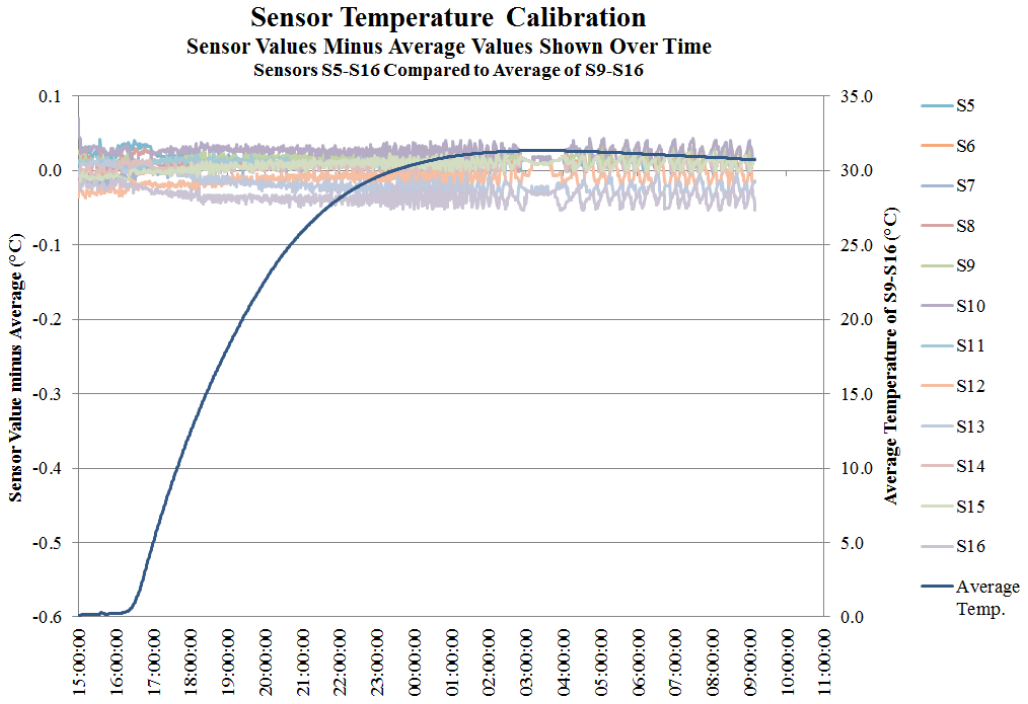

Figure C.1 Sensor Value Minus Average - Sensors S5-S16

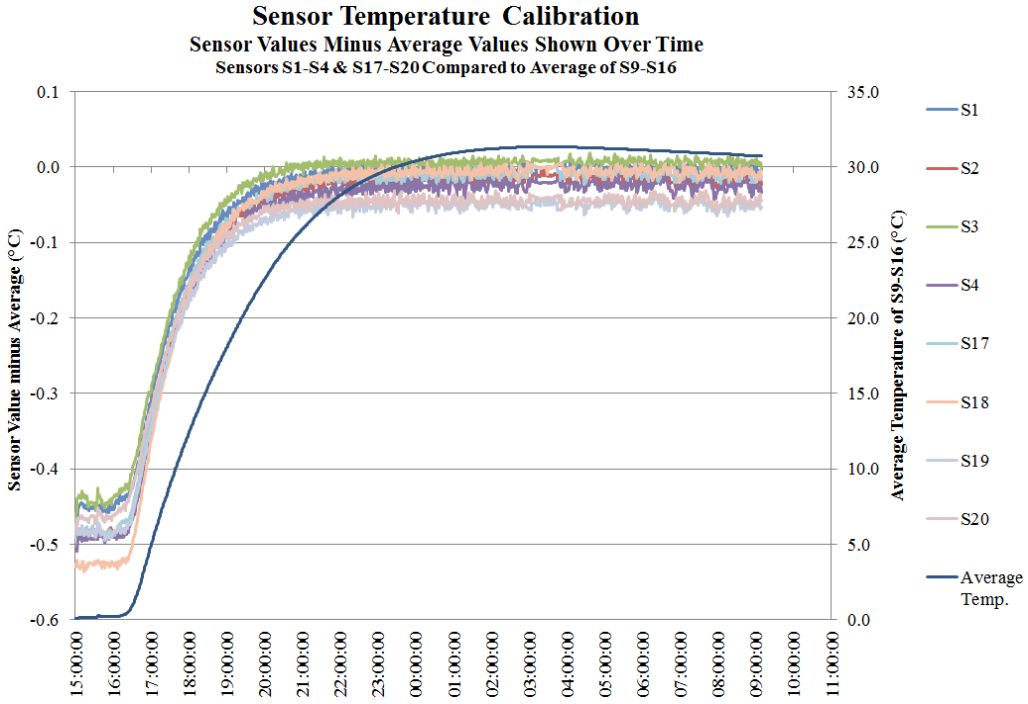

Figure C.2 Sensor Values Minus Average - S1-S4 & S17-S20

Test 2 data from 11:45 to 12:35 showed a higher average temperature and relatively large discrepancies and it is thought that the pump was probably not operating during that period, so that data is excluded from this analysis. However, Appendix C.3 does show the chart that includes this data, should that be of interest. Test 2 data from 12:35 onwards appears to be more reliable and is thus included the main analysis. Figure C.3 shows Test 2 results, displaying the difference between sensor values from S1-S4, S9-S20 and the baseline.

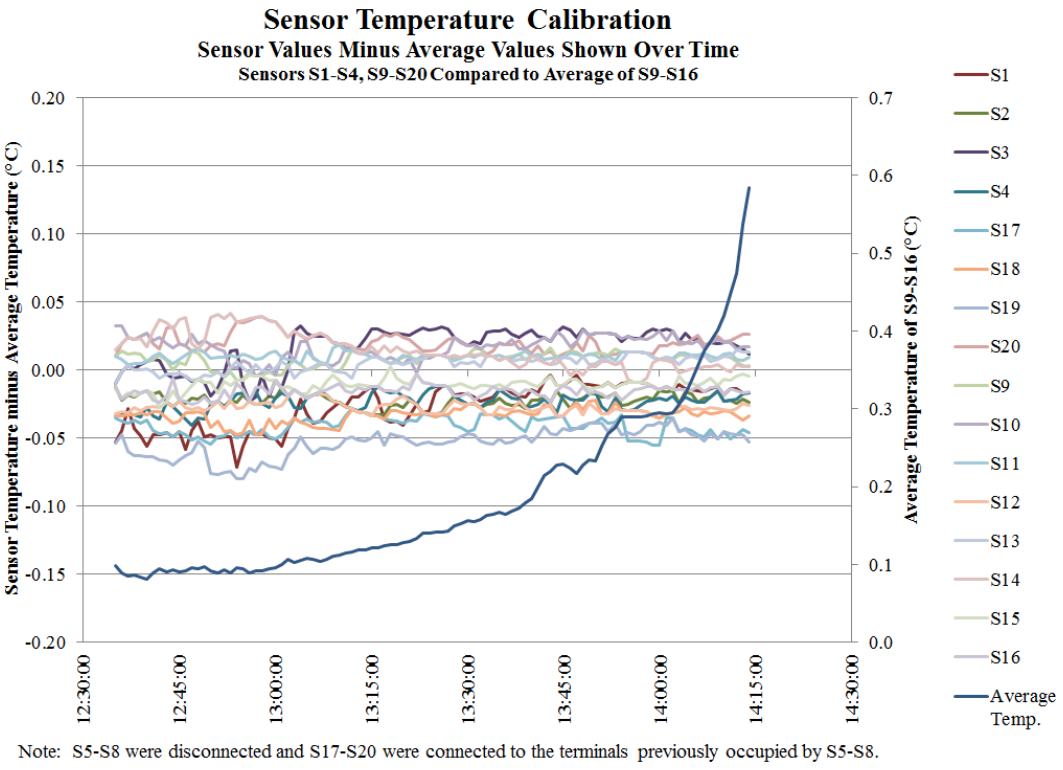

Figure C.3 Sensor Values Minus Average - Sensors S1-S4, S9-S20

Table C.1 shows the average and standard deviation values of the difference between each individual sensor measurement and the baseline value (i.e. the average value of S9-

S16). Worded another way, for each minute, the average of S9-S16 is calculated and subtracted from each sensor value. For each sensor there is now a collection of 'differences' which is averaged and analyzed to determine its standard deviation.

Table C.1 Average Difference (between Sensor and Baseline) and Standard Deviation

Sensor #	Test 1 Average	Test 1 Standard Deviation	Test 2 Average	Test 2 Standard Deviation
S1			-0.03	0.016
S2			-0.02	0.005
S3			0.02	0.015
S4			-0.02	0.006
S5	0.01	0.008		
S6	0.01	0.008		
S7	0.01	0.008		
S8	0.01	0.006		
S9	0.02	0.006	0.01	0.006
S10	0.02	0.008	0.02	0.008
S11	0.01	0.005	0.01	0.003
S12	-0.01	0.010	-0.03	0.004
S13	-0.02	0.012	0.00	0.005
S14	0.01	0.006	0.01	0.013
S15	0.01	0.008	-0.01	0.005
S16	-0.04	0.009	-0.02	0.004
S17			-0.04	0.007
S18			-0.03	0.005
S19			-0.05	0.010
S20			0.02	0.007

C.4 Conclusion

Most sensors measurements were within 0.03 ℃ of the average temperature most of the time. S19 values differed the most, and tended to measure about 0.05 ℃ colder with a

standard deviation of 0.01. All of these values are well within the accuracy value stated in the specifications of ±0.25 ℃.

C.5 Appendix

C.5.1 Appendix C.1

The program shown in Table C.2 is believed to be the program used during sensor calibration. It was last modified November 29th, 2010, long after the calibration was complete. But based on personal memory, it is believed that this program was recovered from one of the CR1000's or from a laptop. The code is quite different from the code implemented at the EEEL building and this is consistent with personal memory of the calibration and the test results.

Table C.2 CRBasic Program Probably Used for Calibration

```
'CR1000 Series Datalogger
'To create a different opening program template, type in new
'instructions and select Template | Save as Default Template
'date:
'program author:


'Declare Public Variables
'Example:
Public Batt_Volt
Public PanelT
Dim i
Public Temp109(20)



'Define Data Tables


DataTable (Minute,1,-1)
        DataInterval (0,1,Min,10)
        Minimum (1,Batt_Volt,FP2,False,False)
        Average (1,PanelT,FP2,False)
        Average (20,Temp109(1),FP2,False)
```

```
EndTable


'Main Program
BeginProg
        Scan (15,Sec,0,0)
                Battery (Batt_Volt)
                PanelTemp (PanelT,_60Hz)

                'Measure first 16 sensors on thermistor multiplexer
                'Turn on MUX
                PortSet (1,1 )
                'Begin loop
                For i = 1 To 16
                        'Advance port
                        PulsePort (2,10000)
                        Delay (0,10,mSec)
                        'Measure Sensor
                        Therm109 (Temp109(i),1,1,Vx1,0,_60Hz,1.0,0)
                Next i
                PortSet (1,0)

                'Measure next 4 sensors on multiplexer using same
```

```
'SE channel on logger but different VX channel
Delay (0,1000,mSec)
PortSet (1,1 )
'Advance port
PulsePort (2,10000)
Delay (0,10,mSec)
'Measure Sensor
Therm109 (Temp109(17),1,1,Vx2,0,_60Hz,1.0,0)
'Advance port
PulsePort (2,10000)
Delay (0,10,mSec)
'Measure Sensor
Therm109 (Temp109(18),1,1,Vx2,0,_60Hz,1.0,0)
'Advance port
PulsePort (2,10000)
Delay (0,10,mSec)
'Measure Sensor
Therm109 (Temp109(19),1,1,Vx2,0,_60Hz,1.0,0)
'Advance port
PulsePort (2,10000)
Delay (0,10,mSec)
'Measure Sensor
```

```
            Therm109 (Temp109(20),1,1,Vx2,0,_60Hz,1.0,0)
            PortSet (1,0)


            CallTable (Minute)
        NextScan
EndProg
```

C.5.2 Appendix C.2

Upon reviewing the program two years after the calibration, it is concluded that during Test 1, the time that measurements differed by nearly 0.5 ℃, the multiplexor was probably operating in 4X16 mode and that wiring may have been as shown in Table C.3.

Table C.3 Wiring Chart

Function	**Colour**	**Multiplexor**	**CR1000**
S1 109 BAM Excitation	Black	1H Terminal	
S1 109 BAM Signal	White	1L Terminal	
S1 109 BAM Shield	Clear	Ground	
S2 109 BAM Excitation	Black	3H Terminal	
S2 109 BAM Signal	White	3L Terminal	
S2 109 BAM Shield	Clear	Ground	
S3 109 BAM Excitation	Black	5H Terminal	
S3 109 BAM Signal	White	5L Terminal	
S3 109 BAM Shield	Clear	Ground	
		. . .	
S16 109 BAM Excitation	Black	31H Terminal	
S16 109 BAM Signal	White	31L Terminal	
S16 109 BAM Shield	Clear	Ground	
S17 109 BAM Excitation	Black	2H Terminal (Note the terminal is adjacent to that shared by S1)	
S17 109 BAM Signal	White	2L Terminal	
S17 109 BAM Shield	Clear	Ground	
S18 109 BAM Excitation	Black	4H Terminal	
S18 109 BAM Signal	White	4L Terminal	
S18 109 BAM Shield	Clear	Ground	
S19 109 BAM Excitation	Black	6H Terminal	
S19 109 BAM Signal	White	6L Terminal	
S19 109 BAM Shield	Clear	Ground	
S20 109 BAM Excitation	Black	8H Terminal	
S20 109 BAM Signal	White	8L Terminal	
S20 109 BAM Shield	Clear	Ground	
Mux Power	Red	12 V	12 V
Power Reference	Black	Ground	Ground
Mux Clock	Green	CLK	C(2)
Mux Reset	White	Res	C(1)
Shield	Clear		G
Excitation Source for S1-S16	Red	COM ODD H	VX1
Excitation Source for S17-S20	Black	COM EVEN H	VX2
Signal Return S1-16	White	COM ODD L	SE(1)

Function	Colour	Multiplexor	CR1000
Signal Return S17-S20	Green	COM EVEN L	SE(1)
Shield	Shield	COM ground	G

A RES24.9K-0.1 completion resistor connects SE(1) and the ground on the CR1000.

It is thought that the doubling up mentioned in the email refers to the fact that in 4X16 mode, the PulsePort command advances the channels in sets (e.g. {1H, 1L, 2H, 2L}, {3H, 3L, 4H, 4L}, etc), and that the first four sets include two sensors but the last 12 sets only include one sensor each.

An alternative to this wiring chart would be that the sensor white wires of S17-S20 were instead connected to 1L, 3L, 5L and 7L, and green wire performing the function of Signal Return S17-S20 at the bottom of the table would not be needed.

C.5.3 Appendix C.3

Figure C.4 shows the data captured for the full period after 11:45 June 25th, 2010. The wide discrepancy of data until about 12:35 would suggest that the sensors were not in the water or the pump was not turned on.

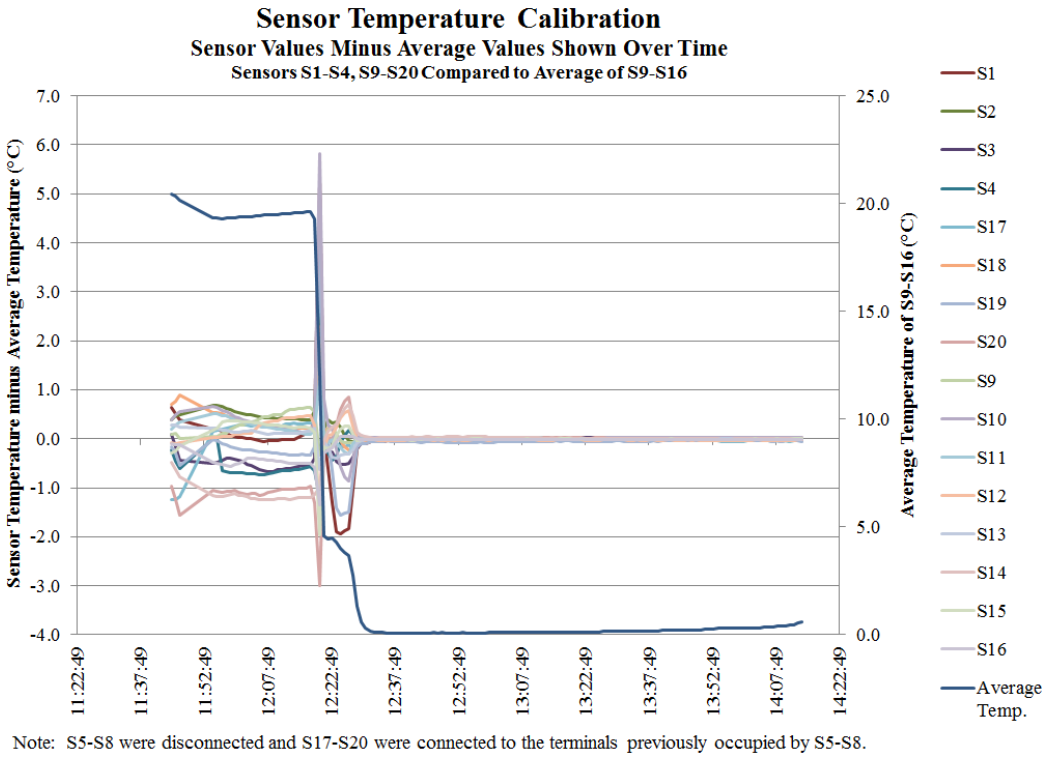

Figure C.4 Test 2 - Sensors Values Minus Average - Showing Period Excluded from Analysis and Calculations (11:45 – 12:35)

APPENDIX D: 109 TEMPERATURE PROBE AND CR1000 UNCERTAINTY ANALYSIS

Prepared by Chris Lashmar, August, 2012

D.1 Introduction

The purpose of this paper is to explore and recommend an approach for identifying the overall uncertainty for the 109 temperature probe and CR1000 system.

D.2 Error Categories

Error can be defined as the measurement value minus the true value (JCGM/WG2, 2008). There are three major categories of errors: equation errors, precision errors and bias errors.

D.2.1 Equation Errors

In this analysis, equation errors are inaccuracies that occur due to errors in the Steinhart and Hart equation which converts a voltage reading to a temperature value.

D.2.2 Precision or Random Errors

Precision or random errors are defined by ASHRAE (2009, p. 36.1) as "Statistical error caused by chance and not recurring. This term is a general category for errors that can take values on either side of an average value. To describe a random error, its distribution must be known."

D.2.3 Bias or Systematic Errors

Bias or systematic errors are defined as "Persistent error not due to chance; systematic errors are causal. It is likely to have the same magnitude and sign for every instrument constructed with the same components and procedures. Errors in calibrating equipment cause systematic errors because all instruments calibrated are biased in the direction of the calibrating equipment error. Voltage and resistance drifts over time are generally in one direction and are classed as systematic errors." (ASHRAE, 2009, p. 36.1).

D.3 Errors vs. Uncertainties vs. Accuracy

Although the terms "accuracy", "error", and "uncertainty" are sometimes used interchangeably, they can also have slightly different meanings. It is worth identifying these similarities and differences when attempting to consolidate information across different sources.

Working Group 2 of the Joint Committee for Guides in Metrology (JCGM/WG2, 2008) states that **measurement accuracy** is "closeness of agreement between a measured quantity value and a true quantity value of a measurement" but "is not a quantity and is not given a numerical quantity value."

However, Campbell Scientific (2009, p. 384) provides the following definition of accuracy: "A measure of the correctness of a measurement" implying a quantity value. Supporting this notion is the fact that, within the specification section of the CR1000

Operators Manual, numerical range values are assigned to the accuracy specification component; no mention of uncertainties is made. This is by no means unique to Campbell Scientific and in fact it appears that the JCGM is providing a definition not used in practice by instrumentation suppliers. This conclusion is based on random search of several instruments, not a large and rigorous study. The discrepancy in terminology does appear to be inconsequential but is nevertheless identified here.

As stated previously, the **error** is the measurement value minus the true value. Unfortunately, "true values are by nature indeterminate" (JCGM/WG1, 2008). An **uncertainty** can be described as an estimation of probable error (ASHRAE, 2009, p. 36.1-36.4). If there is a 95% **level of confidence** that a temperature reading is 25 ℃ ±0.2 ℃ then it can be said that in 95% of the cases where the measured value is 25 ℃, the actual temperature would reside between 24.8 ℃ and 25.2 ℃. The ±0.2 ℃ is the uncertainty. When a manufacturer provides a specification for a temperature sensor indicating an accuracy of ±0.20 ℃, then the manufacturer is indicating that the true value will be within 0.20 ℃ including both bias and precision errors (Mills & Chang, 2004). Thus, it is known that there MAY be a bias error but the size and direction of the actual bias are not identified. All that is known is the sum of the precision and bias errors inherent within the sensor.

D.4 Levels of Confidence and Probability Distributions

D.4.1 Gaussian or Normal Distribution

It is worth further discussing the concepts of level of confidence and probability distribution. A **Gaussian or normal distribution**, more commonly known as a **Bell Curve**, is a type of probability distribution that many people are familiar with. In a classroom situation, a bell curve occurs when the student marks are distributed in a manner that most marks are near the average (or have the highest probability of occurring near the average), with a steady decrease in the frequency of marks as the marks deviate from the average value. The same is true with other measurements. In a series of measurements taken at a given set of conditions, the measurement values vary over some range with more values occurring as they approach the average value, or mean value, as shown in Figure D.1. In a Gaussian distribution, one standard deviation is the range of values closest to the mean that contains 68% of the observations. Two standard deviations include about 95% of the observations.

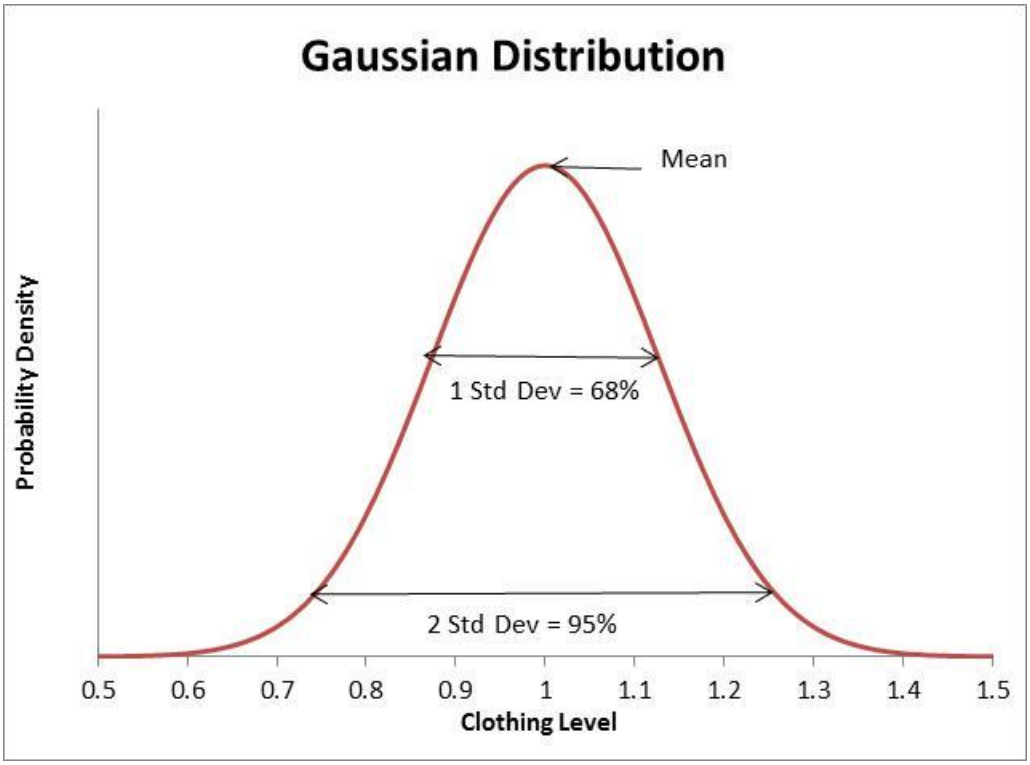

Figure D.1 Gaussian Distribution

D.4.2 Uniform or Rectangular Distribution

It is often the case that neither level of confidence nor the uncertainty distribution is identified in the manufacturer's specifications. In this case, the JCGM/WG1 recommends using, not a Gaussian distribution, but a **uniform** or **rectangular distribution** whereby all values fall within the specified range with even probability. This is supported by Swenson (2010), who provides technical support on the Campbell Scientific User Forums. If a certain level of confidence must be derived from a uniform distribution for the purposes of the experimental discussion, then the following conversions can be made.

Assume that the instrument accuracy is given as ±a.

The standard deviation(σ) is calculated as $\sigma = a/\sqrt{3}$ which has a level of confidence of 57.74%. (JCGM/WG1, 2008. p. 70)

The 95% level of confidence can be determined by multiplying the standard deviation by 1.65. Alternatively, it can be determined by multiplying the accuracy value by 0.95, the level of confidence.

The 99% level of confidence can be determined by multiplying the standard deviation by 1.71 or by multiplying the accuracy value by 0.99.

For example: If the instrument reads 25 ℃ and the measurement accuracy is ±0.20 ℃, then the 95% level of confidence is calculated as $25\ °C \pm (\frac{0.2}{\sqrt{3}} \times 1.65)\ °C$ or $25\ °C \pm 0.19$ ℃. This is the same as multiplying 0.20 by 0.95.

D.5 109 System Uncertainty Components

The overall uncertainty of a measurement taken using the 109 temperature probe and the CR1000 is comprised of uncertainties arising from the CR1000, the RES24.9K-0.1 completion resistor, the interchangeability of the thermistor, and the Steinhart and Hart equation. No uncertainties are identified with the multiplexor.

Although some of the component uncertainty ranges are dependent on temperature, at a given temperature the component uncertainties are treated as being independent of each other. This point may be confusing because the resistance is calculated entirely based on the voltage drop measured by the CR1000 so the measured resistance is dependent on the measured voltage. But the voltage and resistance are not two separate variables that show up in the temperature equation simultaneously, and the uncertainty effects can arise independently, so it is believed that these should be treated independently.

Overall uncertainty is often determined by propagating component uncertainties using the method of partial derivatives. With some equations this can become difficult and, with tools such as Excel available, it is probably easier to solve numerically using the steps that will be described here. Basically, the effect of each component's uncertainty on the final temperature is determined individually, and then all uncertainties are combined at the end.

D.5.1 Temperature Calculation

Before the uncertainties are calculated, it is useful to know the basic temperature calculation. Using the measured voltage as the starting point, the temperature is calculated by the next two equations as provided by Campbell Scientific (2010). First, calculate the thermistor resistance, R_T as

$$R_T = 24900 \times \left(\frac{V_{ex}}{V} - 1\right)$$ **Equation 1**

Where: 24900 is the resistance of the fixed resistor in ohms

V_{ex} is 2500 mV, the excitation voltage

V is the measured voltage (mV).

Then, calculate the temperature T_k in degrees Kelvin using the Steinhart and Hart equation:

$$T_k = \frac{1}{A + B\ln(R_T) + C(\ln(R_T))^3}$$ **Equation 2**

Where: A = 1.129242 X 10^{-3}

B = 2.341077 X 10^{-4}

C = 8.775468 X 10^{-8}.

If instead, the temperature is the known value, the calculations are more complicated and are derived here. First let

$$X = \ln(R_T).$$ **Equation 3**

Restate Equation 2 as

$$T_k = \frac{1}{A + BX + CX^3}$$ **Equation 4**

Rearrange Equation 4:

$$CX^3 + BX + A - \frac{1}{T_k} = 0.$$ **Equation 5**

Note that this takes the form of a cubic polynomial. To avoid simplifying the result by hand, a tool such as www.wolframalpha.com can be used to determine the value of X.

The resulting equation is described here in two parts. First, to save repetition of a large component of the equation, calculate a variable that will be arbitrarily called Z:

$$Z = \sqrt[3]{\sqrt{\left(27C^2T_k^2 \times (1 - AT_k)\right)^2 + 108B^3C^3T_k^6} + 27C^2T_k^2 \times (1 - AT_k)}$$ **Equation 6**

Then calculate X as

$$X = \frac{Z}{3\sqrt[3]{2}CT_k} - \frac{\sqrt[3]{2}BT_k}{Z}$$ **Equation 7**

Recalling that X is actually just ln(R_T), the resistance can now be calculated:

$$R_T = exp\left(\frac{Z}{3\sqrt[3]{2}CT_k} - \frac{\sqrt[3]{2}BT_k}{Z}\right)$$ **Equation 8**

And now the expected measured voltage can be calculated as

$$V = \frac{24900V_{ex}}{R_T + 24900}$$ **Equation 9**

D.5.2 CR1000 Datalogger Uncertainty

The temperature uncertainty due to the CR1000 is determined by first calculating the uncertainty in the voltage, U_V, in mV as provided by Campbell Scientific (2009):

$$U_V = V \times 0.0006 + 2.004$$ **Equation 10**

Where: The value of 0.0006 is used when the CR1000 panel temperature is between 0 ℃ and 40 ℃.

The value of 2.004 is the calculated offset value when the input range of the sensor is 2500 mV and it is measured using the single ended channel (i.e. 3* 0.667 + 0.003 = 2.004).

To calculate the upper value of the temperature range due to the voltage uncertainty, sum the measured voltage and the voltage uncertainty and substitute the result back into Equation 1 and repeat Equation 2 as shown in the next two equations:

$$R_{T+} = 24900 \times \left(\frac{V_{ex}}{V + U_V} - 1\right)$$ **Equation 11**

$$T_{C+} = \frac{1}{A + B\ln(R_{T+}) + C(\ln(R_{T+}))^3}$$ **Equation 12**

To calculate the lower temperature value, subtract the voltage uncertainty from the measured voltage and substitute the results back into Equation 1 and Equation 2 as shown in the next two equations:

$$R_{T-} = 24900 \times \left(\frac{V_{ex}}{V - U_V} - 1\right)$$ **Equation 13**

$$T_{C-} = \frac{1}{A + B\ln(R_{T-}) + C(\ln(R_{T-}))^3}$$ **Equation 14**

Finally, the positive and negative temperature uncertainties due to the CR1000 are as follows:

$U_{C+} = T_{C+} - T_K$ **Equation 15**

$U_{C-} = T_K - T_{C-}$ **Equation 16**

Where T_K is the actual measured temperature in degrees Kelvin.

D.5.3 Completion Resistor Uncertainty

The 24900 Ohm resistor has two uncertainty components as described by Campbell Scientific (2010): 0.1% of the 24900 ohm resistance, and a temperature based component that varies 10ppm/ ℃ away from 25 ℃. Combining these two components, the higher resistance value is calculated as:

$$R_{T+} = R_T\left(1.001 + \left|\frac{10}{10^6} \times (25 + 273.15 - T_K)\right|\right). \quad \textbf{Equation 17}$$

And the lower value is calculated as

$$R_{T-} = R_T\left(\frac{1}{1.001} - \left|\frac{10}{10^6} \times (25 + 273.15 - T_K)\right|\right). \quad \textbf{Equation 18}$$

A higher resistance value indicates a lower temperature, so the upper temperature due to thermistor uncertainty is calculated as

$$T_{T+} = \frac{1}{A + B\ln(R_{T-}) + C(\ln(R_{T-}))^3}. \quad \textbf{Equation 19}$$

And the lower temperature is calculated as

$$T_{T-} = \frac{1}{A + B\ln(R_{T+}) + C(\ln(R_{T+}))^3}. \quad \textbf{Equation 20}$$

Finally, the positive and negative temperature uncertainties due to the thermistor are as follows:

$$U_{T+} = T_{T+} - T_K \qquad \textbf{Equation 21}$$

$$U_{T-} = T_K - T_{T-} \qquad \textbf{Equation 22}$$

D.5.4 Thermistor Interchangeability Uncertainty

The thermistor interchangeability error is 0.2 ℃ for temperatures above 0 ℃ and increases to about 0.5 ℃ at -50 ℃ as shown by the red line in Figure D.2. The label "thermistor interchangeability error" implies the error occurs between thermistors, so it seems likely that the thermistor interchangeability error is largely a bias error, rather than a precision error. This is mostly true for the 107 sensor as the *Model 107 Temperature Probe Instruction Manual* says that "For the range of 0 ℃ to 50 ℃, the interchangeability error is predominantly offset and can be determined with a single point calibration." If this is also true for the 109 sensor, then the calibration process performed with multiple sensors in an ice bath might allow one to reduce this uncertainty; however, the water will be warmed as it is circulated through the pump and touches the basin walls, so it is hard to know how close to 0 ℃ the water temperature actually is without relying on the measured values.

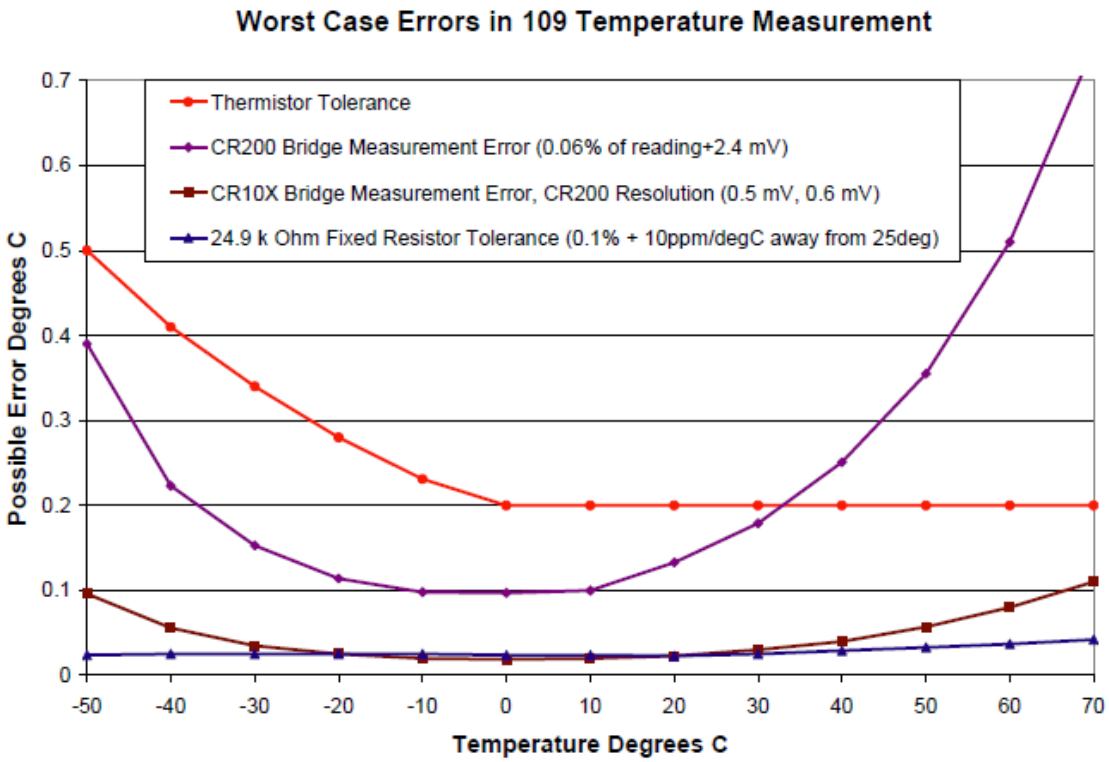

Figure D.2 Worst Case Errors in 109 Temperature Measurement. Source: Campbell Scientific 109 & 109BAM Temperature Probe Instruction Manual

The error values for this figure were entered into Excel for temperatures below 0 ℃ and a second order polynomial was fitted to the curve with an R^2 value of 0.9998. The resulting polynomial is as follows:

$$U_I = \pm(6.69643 \times 10^{-5}x^2 - 0.00261x + 0.200893) \text{ for x } < 0 \quad \textbf{Equation 23}$$

$$U_I = \pm 0.2 \text{ for x >=0} \quad \textbf{Equation 24}$$

Where: U_I is the uncertainty due to the thermistor interchangeability (℃)

x is the temperature (℃).

Therefore, for all temperatures greater than 0 ℃, an error value of 0.2 ℃ is used, and for temperatures less than 0 ℃, the polynomial is used.

D.5.5 Steinhart and Hart Uncertainty

The uncertainty associated with the Steinhart and Hart equation is extremely small compared to the other components, but is included here as proof.

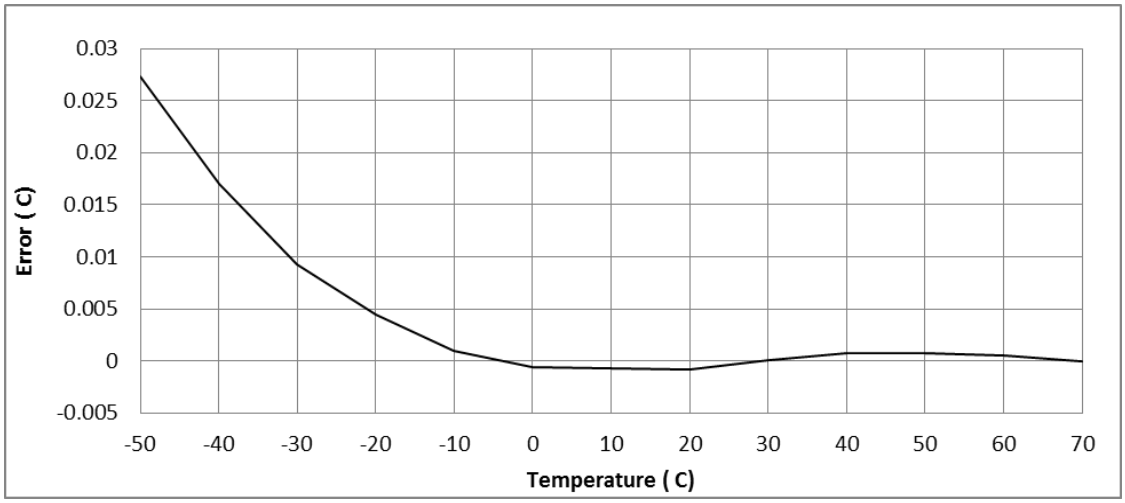

Figure D.3 Steinhart and Hart Tabulated Errors. Source: Campbell Scientific 109 & 109BAM Temperature Probe Instruction Manual

Based on Figure D.3, a table of values were created as shown in Table D.1. For any given measured temperature, the corresponding error can be interpolated from this table using Excel. A 4^{th} or 5^{th} order polynomial created in Excel would also have worked very well instead of interpolation.

Table D.1 Steinhart and Hart Errors

Temperature	Error
-50	0.0273
-40	0.017
-30	0.0093
-20	0.0044
-10	0.001
0	-0.00065
10	-0.0007
20	-0.0008
30	0.0001
40	0.0007
50	0.0007
60	0.0005
70	0

D.6 Overall Temperature Uncertainty

ASHRAE recommends calculating an overall uncertainty by combining the bias and precision uncertainties using the method of taking the square root of the sum of the squares (SRSS):

$$U_{Total} = \sqrt{\sum U_{Precision}^2 + \sum U_{Bias}^2} \qquad \textbf{Equation 25}$$

Figliola and Beasley (1991) modify this slightly, indicating that $U_{Precision}$ be determined at the 95% level of confidence to determine U_{Total} at the 95% level of confidence (p. 157).

Mills and Chang (2004) argue that combining bias and precision uncertainties in this manner is misleading because the formula is based on the assumption of a Gaussian distribution which is not true for the bias errors (p.31). The bias errors could accumulate to a worst case scenario or they could cancel each other out, but it is unlikely that they

will follow the Gaussian distribution. Mills and Chang suggest that it is more useful to provide precision uncertainties and "an intelligent discussion of possible bias errors and their magnitudes".

Further complicating matters is the recommendation by the JCGM/WG1 (2008) to assume a uniform distribution if the distribution is unknown (p.13), as is the case with the equipment specifications. The JCGM/WG1 say later that if the overall uncertainty is dominated by a uniform distribution, the central limit theorem may not apply (p. 71), meaning that the SRSS method may also become less accurate. In the case of the 109 sensors and CR1000 datalogger, all uncertainties are assumed to follow a uniform distribution and two of them, the CR1000 and thermistor interchangeability error, dominate the overall uncertainty. The JCGM/WG1(2008) points out that more accurate combined distributions can be determined by convolving the equations, but this assumes an equation of the form

$$Y = c_1X_1 + c_2X_2 + \cdots c_nX_n \qquad \textbf{Equation 26}$$

rather than the form used in Equation 2 which calculates temperature. At any given temperature, the small input uncertainties create a temperature variation that is close to linear and so maybe it is more accurate to convolve the two dominating distributions, but it is not clear this is the case. So the more conservative option, where the 95% level of confidence includes a slightly larger interval, is described here. This option is easier to implement and more common, although typically where normal distributions are assumed.

The basic approach is to determine one standard deviation for each input distribution. For uniform distributions, this is calculated as

$$\sigma_x = \frac{U_x}{\sqrt{3}}$$ **Equation 27**

Where: U_x is the uncertainty for a given component.

The standard deviation values are combined using the SRSS method to determine the overall standard deviation. Multiply this by a factor of 2 to achieve coverage (k) of at least 95%.

So the final formula for calculating the overall uncertainty at the 95% level of confidence based on equipment specifications is as follows:

$$U_+ = 2 \times \sqrt{\frac{U_{C+}^2 + U_{T+}^2 + U_I^2 + U_S^2}{3}}$$ **Equation 28**

$$U_- = -2 \times \sqrt{\frac{U_{C-}^2 + U_{T-}^2 + U_I^2 + U_S^2}{3}}$$ **Equation 29**

As it turns out, there is negligible difference between the positive and negative uncertainties as demonstrated in Figure D.4. When the positive and negative uncertainty values are averaged and graphed, the results appear as shown in Figure D.5. The graph shows the uncertainty for each component, at one standard deviation (k=1), the overall

uncertainty at one standard deviation (k=1), and the overall uncertainty at two standard deviations (k=2).

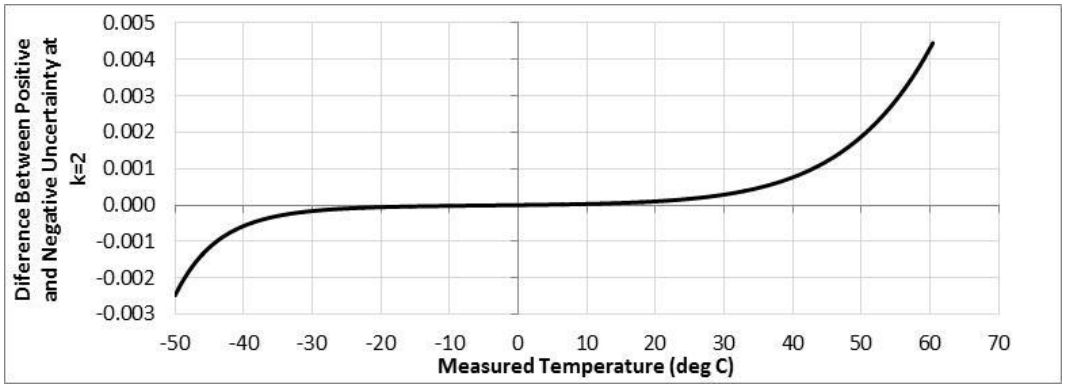

Figure D.4 Difference between Positive and Negative Uncertainties at k=2 (Over 95% Level of Confidence)

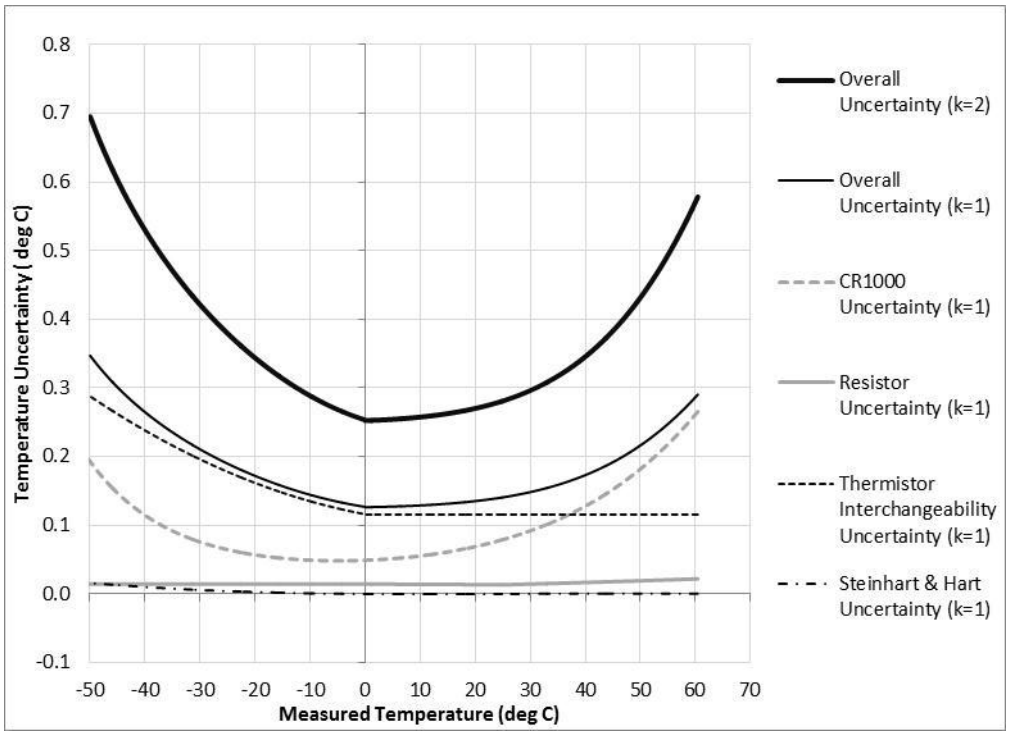

Figure D.5 Measurement Uncertainties of 109 Temperature Sensor with CR1000 Datalogger Based on Equipment Specifications. When k=1, the Level of Confidence is between 58% and 68%. When k=2, the Level of Confidence is over 95%.

When field measurements are recorded, there will be some uncertainty introduced as a result of the conditions in the field. The JCGM/WG1 warns that uncertainty components should not be "double-counted" (p.14). While all uncertainties originating from the equipment will appear in the results of the field measurements, the bias component will not be detectable (even though it may be large) unless there something which provides a calibration point (e.g. melting or freezing of water). The precision uncertainty originating from the equipment itself will be combined with the random effects arising from the field conditions. As mentioned previously, the thermistor interchangeability error is likely predominantly bias error from 0 ℃ to 50 ℃ and this is the dominating factor in the overall uncertainty throughout much of the temperature range. The CR1000 uncertainty affects the overall value less and it is unclear how much of that uncertainty is due to bias and how much is random effects. Lacking this information, the most prudent approach might be to include the standard deviation of the recorded values in the overall uncertainty calculation. The standard deviation, S, of the measured values is calculated as

$$S = \sqrt{\frac{\sum_{i=1}^{n}(T_i - \bar{T})^2}{n-1}}$$ **Equation 30**

Where: T_i is each temperature measurement

$\bar{T}$ is the average of the temperature measurements

n is the number of measurements taken over some period of interest.

This is now incorporated into the overall formulas

$$U_+ = 2 \times \sqrt{\frac{U_{C+}^2 + U_{T+}^2 + U_I^2 + U_S^2}{3} + S^2}$$ **Equation 31**

$$U_- = -2 \times \sqrt{\frac{U_{C-}^2 + U_{T-}^2 + U_I^2 + U_S^2}{3} + S^2.}$$ **Equation 32**

So to summarize, Equation 31 and Equation 32 determine the overall positive and negative uncertainty values at over a 95% level of confidence. The overall distribution is based on the combination of four assumed uniform distributions, and one assumed Gaussian distribution.

References

ASHRAE. (2009). *ASHRAE Handbook, Fundamentals, S-I Edition*. Atlanta, GA: American Society of Heating, Refrigerating and Air-Conditioning Engineers, Inc.

Campbell Scientific. (2009). *CR1000 Measurement and Control System Operator's Manual.* Retrieved August 22, 2012 from http://www.campbellsci.ca/Catalogue/CR1000_Man.pdf

Campbell Scientific. (2010a). *109B and 109BAM Temperature Probe Instruction Manual.* Campbell Scientific (Canada) Corp.

Campbell Scientific. (2010b). *Model 107 Temperature Probe Instruction Manual.* Campbell Scientific, Inc.

Figliola, R. S., & Beasley, D. E. (1991). *Theory and Design for Mechanical Measurements*. Ontario, Canada: John Wiley & Sons, Inc.

Dietrich, C. F. (1973). *Uncertainty, Calibration and Probability – The Statistics of Scientific and Industrial Measurement*. London, UK: Adam Hilger Rank Precision Industries Ltd.

Mills, A. F., & Chang, B. H. (2004). *Error Analysis of Experiments A Manual for Engineering Students*. Retrieved August 22, 2012 from http://www.seas.ucla.edu/mae/Error_Analysis_of_Experiments.pdf

Swenson, J. (2010). *Campbell Scientific User Forums.* Retrieved August 22, 2012 from http://63.255.173.180/forum/messages.cfm?threadid=F6A5B601-EED8-D3DB-AC8229D35460664E

Working Group 1 of the Joint Committee for Guides to Metrology (JCGM/WG1). (2008). *JCGM 100:2008 GUM 1995 with minor corrections Evaluation of measurement data - Guide to the expression of uncertainties in measurement.* The Joint Committee for Guides in Metrology.

Working Group 2 of the Joint Committee for Guides to Metrology (JGCM/WG2). (2008). *JCGM 200:2008 International vocabulary of metrology - Basic and general concepts and associated terms (VIM).* The Joint Committee for Guides in Metrology.

APPENDIX E: ELLISDON M1.03 EARTHTUBES PLAN DRAWING

Provided by EllisDon.

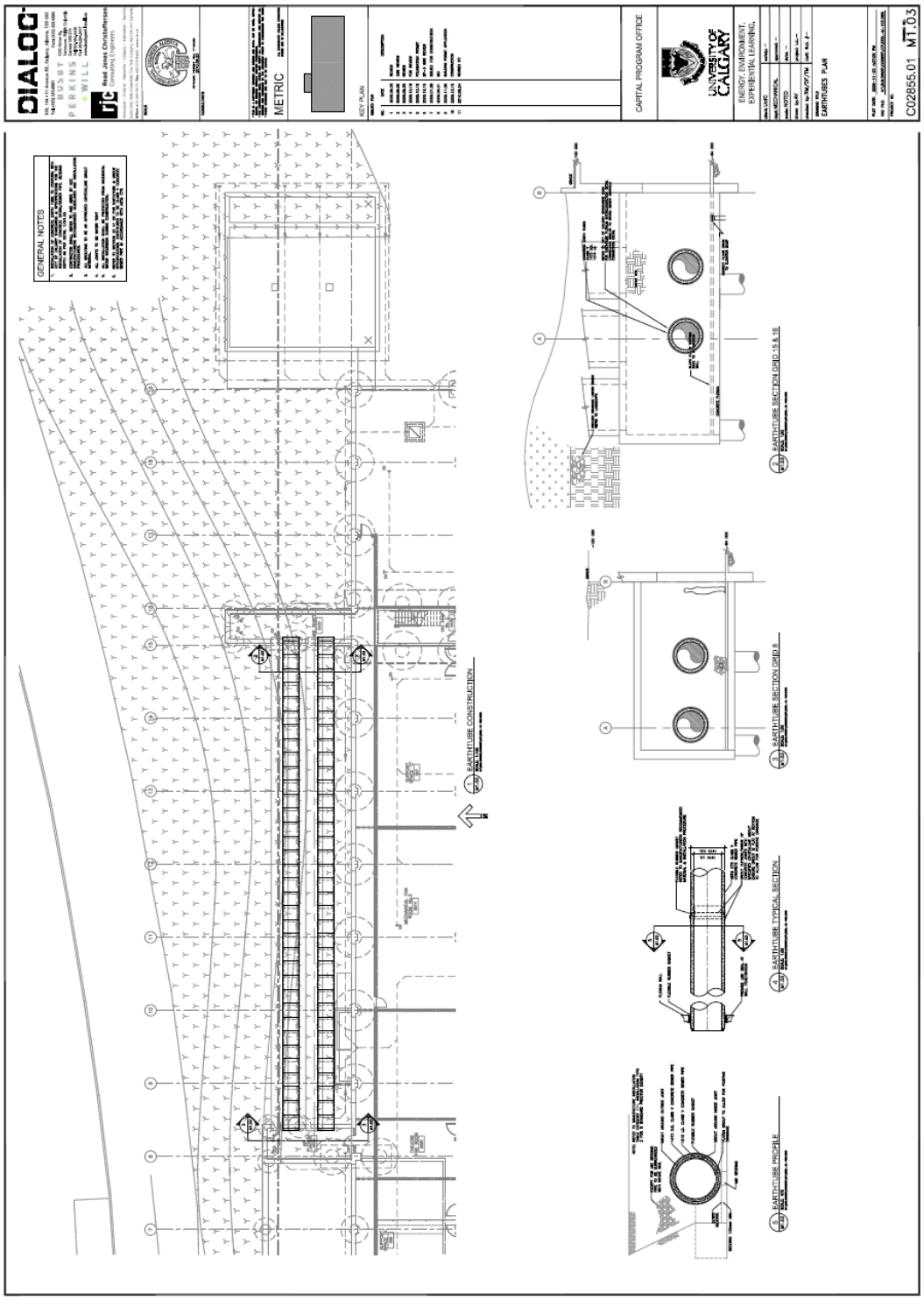

APPENDIX F: REYNOLDS NUMBER CALCULATION

F.1 General Introduction

As defined in the ASHRAE Handbook Fundamentals (ASHRAE, 2009, p. 3.3), "Laminar and turbulent flows can be differentiated using the Reynolds number Re."

$$Re_L = VL/\nu$$

where, L is the characteristic length scale and ν is the kinematic viscosity of the fluid. In flow through pipes, tubes, and ducts, the characteristic length scale is the hydraulic diameter D_h. For a round pipe, D_h equals the pipe diameter D. In this research:

$$L = D_h = D = 1.2 \text{ m}$$

$$\nu = \nu_{air} = 1.62*10^{-4} \text{ ft}^2/\text{s} = 0.15*10^{-4} \text{ m}^2/\text{s} \text{ (p. 3.1)}$$

The EEEL ET system uses two 3.73 kW TECO TEFC motor driven fans to draw ambient air through the ducts (Appendix B). Each fan has a normal flow of 2360 L/s (2.36 m^3/s, 1750 rpm) to a minimum of 826 L/s (0.826 m^3/s).

$$V = Q/A$$

where V is the airflow velocity, Q is the airflow rate and A is the discharge area. In this research, it is assumed the two ducts both draw air from inlet to discharge, two fans are always set at the same speed, and the entering air mixes evenly and has the same velocity at any point inside the ducts. The airflow capacity for each duct should be half of the total airflow capacity.

That is:

$$Q_{each} = Q_{total}/2$$

$$A_{each} = \pi(D/2)^2 = 3.14*(1.2\ m/2)^2 = 1.13\ m^2$$

F.2 Detailed Calculations

F.2.1 Supply Fan Operated with Rated Maximum Speed

When supply fans are operating at rated maximum speed, for airflow in each duct:

$$Q_{max} = 2.36\ m^3/s$$

$$V_{max} = Q_{max} /A_{each} = (2.36\ m^3/s)/1.13\ m^2 = 2.1\ m/s$$

$$Re_{max} = V_{max}L/\nu_{air} = 2.1\ m/s*1.2\ m/(0.15*10^{-4}\ m^2/s) = 168000 > 10{,}000$$

"Laminar flow in pipes or ducts exists when the Re < 2300. Fully turbulent flow exists when Re > 10,000. For 2300 <Re < 10,000, transitional flow exists, and predictions are unreliable (ASHRAE, 2009, p. 3.3)." The airflow of 2.1 m/s under the maximum speed operation (1750 rpm for each supply fan) in this system is therefore turbulent.

F.2.2 Supply Fan Operated with Minimum Speed

When supply fans are operating at minimum speed, for airflow in each duct:

$$Q_{min} = 0.826\ m^3/s$$

$$V_{min} = Q_{min}/A_{each} = (0.826\ m^3/s)/1.13\ m^2 = 0.73\ m/s$$

$$Re_{min} = V_{min}L/\nu_{air} = 0.73\ m/s*1.2\ m/(0.15*10^{-4}\ m^2/s) = 58400 > 10{,}000$$

According to Fan Law 1(McQuiston et al., 2005, p. 398):

$$Q_1/Q_2 = rpm_1/rpm_2$$

where $Q_{max} = 2.36\ m^3/s$, $Q_{min} = 0.826\ m^3/s$, $rpm_{max} = 1750$ rpm

$$rpm_{min} = Q_{min} * rpm_{max}/Q_{max} = 0.826\ m^3/s * 1750\ rpm/2.36\ m^3/s = 613\ rpm$$

The airflow of 0.73 m/s under the minimum speed operation (613 rpm of each supply fan) in this system is therefore also turbulent.

F.2.3 Airflow Condition Boundaries Calculation

Under the same assumption as above, airflow conditions under certain air velocity can be calculated.

F.2.3.1 Laminar Airflow

When Re < 2300, the airflow is laminar.

$$Re_{Laminar} = V_{Laminar} L/\nu_{air} < 2300$$

$$V_{Laminar} < 2300\nu_{air}/L$$

$$V_{Laminar} < 2300 * 0.15 * 10^{-4}\ m^2/s/1.2\ m$$

$$V_{Laminar} < 0.03\ m/s$$

$$Q_{Laminar} = V_{Laminar} A = 0.03\ m/s * 1.13\ m^2 = 0.034\ m^3/s$$

$$rpm_{Laminar} = Q_{Laminar} * rpm_{max}/Q_{max} = 0.034\ m^3/s * 1750\ rpm/2.36\ m^3/s = 25\ rpm$$

That is when each of the supply fans of this ET system is operating slower than 25 rpm, the entering air will be under laminar flow. This is beyond the supply fan operating range, and will only occur very briefly during the fan's starting up and shutting down.

F.2.3.2 Turbulent Airflow

When Re > 10,000, the airflow is Turbulent.

$$Re_{Turbulent} = V_{Turbulent}L/\nu_{air} > 10000$$

$$V_{Turbulent} > 10000\nu_{air}/L$$

$$V_{Turbulent} > 10000*0.15*10^{-4}\ m^2/s/1.2\ m$$

$$V_{Turbulent} > 0.13\ m/s$$

$$Q_{Turbulent} = V_{Turbulent}A = 0.13\ m/s * 1.13\ m^2 = 0.15\ m^3/s$$

$$rpm_{Turbulent} = Q_{Turbulent}* rpm_{max}/Q_{max} = 0.15\ m^3/s*1750\ rpm/2.36\ m^3/s = 111\ rpm$$

That is when each of the supply fans of this ET system is operating faster than 111 rpm, the entering air will be under turbulent flow. This will be always true when each supply fan is operating normally.

F.2.3.3 Transitional Airflow

When 2300 <Re < 10,000, the airflow is transitional. According to calculations above:

$$0.03\ m/s < V_{Transitional} < 0.13\ m/s$$

$$25\ rpm < rpm_{Transitional} < 111\ rpm$$

That is when the supply fan of this ET system is operating between 25 and 111 rpm, the entering air will be under transitional flow. Again, this is beyond the supply fan operating range, and will only occur very briefly during the fan's starting up and shutting down.

F.3 Discussion

One thing should be noted that, the assumption this author made that "the entering air mixes evenly and have the same air velocity at any point inside the ducts" will not be true in real life. Moreover, according to Chapter 4, under the actual operation of the ET system, the airflow inside the south duct was backwards. As the airflow rates in both ducts are unknown, this makes calculation impossible. Air distribution when entering and moving through a duct is complicated, and could be studied with computational fluid dynamic techniques. This author's research scope does not require that level of analysis. The knowledge of duct airflow condition is sufficient.

References

ASHRAE. (2009). *ASHRAE Handbook, Fundamentals, I-P Edition*. Atlanta, GA: American Society of Heating, Refrigerating and Air-Conditioning Engineers, Inc.

McQuiston, F. C., Parker, J. D., & Spitler, J. D. (2005). *Heating, Ventilating, and Air Conditioning Analysis and Design* (6th ed.). Hoboken, NJ: John Wiley &Sons, Inc.

APPENDIX G: MEDIAN DAILY GROUND TEMPERATURE CHANGES INSIDE STRINGS

Graphs below show soil temperature changes inside strings from February 15th, 2011 to September 30th, 2012.

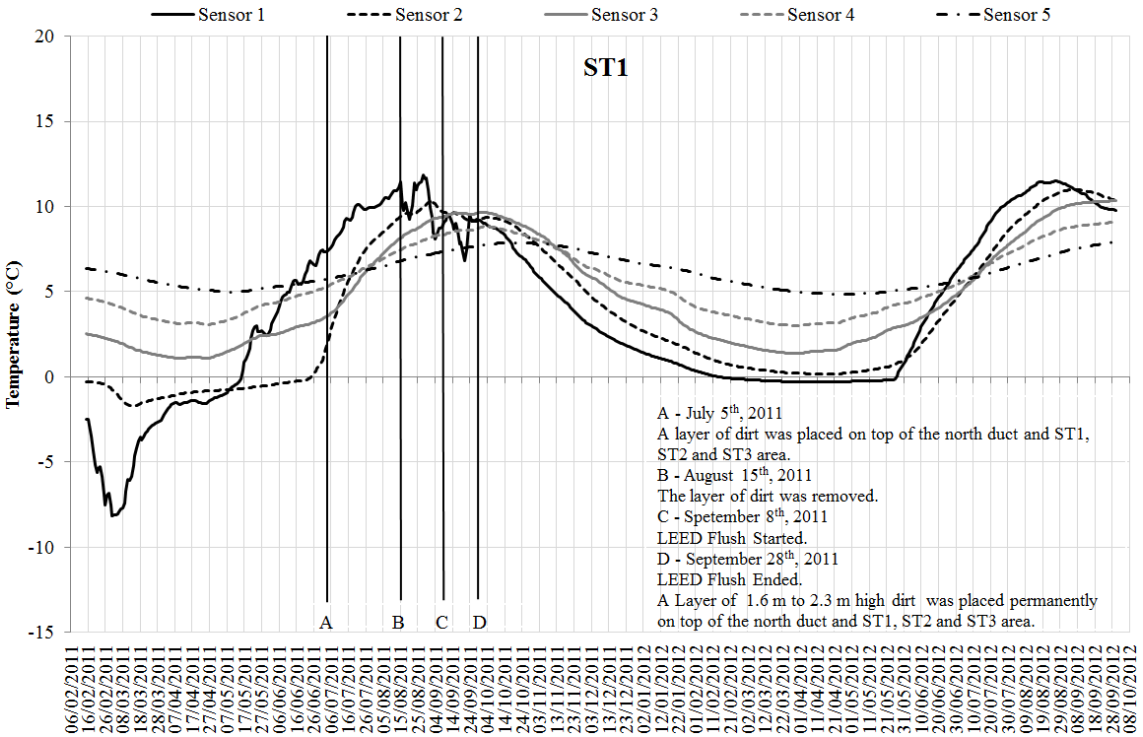

Figure G.1 ST1 Median Daily Ground Temperatures

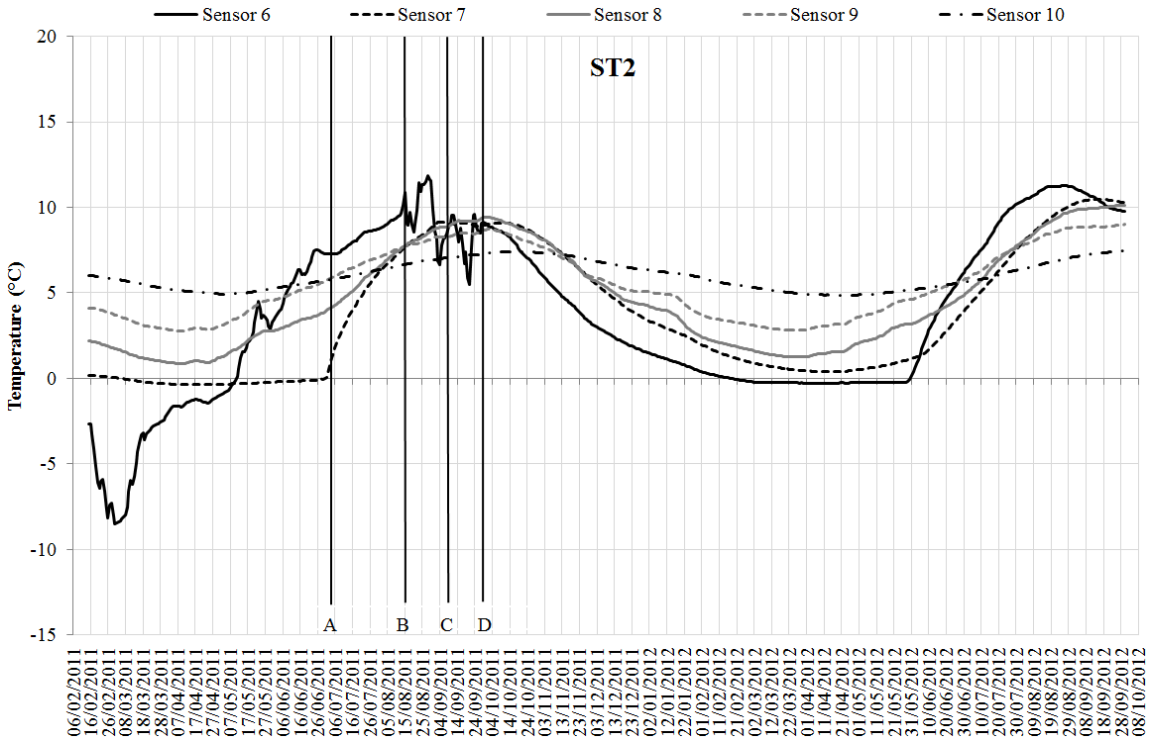

Figure G.2 ST2 Median Daily Ground Temperatures

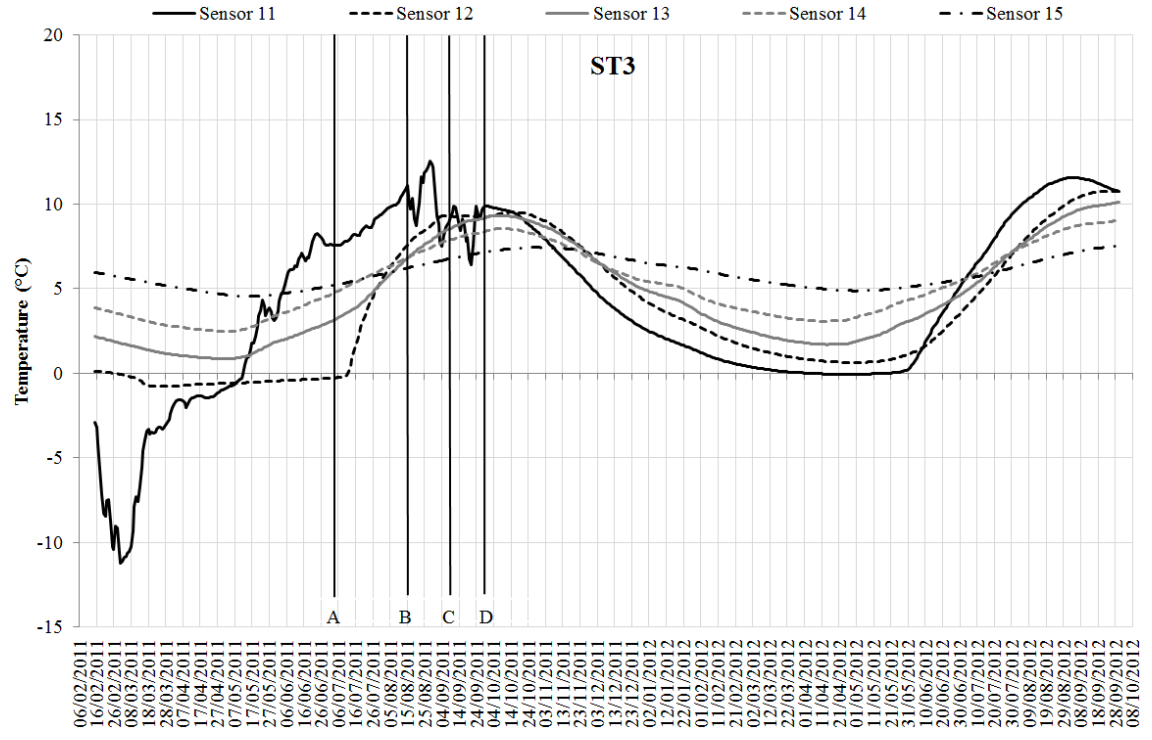

Figure G.3 ST3 Median Daily Ground Temperatures

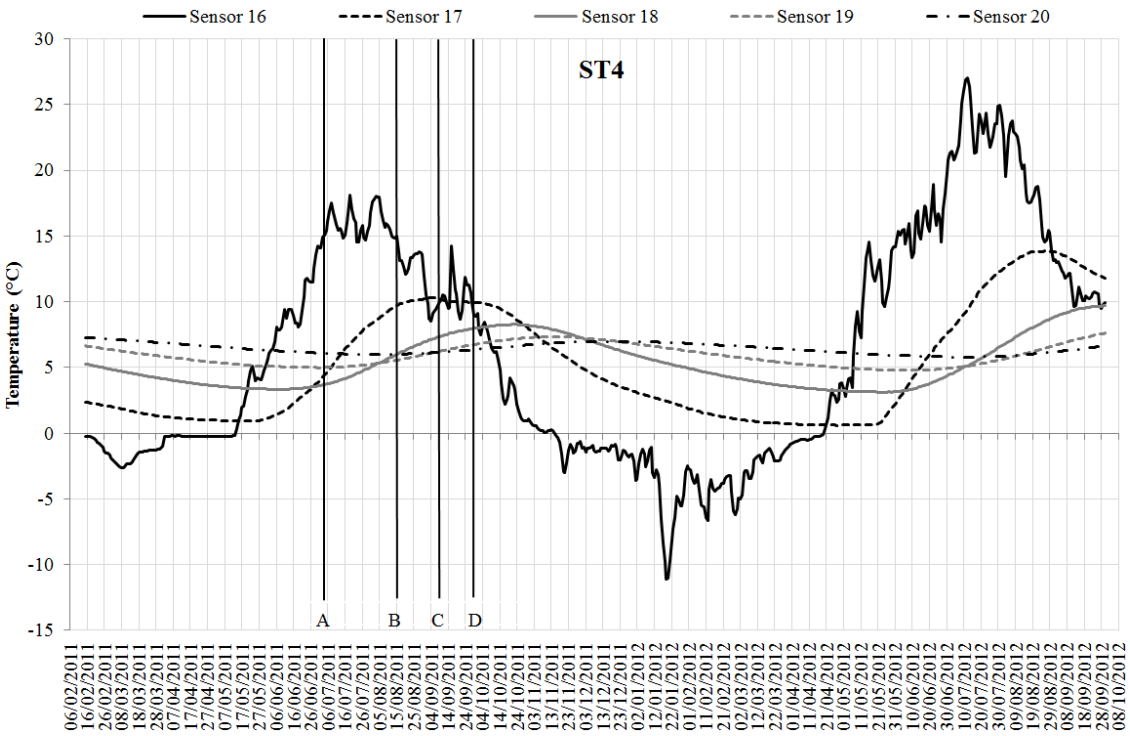

Figure G.4 ST4 Median Daily Ground Temperatures